The University of Nottingham
UNITED KINGDOM · CHINA · MALAYSIA

Optimisation of treatment of cancer based on principles of pharmacokinetics

Jong Bong Lee

School of Pharmacy
University of Nottingham
Nottingham
United Kingdom

Thesis submitted to The University of Nottingham for the degree of

Doctor in Philosophy

TABLE OF CONTENTS

TABLE OF CONTENTS 2

ACKNOWLEDGEMENTS 8

LIST OF PUBLICATIONS 10

LIST OF ABBREVIATIONS 11

ABSTRACT 15

LIST OF FIGURES 17

LIST OF TABLES 25

1. INTRODUCTION 29

1.1. Principles of pharmacokinetics in discovery and development of anticancer agents 29

1.1.1. Cancer and metastasis 29

1.1.2. Limitations of current chemotherapy 30

1.1.3. Pharmacokinetic development and optimisation of anticancer agents. 31

1.2. Maximising exposure of intestinal lymphatic system to drugs 34

1.2.1. Cancer and the lymphatic system 34

1.2.2. Lymphoma and lymphadenopathy in the abdominal lymphatics 37

1.2.3. Targeting the intestinal lymphatic system 39

1.3. Pharmacokinetic optimisation of cyclin-dependent kinase inhibitors 42

1.3.1. Pharmacokinetic optimisation in discovery and development of orally bioavailable anticancer agents 42

1.3.2. Development of cyclin-dependent kinase inhibitors 43

1.4. Project hypotheses and aims 44

1.4.1. Intestinal lymphatic system targeting of anticancer agents by lipophilic prodrug approach 45

1.4.2. Pharmacokinetic development of CDK9 inhibitors 46

2. MATERIALS AND METHODS 48

2.1. Materials 48

2.2. Chemical synthesis 49

2.2.1. General synthetic scheme for esterification 49

2.3. Chylomicron and artificial lipid particle association assay 50

2.3.1. Preparation of artificial lipid particle emulsion 50

2.3.2. Preparation of human plasma-derived chylomicron emulsion 50

2.3.3. Assay procedure 51

2.4. Prodrug conversion assay 52

2.5. Triglyceride solubility measurement 53

2.6. Cell growth inhibition assay 53

2.7. Permeability assay 54

2.7.1. Cell culture 54

2.7.2. Caco-2 permeability assay 54

2.8. Solubility assay 55

2.8.1. Preparation of biorelevant media 55

2.8.2. Assay procedure 56

2.9. Liver microsomal stability assay 57

2.9.1. Assay procedure 57

2.9.2. Calculations 57

2.10. *In silico* simulations 59

2.10.1. Simulation of absorption 59

2.10.2. Simulation of oral bioavailability 61

2.10.3. Simulation of absorption sites 62
2.10.4. Deconvolution of plasma concentration-time profiles 63
2.11. Analytical methods for determination of concentration 63
2.11.1. Sample preparation 63
2.11.2. Analytical conditions 66
2.12. Animal experiments 69
2.12.1. Animals 69
2.12.2. Pharmacokinetic study 70
2.12.3. Biodistribution study 71
2.12.4. Postprandial continuous lymph collection 71
2.12.5. Colonic administration 72
2.13. Statistical analyses 72

3. DEVELOPMENT AND VALIDATION OF SIMPLE AND SENSITIVE BIOANALYTICAL METHOD FOR DETECTION OF BEXAROTENE IN RAT PLASMA 74
3.1. Introduction 74
3.2. Scheme of work 77
3.3. Validation criteria 77
3.3.1. Selectivity 77
3.3.2. Accuracy and precision 78
3.3.3. Sensitivity 78
3.3.4. Linearity 78
3.3.5. Recovery 79
3.3.6. Freeze and thaw stability 79
3.3.7. Bench-top, short-term and long-term stability 79
3.3.8. Autosampler stability 80

3.3.9. Stock solution stability 80
3.4. Results and discussion 81
3.4.1. Method development 81
3.4.2. Method validation 82
3.4.3. Pharmacokinetic study in rats 86
3.4.4. Assessment of the suitability of the analytical method to human and mouse plasma. 88
3.5. Conclusion 90

4. INTESTINAL LYMPHATIC SYSTEM TARGETING BY LIPOPHILIC PRODRUG APPROACH 91
4.1. Introduction 91
4.2. Scheme of work 92
4.3. Results 93
4.3.1. Preparation of prodrugs of BEX 93
4.3.2. Association with lipoproteins 96
4.3.3. Conversion of BEX prodrugs to BEX 97
4.3.4. TG solubility of BEX and its prodrugs 100
4.3.5. Plasma pharmacokinetics of BEX and selected prodrugs 100
4.3.6. Biodistribution of BEX and selected prodrugs to the intestinal lymphatics 104
4.3.7. Application of the prodrug approach to intestinal lymphatic targeting of RA 105
4.3.8. *In vitro* efficacy and synergism 107
4.4. Discussion 108
4.5. Conclusion 118

5. PERMEABILITY OF DRUGS: QUANTITATIVE ANALYSIS OF LAB-TO-LAB VARIABILITY IN CACO-2 PERMEABILITY ASSAYS 119

5.1. Introduction 119

5.2. Scheme of work 120

5.3. Results and discussion 121

5.3.1. Permeability assay 121

5.3.2. Simulation of F_a 123

5.4. Conclusion 126

6. PHARMACOKINETIC DEVELOPMENT OF CDK9 INHIBITORS 128

6.1. Introduction 128

6.2. Scheme of work 130

6.3. Results 130

6.3.1. *In vitro* pharmacokinetic evaluation of candidate CDK9 inhibitors 130

6.3.2. *In silico* simulation of pharmacokinetic properties 136

6.3.3. *In vivo* evaluation of pharmacokinetics 137

6.3.4. Biopharmaceutical development of compound DF030263 139

6.4. Discussion 146

6.4.1. Rational drug development approach utilising in vitro-in silico-in vivo pharmacokinetic evaluations 146

6.4.2. Biopharmaceutical development of compound DF030263 152

6.5. Conclusion 157

7. GENERAL DISCUSSION AND FURTHER WORK 159

7.1. General discussion 159

7.2. Further work 166

7.2.1. Intestinal lymphatic system targeting of anticancer agents by lipophilic prodrug approach 166

7.2.2. Pharmacokinetic development of CDK9 inhibitors 167

APPENDICES 170

Appendix 1. Synthesis and characterisation results 170

Appendix 2. Establishment of a "user-defined permeability model" 186

Appendix 3. TG measurements in each test medium used for further conversion studies of BET and BCY (mg/mL, n = 3) 188

REFERENCES 189

ACKNOWLEDGEMENTS

First of all, I would like to express my sincere gratitude to my supervisors Dr. Pavel Gershkovich and Prof. Peter Fischer for their immense support for my PhD project. Especially Dr. Pavel Gershkovich has shown great patience in guiding me to the right path, often when I failed to acknowledge the true meaning of research. He has allowed me to properly grasp the fascination of research and certainly his influence will remain in me throughout my career. I have learned the logical process of reasoning from Prof. Peter Fischer and he has also shown me how to be excited from my research outcomes.

Secondly, I would like to thank my wife, Uijin Jeong, who has been by my side all along the PhD course. She has provided emotional comfort and been extremely supported during my studies. I also appreciate the support from my family and friends all throughout.

I am grateful to many other academic members and staff. In the University of Nottingham, I thank Dr. Tracey Bradshaw for her kindness and insight in designing *in vitro* efficacy studies, Prof. David Barrett and Dr. Catherine Ortori for their help in analytical chemistry, Dr. Cornelia de Moor especially for her supervision for studies towards the end of my PhD and Dr. Michael Stocks, Dr. Fadi Soukarieh, Dr. Anthony Wilson and Dr. Christophe Fromont for their supervision in medicinal chemistry. At Rutgers University, I greatly appreciate support from Dr. Leonid Kagan in the collaborative research and also Dr. Gregory Voronin for his help in research. At Sungkyunkwan University, I would like to thank Prof. Sun Dong Yoo for our collaborative research and the mentoring he provided throughout.

I would like to think myself as extremely lucky as I had the privilege of receiving help from so many colleagues in and out of the university. Our members of the Gershkovich

group were the most precious colleagues and among them, I would like to thank Atheer Zgair the most. He has been a helpful colleague, thoughtful advisor, discussion partner and an idea bank. Also my best regards to Jonathan Wong, Paloma Benito-Gallo, Sally Gittings, Dhiaa Taha, Joseph Ali, Chaolong (Louis) Qin, Carlos Sanders and Wanshan Feng for their company in our group. I also have appreciation for Aimie Garces for her help in synthesis, Mohammed Al-Hayali for his help with cell work and Rui (Tony) Gao for chemistry work. I enjoyed very much working with Xiaowei Zang and Manting Chiang at Rutgers and would like to thank them for all their help. Also my gratitude to my friend and collaborators Tae Hwan Kim and Min Gi Kim in Sungkyunkwan. I would also like to thank the undergraduate and MSc students who participated in the project, Amy Hume, Cecilia Adrower, Elena Cipolla, Chunlong (Ian) Lau, Jed Malec, Tecashanell McIntosh, Ting-Hoi Chan, Ting Qian Ooi and Wan Tying Soh, I could not have completed the project without you all.

Last but not least, I love my mates in our university baseball club, the Nottingham Thieves. They made my life in Nottingham so much enjoyable!

I would like to acknowledge Cancer Research UK, Wellcome Trust, School of Pharmacy for funding in research. I would like to thank Simulations Plus, Inc (Lancaster, CA, USA) for providing GastroPlus™ for research.

Jong Bong Lee

October 2017



LIST OF PUBLICATIONS

Lee JB, Zgair A, Taha DA, Zang X, Kagan L, Kim TH, Kim MG, Yun H-Y, Fischer PM, Gershkovich P, Quantitative analysis of lab-to-lab variability in Caco-2 permeability assays, *Eur J Pharm Biopharm*. **2017** May; 114:38-42.

Lee JB, Zgair A, Kim TH, Kim MG, Yoo SD, Fischer PM, Gershkovich P, Simple and sensitive HPLC-UV method for determination of bexarotene in rat plasma, *J Chromatogr B Analyt Technol Biomed Life Sci.* **2016** Nov; 1040:73-80.

LIST OF ABBREVIATIONS

ACAT	Advanced compartmental absorption and transit
ADME	Absorption, distribution, metabolism and excretion
AUC	Area under the curve
BCS	Biopharmaceutical classification system
BEX	Bexarotene
C_0	Concentration extrapolated to time zero
CDKs	Cyclin-dependent kinases
CL_h	Hepatic clearance
CL_{int}	Intrinsic clearance
CLL	Chronic lymphocytic leukaemia
CM	Chylomicrons
C_{max}	Maximum concentration observed
CT	Computerised tomography
CTCL	Cutaneous T-cell lymphoma
DLBCL	Diffuse large B-cell lymphoma
DMEM	Dulbecco's modified eagle medium
DMSO	Dimethyl sulfoxide
E_h	Hepatic extraction ratio

F_a	Fraction absorbed in humans
FaSSGF	Fasted state simulated gastric fluid
FaSSIF	Fasted state simulated intestinal fluid
FBS	Fetal bovine serum
FDA	US Food and Drug Administration
FeSSIF	Fed state simulated intestinal fluid
F_h	The fraction of the compound that passes through liver unchanged
F_{oral}	Oral bioavailability
GI	Gastrointestinal
GI_{50}	The concentration that inhibited cell growth by 50%
HBSS	Hank's balanced salt solution
HEPES	4-2-Hydroxyethyl-1- piperazineethanesulfonic acid
HIV	Human immunodeficiency virus
HPLC	High performance liquid chromatography
HQC	High quality control
IS	Internal standard
LLOQ	Lower limit of quantification
LQC	Low quality control
MLN	Mesenteric lymph nodes

MQC	Medium quality control
MTT	Thiazolyl blue tetrazolium bromide
NHL	Non-Hodgkin's lymphoma
P_{app}	Apparent permeability coefficient
PBPK	Physiologically-based pharmacokinetic
P_{eff}	Effective permeability in human
PEG400	Polyethylene glycol 400
PK/PD	Pharmacokinetics and pharmacodynamics
PPAR	Peroxisome proliferator-activated receptor
QC	Quality control
RA	Retinoic acid
RAR	Retinoic acid receptor
RE	Relative error
RMSE	Root mean square error
RSD	Relative standard deviation
RXR	Retionid X receptor
$t_{1/2}$	Half-life
TDM	Therapeutic dose monitoring
TEER	Transepithelial electrical resistance
T_{max}	Time of maximum concentration observed

V_{ss}	Volume of distribution at steady state

ABSTRACT

The main hypothesis of this research project was that optimisation of treatment based on pharmacokinetic principles is on its own a powerful approach in improvement of treatment outcomes. This work therefore focused on optimisation of treatment of cancer based on principles of pharmacokinetics using two main approaches 1) lipophilic prodrug approach to specifically target the intestinal lymphatic system following oral administration and 2) identification of orally bioavailable candidate anticancer agents and biopharmaceutical development to increase the bioavailability for sufficient systemic exposure to the drug. The first approach was the prodrug derivatisation to take advantage of the physiological process of intestinal lymphatic transport in order to deliver anticancer agents to the mesenteric lymph nodes. Similar prodrug approaches have been researched by other groups but the main focus previously was on increasing the overall bioavailability where they mostly used long-chain or triglyceride mimetic prodrug moieties. However, in this project, through a series of stability and chylomicron association studies, it was revealed that activated ester prodrugs are the most suitable forms for yielding high concentrations of active drugs in the mesenteric lymph nodes. It was remarkable that using this novel approach significantly higher concentrations of the active drugs were achievable in the intestinal lymphatics without affecting the systemic exposure. The second approach taken in this PhD project was achieving sufficient systemic exposure of anticancer agents by identification of orally bioavailable candidate and improvement of oral bioavailability by biopharmaceutical development. The candidates with promising pharmacokinetic properties were rank-ordered by application of a rational drug discovery and development approach of integrated *in vitro-in silico* assessments. Following *in vivo*

confirmation studies, oral bioavailability was further enhanced for a compound that exhibited a double-peak phenomenon. The results of the two approaches indicate that pharmacokinetic optimisation can be useful in development of anticancer agents to improve the treatment outcomes of cancer.

LIST OF FIGURES

Figure 1-1. Estimated age-standardised cancer incidence and mortality rates (per 100,000 in Europe, 2012). Adapted with permission of the publisher [1]. 30

Figure 1-2. Physiological diagram of the lymphatic system. (A) Distribution of lymphatic vessels. (B) Drainage of molecules into lymphatic vessels. Adapted with permission of the publisher [6]. 34

Figure 1-3. Schematic description of the process of lymphatic metastasis. (A) Lymphangiogenesis is promoted by cancer cells. (B) Cancer cells migrate through the lymphatic vessels to form distant metastasis. Adapted with permission of the publisher [31]. 36

Figure 1-4. Persistent lymphadenopathy in a 62-year-old woman with lymphoma. (A) Computerised tomography (CT) image shows lymphadenopathy in the mesentery of the right lower quadrant (arrow). (B) Posttreatment CT image obtained 2 years later shows persistent, unchanged lymphadenopathy (arrow). The disease was in remission when this image was obtained. Adapted with permission of the publisher [42]. 38

Figure 1-5. Schematic representation of the intestinal lymphatic transport of lipophilic drugs when co-administered orally with long chain triglycerides. Adapted with permission of the author [65]. 39

Figure 1-6. *Ex vivo* CM association model showing correlation of affinity to CM (%) with lymphatic absorption. Adapted with permission of the publisher [39]. 40

Figure 3-1. Schematic diagram of workflow for development, validation and application of bioanalytical method for BEX in rat plasma. 77

Figure 3-2. Representative chromatograms from rat plasma. A, Rat plasma spiked with 10 µg/mL of IS; B, rat plasma spiked with 10 ng/mL BEX and 10 µg/mL of IS (LLOQ sample); C, rat plasma spiked with 100 ng/mL BEX and 10 µg/mL of IS (calibration curve sample); D, rat plasma sample obtained in pharmacokinetic study 1 h following intravenous bolus administration of 2.5 mg/kg BEX. All observed at λ = 259 nm..... 83

Figure 3-3. Plasma concentration-time profiles of BEX following intravenous bolus administration at 2.5 mg/kg in rats (n = 3). 87

Figure 3-4. Representative chromatograms from human plasma. A, blank human plasma observed at λ = 259 nm; B, human plasma spiked with 400 ng/mL BEX observed at λ = 259 nm (MQC sample); C, blank human plasma observed at λ = 220 nm; D, human plasma spiked with 10 µg/mL of IS observed at λ = 220 nm. 89

Figure 3-5. Representative chromatograms from mouse plasma. A, blank mouse plasma; B, mouse plasma spiked with 400 ng/mL BEX and 10 µg/mL of IS (MQC sample). All observed at λ = 259 nm. 89

Figure 4-1. Schematic diagram of lipophilic prodrug approach for BEX and RA to target the intestinal lymphatic system. 93

Figure 4-2. Chemical structures of BEX and its prodrugs. 94

Figure 4-3. Association % of compounds with human chylomicron and artificial emulsion prepared from Intralipid®, representing potential of intestinal lymphatic system targetability. *, $p<0.05$; **, $p<0.01$ (mean ± SD, n = 5 or 6). Association of BTG with artificial emulsion could not be measured due to constraints in analytical methods. 96

Figure 4-4. Correlation graph between association (%) of compounds with human chylomicron and artificial emulsion prepared from Intralipid® (mean ± SD). Moderate correlation with coefficient of correlation (R^2) of 0.694 was found between the two test media..... 97

Figure 4-5. Half-lives of prodrugs in rat plasma and FaSSIF with added esterase activity (20 IU/mL), representing their converting rate to BEX (mean ± SD, n = 3). Half-lives of BOT and B27 in FaSSIF + esterase were not obtainable because no prodrug cleavage was observed. 98

Figure 4-6. Detailed bio-relevant assessment of stability of BET and BCY mimicking various *in vivo* situations (mean ± SD, n = 3). Bars in light orange represent stability of prodrugs when they are spiked in the form of drug-chylomicron (CM) complex as it would be the associated form that reaches intestinal lymphatics. Bars in dark blue were tested to evaluate if the presence of Intralipid® was inhibitory towards the enzymatic activity. Bars in light blue represent stability tested *ex vivo* with postprandial lymph where CM is present in abundant amount. **, $p<0.01$..... 99

Figure 4-7. *In vivo* pharmacokinetic profiles of BEX and their prodrugs. A, BEX (2.5 mg/kg) and its prodrugs (equivalent to 2.5 mg/kg of BEX) following i.v. administration in rats (mean ± SD, n = 3). B, BEX (10 mg/kg) and its prodrugs (equivalent to 10 mg/kg of BEX) following oral administration in rats (mean ± SD, n =4 to 6). For both A and B, administered compounds are mentioned as the title of each graph. Symbols represent the compound quantified and the medium of samples, as specified in the legends below each graph. Concentrations in plasma and lymph are presented in ng/mL. Concentrations in mesenteric lymph nodes (MLN) are presented in ng/g. 102

Figure 4-8. Maximum achievable concentration of BEX and its prodrugs in plasma, lymph and mesenteric lymph nodes (MLN) following oral administration in lipid-coadministration conditions in rats. Concentrations in plasma and lymph are presented in ng/mL. Concentrations in MLN are presented in ng/g. 103

Figure 4-9. Maximal observed concentration of BEX achieved in mesenteric lymph nodes (MLN) (ng/g) following oral administration of BEX, BET, BTG and BCY (mean ± SD). **, p<0.01; ***, p<0.001. 105

Figure 4-10. Application of the prodrug approach to RA (retinoic acid). A, chemical structures of RA and its prodrugs; B, association with human chylomicrons and artificial emulsion (mean ± SD, n = 6); C, half-life in rat plasma and fasted state simulated intestinal fluid (FaSSIF) with esterase (mean ± SD, n = 3); D, *in vivo* pharmacokinetic profiles in plasma and intestinal lymphatics following oral administration of RA (10 mg/kg) or RAC (at equivalent to 10 mg/kg RA) in rats (mean ± SD, n = 5 or 6); E, maximum concentration of RA achieved in mesenteric lymph nodes (MLN) (ng/g) following oral administration of RA and RAC (mean ± SD). *, p<0.05. 106

Figure 4-11. Assessment of cell growth inhibition and synergism of BEX and RA using MTT assay in DLBCL cell lines of DOHH2 and VAL. A, dose-response curves showing cell growth inhibition of BEX in presence of various concentration of RA; B, isobolograms indicating effective synergism between BEX and RA. Blue lines represent expected effectiveness when the two drugs are additive, where the *y*-intercept is GI_{50} of BEX and *x*-intercept is GI_{50} of RA. Orange dots represent GI_{50} observed with synergism (mean ± SD); C, synergism expressed by reduced GI_{50} of BEX in presence of RA. All MTT assay results shown from 4 trials of n = 6 (mean ± SD). *, p<0.05; **, p<0.01; ***, p<0.001. 108

Figure 4-12. Examples of enzymatic hydrolysis of activated esters. Adapted with permission of the publisher [174]..... 114

Figure 5-1. Schematic diagram of analysing lab-to-lab variability in Caco-2 assay and investigating potential impact of the variability in prediction of oral absorption. 121

Figure 5-2. Correlation between Caco-2 P_{app} values from experimental results (i.e. our laboratory) and human P_{eff} values from the literature (A) and human F_a values from literature (B). P_{eff} values are from reference [183] and F_a values are from references [177-180, 184-187]. 123

Figure 5-3. Root mean square error (RMSE) for simulated F_a values of application set compounds belonging to different BCS classes. 125

Figure 6-1. Schematic diagram of pharmacokinetic development of CDK9 inhibitors 130

Figure 6-2. Chemical structures of the candidate CDK9 inhibitors. 131

Figure 6-3. Plasma concentration-time profiles of HS3-77 following intravenous and oral administration in rats (n = 3, mean ± SD). 138

Figure 6-4. *Above*, mean plasma concentration-time profiles of DF030263 in fasted rats following intravenous (2 mg/kg) and oral (12 mg/kg) administration (n = 4, each group). *Below*, individual plasma concentration-time profiles of DF030263 in 4 fasted rats following oral administration (12 mg/kg). 140

Figure 6-5. Deconvolution results of plasma concentration-time profiles obtained from oral bioavailability evaluation of DF030263. Connected lines represent mean and dotted lines represent SD. A, cumulative input vs time; B, input rate vs time; C, individual graphs for cumulative input vs time; D, individual graphs for input rate vs time. 142

Figure 6-6. Solubility of DF030263 in FaSSGF, FaSSIF and FeSSIF at various pH (n = 3). FaSSGF, fasted state simulated gastric fluid; FaSSIF, fasted state simulated intestinal fluid; FeSSIF, fed state simulated intestinal fluid. 143

Figure 6-7. *In silico* simulation of intestinal absorption of DF030263 at each compartment of the gastrointestinal tract. *Asc Colon, ascending colon; Amt Abs, total amount absorbed in the gastrointestinal tract. 144

Figure 6-8. Mean plasma concentration-time profiles of DF030263 in rats following oral administration at fed state (12 mg/kg, n = 6) and colonic administration (12 mg/kg, n = 3). 145

Figure 6-9. Structure-property relationship of the candidate CDK9 inhibitors. 150

Appendix Figure 2-1. Establishment of a “user-defined permeability model” in GastroPlus™. 187

LIST OF TABLES

Table 2-1. Composition of the simulated fluids (mM) 56

Table 2-2. Dose and formulation input parameters of application set compounds for GastroPlus™ simulation 60

Table 2-3. Input parameters for *in silico* simulation of DF030263 compound..... 62

Table 2-4. Sample preparation conditions for compound studied in Chapter 3..... 64

Table 2-5. Sample preparation conditions for compounds studied in Chapter 4 64

Table 2-6. Sample preparation conditions for compound studied in Chapter 5..... 65

Table 2-7. Sample preparation conditions for compound studied in Chapter 6..... 65

Table 2-8. Analytical method conditions for compounds studied in Chapter 3 (Waters Alliance module used)..... 67

Table 2-9. Analytical method conditions for compounds studied in Chapter 4 (Waters Alliance module used)..... 67

Table 2-10. Analytical method conditions for compounds studied in Chapter 5 (Waters 600 pump and 717 autosampler system used) 67

Table 2-11. Analytical method conditions for compounds studied *in vitro* in Chapter 6 (Waters 600 pump and 717 autosampler system used) 68

Table 2-12. Analytical method conditions for compounds studied *in vivo* in Chapter 6 (Waters Alliance module used) 69

Table 3-1. Intra- and inter-day validation results of the analytical method of BEX in rat plasma using HPLC-UV (n = 6) 84

Table 3-2. Stability results of rat plasma samples of BEX under various storage conditions (n = 6) 86

Table 3-3. Pharmacokinetic parameters of BEX obtained following intravenous bolus administration of 2.5 mg/kg BEX in rats (n = 3) 87

Table 3-4. Intra-day validation results of the analytical method of BEX in human and mouse plasma using HPLC-UV (n = 6) 88

Table 4-1. Physicochemical properties of BEX and its prodrugs 95

Table 4-2. Plasma pharmacokinetic parameters of BEX following administration of BEX or its prodrugs by i.v. and p.o. administration (mean ± SD). 103

Table 5-1. P_{app} values of training set compounds from our laboratory and six different literature datasets 122

Table 5-2. Caco-2 P_{app} values and simulated F_a values of application set compounds 124

Table 5-3. Different experimental settings used in different laboratories for Caco-2 permeability assays 126

Table 6-1. Caco-2 permeability results of CDK9 inhibitor candidates (mean ± SD) 131

Table 6-2. Solubility of CDK9 inhibitor candidates in biorelevant media and DDW (mean ± SD) 132

Table 6-3. Liver microsomal metabolic stability of CDK9 inhibitor candidates in human and rat liver microsomes (mean ± SD) 133

Table 6-4. *In silico* simulation of pharmacokinetic properties of CDK9 inhibitor candidates 136

Table 6-5. Pharmacokinetic parameters of HS3-77 obtained from *in vivo* pharmacokinetic experiments in rats 138

Table 6-7. Plasma pharmacokinetic parameters obtained from *in vivo* pharmacokinetic experiments for fed state and colonic administration 145

1. INTRODUCTION

1.1. Principles of pharmacokinetics in discovery and development of anticancer agents

1.1.1. Cancer and metastasis

With 14 million new cases and 8.2 million deaths per year, cancer is the major cause of morbidity and mortality in the world [1]. During the past 20 years, deaths from different types of cancer have risen by 38.0% with cases such as lymphoma (46.7%), colorectal cancer (45.7%), prostate (64.5%), and urinary system cancers (90.6%) increasing dramatically [2]. In 2012, breast, prostate and lung cancers were the most common cancers found in Europe (Figure 1-1) [1]. One in two people born after 1960 is expected to be diagnosed with cancer during their lifetime in the UK [3].

A particular threat associated with cancer is metastasis, the invasion of cancer cells from the primary tumour to other distal regions and organs, which is the major cause of death for cancer patients in the majority of cancer types [4, 5]. Primary tumours may be controlled by surgery, radiation therapy and chemotherapy. However, most metastatic tumours are not manageable by surgery or radiation therapy alone and the treatment mainly relies on chemotherapy, which is usually not sufficiently targeted to the affected tissues [6]. As a consequence, 5-year survival rates for cancer patients with metastatic cancer is only 20% across all cancers and therefore development of metastasis results in poor prognosis [4]. For example, when breast cancer is confined to the breast tissue only, the 5-year survival rate of patients is 87.1% but when

metastasis to regional lymph nodes has occurred, it drops to 18.7%. The situation is even more devastating when it comes to lung cancer, where the 5-year survival rate is 41.5% in cases without lymph node involvement, which decreases dramatically to 4.3% upon progression to metastasis [7].

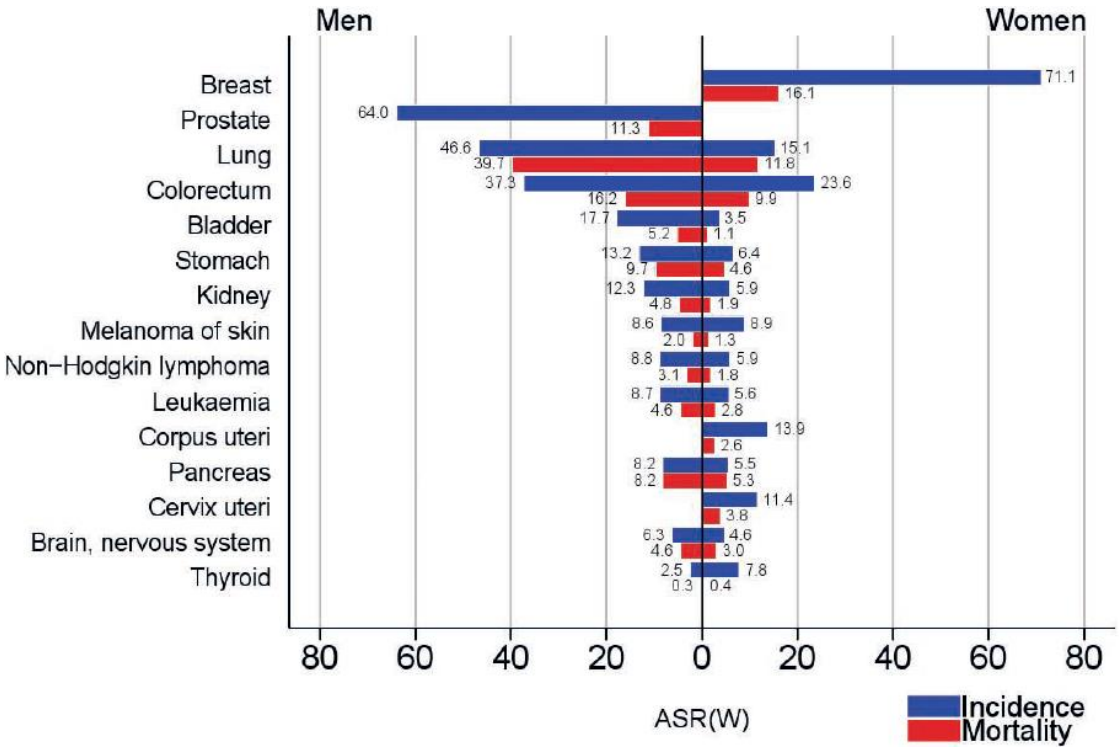


Figure 1-1. Estimated age-standardised cancer incidence and mortality rates (per 100,000 in Europe, 2012). Adapted with permission of the publisher [1].

1.1.2. Limitations of current chemotherapy

Pharmacological treatment of cancer is often limited by lack of efficacy and side effects. Insufficient efficacy is frequently due to unfavourable pharmacokinetics and biodistribution profiles including poor bioavailability, rapid clearance and limited distribution to the tumour tissues [8]. Side effects of anticancer agents are attributed to the fact that they target vital modulators and regulators controlling growth and maintenance of the cells. They not only disrupt cell-cycle, inhibit growth factors and

induce apoptosis of the cancer cells but also those of the normal cells [9]. Therefore, anticancer agents that specifically target the tissues affected by the tumour and cancer cells are needed for improvement of treatment of cancer.

Despite the fact that numerous targeted cancer chemotherapies have been discovered and developed, cancer patients still suffer from inevitable toxicity and sometimes debilitating side effects. Currently, most anticancer drugs are not molecularly targeted enough to specifically act on the cancer cells and their unexpected side effects continue to be discovered [10]. Targeted anticancer therapies which are supposed to only act on well-defined molecular target or biologic signalling streams still manifest their activity on normal cells due to unforeseen off-target mechanisms [11, 12].

1.1.3. Pharmacokinetic development and optimisation of anticancer agents

Pharmacokinetic development and optimisation of chemotherapy is highly desirable as anticancer agents are known to possess several distinctive features. Firstly, high inter-patient variability is found in terms of pharmacokinetics as inter-individual variation in the absorption, distribution, metabolism and excretion (ADME) can be substantial [13-15]. In addition, anticancer drugs frequently have very narrow therapeutic window which means the drug exposure can easily be toxic or sub-therapeutic without careful control [13, 14, 16]. Lastly, clinical responses including efficacy and toxicity are often delayed and unpredictable [13, 14].

Therefore, therapeutic dose monitoring (TDM) is often employed in chemotherapy to ensure that the drug exposure is within the therapeutic window [15, 17]. In addition, extensive efforts to elucidate the relationship between pharmacokinetics and pharmacodynamics (PK/PD) have been made through modelling and simulation, which contributes to selection of the appropriate dose [17, 18]. Other various pharmacokinetic approaches to optimise chemotherapy include modification of dosing schedules, alteration of ADME of the drugs and application of pharmacogenetics to individualise the treatment [14]. The dose schedule can be optimised by using pharmacokinetic parameters obtained from patients and different dosing regimens can be coordinated, which includes circadian administration [14, 19]. Pharmacogenetics have been studied to tailor individual dosing regimen by defining relationships between genetic polymorphism and the ADME of drugs. An example includes irinotecan where interindividual differences in metabolism and clearance can be observed due to polymorphism in organic anion-transporting polypeptide (OATP) transporter families [13]. Attempts to alter the ADME of drugs have been made by using biomodulators that affect metabolising enzymes and transporters that can assist in improving the efficacy or increasing the therapeutic index. For instance, leucovorin can be coadministered with fluorouracil or mercaptopurine for improving antitumour effects and alleviate side effects [14].

Improvement in pharmacokinetics of chemotherapy can also be achieved by targeted site-specific distribution of the drug to the affected compartment. By pharmacokinetic optimisation that enables delivery of the drug to specific tissues at substantially higher concentration compared to systemic circulation, unnecessary systemic exposure can be avoided. This would allow significantly lower doses than the maximum tolerable

dose to be administered for the required efficacy. Consequently, this would benefit the patients by mitigating unnecessary adverse effects [11, 12].

For treatment of chronic systemic cancers, such as leukaemia, oral administration would be the preferred route to achieve prolonged exposure of the body to the anticancer agents. However, a large portion of potential candidates for anticancer agents are dropped during development due to unfavourable pharmacokinetics such as low bioavailability and insufficient systemic exposure [20, 21]. It should also be noted that low bioavailability is usually also associated with higher inter-individual variability in the exposure [22]. Therefore, pharmacokinetic optimisation is essential in development of orally bioavailable anticancer agents.

It is, therefore, important to consider the principles of pharmacokinetics for optimisation of treatment of cancer. The pharmaceutical science area of pharmacokinetics has long been playing a critical role in drug discovery and development [23] and it is of particular importance in cancer treatment. In this PhD project, two main approaches have been explored: site-specific targeting and increase in systemic exposure. Targeted delivery to the intestinal lymphatic system was studied using lipophilic prodrug approach, for which the background is discussed in Section 1.2. The research for pharmacokinetic optimisation in development of orally bioavailable anticancer agents is further explained in Section 1.3.

1.2. Maximising exposure of intestinal lymphatic system to drugs

1.2.1. Cancer and the lymphatic system

The lymphatic system is a one-way flow system which consists of vessels starting from blind-ended lymphatic capillaries and ending with the thoracic duct, which drains the lymph into the junction between the left subclavian and jugular veins (Figure 1-2) [24]. The lymph fluid originates from lymph capillaries and flows through the lymphatic collecting vessels. The main functions of the lymphatic system are maintaining homeostasis of body fluids, regulation of the immune system, and absorption of dietary lipids in the case of the intestinal lymphatic system.

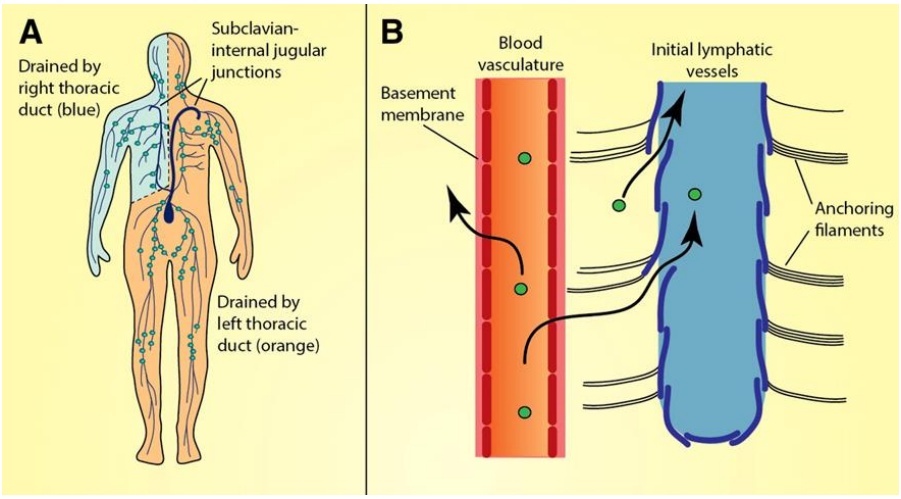


Figure 1-2. Physiological diagram of the lymphatic system. (A) Distribution of lymphatic vessels. (B) Drainage of molecules into lymphatic vessels. Adapted with permission of the publisher [6].

The lymphatic system plays an important role in the pathophysiology of cancer as it can be both a site for the primary cancer and the major route of metastasis. Lymphatic tissues can host a group of cancerous cells called lymphomas. Lymphomas are types of blood cancer that accounts for approximately half of all haematological neoplasms

[25]. Lymphomas are associated with lymphocytes of the lymph nodes and lymphoid tissues and include a variety of heterogeneous malignancies that arise from lymphocytes [26]. The main types of lymphomas are non-Hodgkin's lymphoma (NHL) and Hodgkin's lymphoma. NHL accounts for 4% of all new cases of cancer, and is the sixth most prevailing cancer in the UK as of 2011 [3]. It is challenging for systemic chemotherapy to specifically target the tumour in the lymphatics as only limited amount of drug can be distributed from the systemic circulation into the lymphatic system [27].

The lymphatic system is one of the most important pathophysiological compartments in cancer metastasis as it provides primary transportation route for the spreading of many solid tumours (Figure 1-3) [28]. The incomplete nature of the blind-ended lymphatic capillaries (lacteals) presents an easily accessible path that promotes invasion and metastatic dissemination of cancer cells [29, 30]. As mentioned above, lymph node involvement can be a signal of metastatic progression and thus sentinel lymph node biopsy is often utilised in quantification of metastasis and staging of cancer [6]. However, current chemotherapies available for treatment of metastasis are limited by their poor disposition to the actual site of metastasis [4].

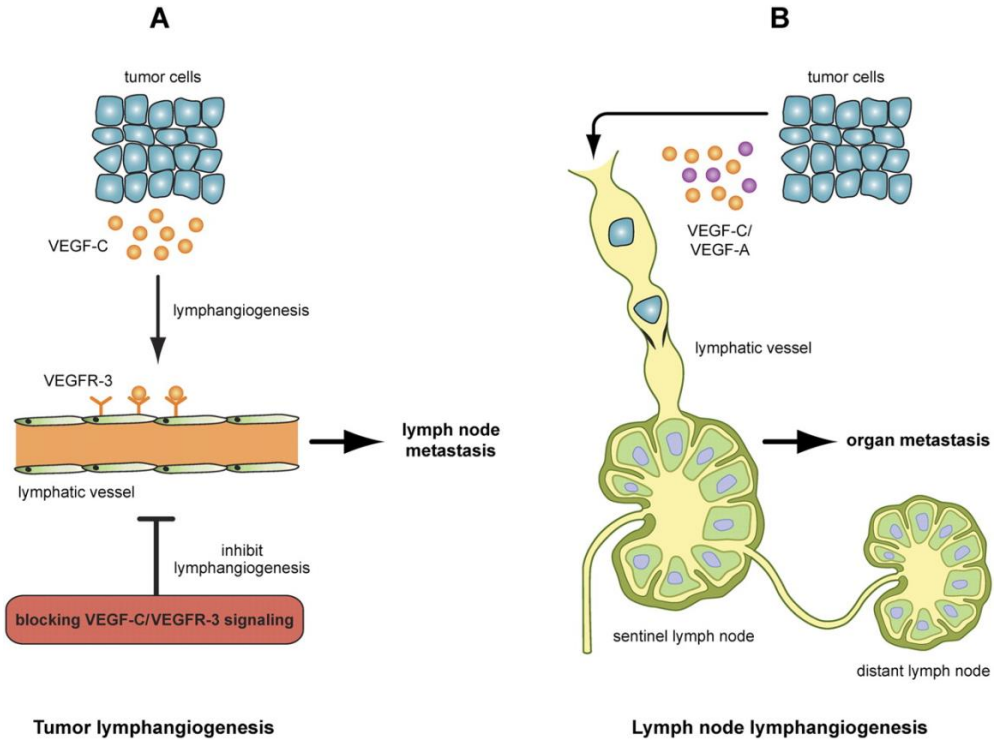


Figure 1-3. Schematic description of the process of lymphatic metastasis. (A) Lymphangiogenesis is promoted by cancer cells. (B) Cancer cells migrate through the lymphatic vessels to form distant metastasis. Adapted with permission of the publisher [31].

Lymphadenectomy, surgical removal of cancer-affected sentinel lymph nodes, is one of the solutions for treatment of metastasis but is often accompanied by reoccurrence [27, 32]. Therefore, non-surgical delivery of anticancer agents to the lymphatic system for treatment of metastasis and lymphomas is an important mode in many cases.

Delivery of anticancer agents specifically to the lymphatic system has been studied using different routes of administration. Interstitial administration of drugs can benefit from the physiological lymphatic uptake that drains interstitial fluid and other molecules to reach the lymphatic system [33]. It has been found that intradermal injection is superior to intramuscular or subcutaneous injection for this purpose [34] and that size of the particle of the drug or formulation is the most determinant factor

for lymphatic targeting [6]. Lymphatic system targeting following intravenous administration has also been reported for formulations such as liposomes and nanoparticles [35, 36]. However, this route requires the particle to penetrate the blood vessel wall, distribute into the interstitial space and then follow the lymphatic uptake process similar to interstitially administered drugs [33]. Mucosal delivery to target the lymphatics has also been studied, mostly for vaccines, through nasal, pulmonary and genital mucosa [37, 38]. It provides ease of administration and therefore improved compliance but still faces problems of safety, stability, and variability [37]. Drug delivery to the lymphatics can be also achieved by the oral route and efficient targeting can be achieved by taking advantage of the physiological intestinal lymphatic transport of lipids and lipophilic molecules [39]. It has been studied previously focussing mostly on potential for increased bioavailability of drugs by circumventing the hepatic first-pass effect [40, 41]. This oral delivery route was the main focus in this PhD project and therefore more discussion is made on this below.

1.2.2. Lymphoma and lymphadenopathy in the abdominal lymphatics

Lymphoma is the most common cause of mesenteric or retroperitoneal lymphadenopathy [42-44]. In most cases this lymphadenopathy is associated with NHL [45-48]. In as many as 30-50% of NHL patients, especially those with diffuse large B-cell or follicular B-cell lymphoma, disease significantly affects abdominal lymph nodes [47, 49-55]. Figure 1-4 shows a representative computerised tomography (CT) scan of one such patient with mesenteric lymphadenopathy which is persistent even in remission stage [42].

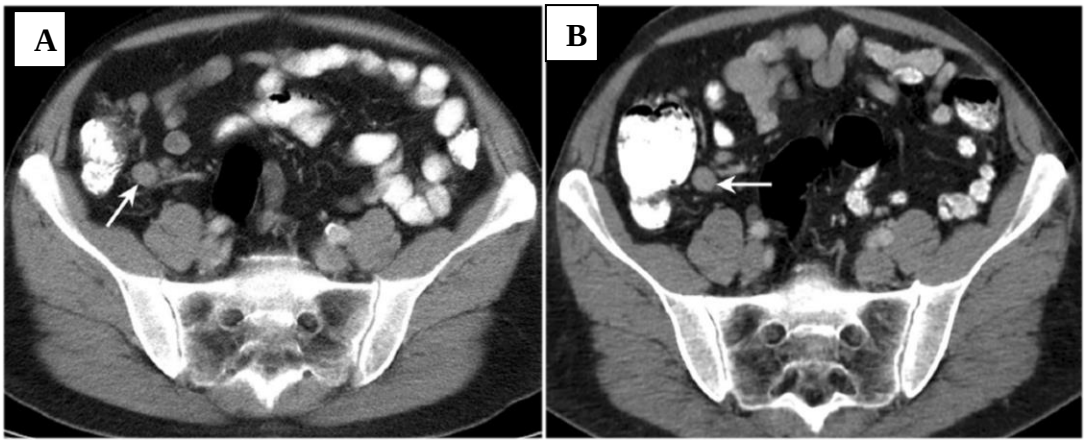


Figure 1-4. Persistent lymphadenopathy in a 62-year-old woman with lymphoma. (A) Computerised tomography (CT) image shows lymphadenopathy in the mesentery of the right lower quadrant (arrow). (B) Posttreatment CT image obtained 2 years later shows persistent, unchanged lymphadenopathy (arrow). The disease was in remission when this image was obtained. Adapted with permission of the publisher [42].

There have been recent important advances in targeted and selective treatments of NHL, including monoclonal antibodies, Bruton's tyrosine kinases inhibitors, phosphoinositide-3-kinase inhibitors and inhibitors of other molecular targets [56]. However, chemotherapy (usually in combination with immune therapy) is still the first-line treatment of NHL patients in many cases [57]. Only a very limited proportion of a drug can usually be distributed from the systemic circulation into the lymphatic system [27, 58]. Consequently, in order to achieve sufficient concentrations of cytotoxic drugs in the affected lymph nodes, the required levels in the systemic circulation would be very high and associated with significant side effects. Therefore, there is an unmet need for targeted increased delivery of anticancer agents to the mesenteric and retroperitoneal lymph nodes for treatment of NHL patients with substantial abdominal lymph nodes involvement in the disease.

1.2.3. Targeting the intestinal lymphatic system

Although most drugs absorbed from the gastrointestinal (GI) system are passed to the portal vein, lipophilic compounds also gain access to the systemic circulation through the intestinal lymphatics (Figure 1-5) [59, 60]. This distribution to the lymphatic system is determined mainly by the association of drugs with large lipoproteins, *i.e.* chylomicrons (CM) in the enterocytes. This is because drug molecules need to be associated with CM in order to utilise them as a carrier to the lymphatic system. In fact, a correlation between CM association and lymphatic absorption is well established (Figure 1-6) [39, 40, 61-64]. Figure 1-6 does not have a large number of drugs studied, but additional correlation have been reported in following studies [39, 40, 61-64].

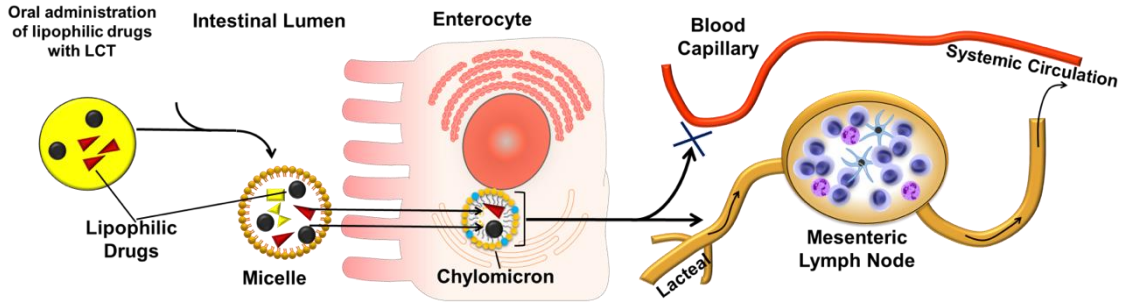


Figure 1-5. Schematic representation of the intestinal lymphatic transport of lipophilic drugs when co-administered orally with long chain triglycerides. Adapted with permission of the author [65].

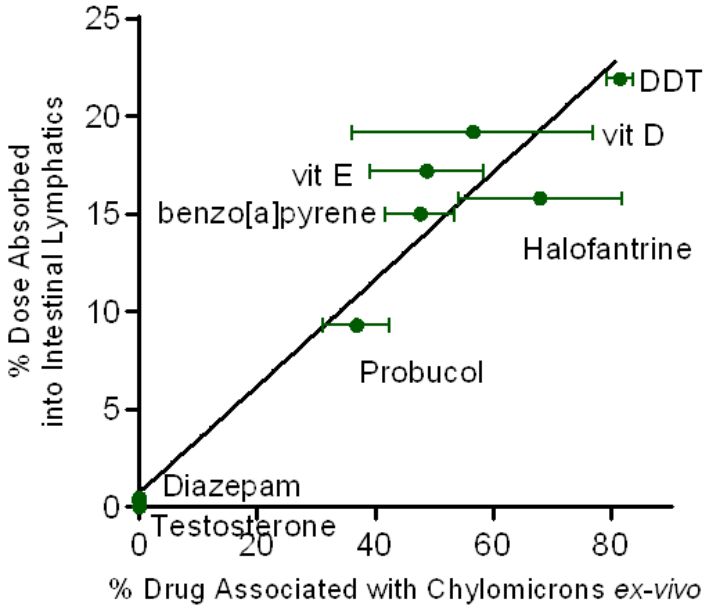


Figure 1-6. *Ex vivo* CM association model showing correlation of affinity to CM (%) with lymphatic absorption. Adapted with permission of the publisher [39].

As mentioned above, intestinal lymphatic transport has been previously studied mostly to increase the oral bioavailability of drugs. In fact, there have been some very successful attempts with enhanced systemic exposure of certain drugs through lymphatic absorption [41]. One of the most successful examples include testosterone, which on its own has <1% oral bioavailability but upon targeting lymphatic transport by prodrug approach, systemic exposure could be increased by 90-fold [66]. However, an issue that has been practically overlooked in the past is that the lymphatic system has functional importance, and drugs that are transported *via* this route reach very high concentrations in lymph fluid and lymph nodes, and therefore can exert their activity within the lymphatic system itself. In a previously reported study, a concentration gradient as high as 500-fold was found between the lymph and plasma for a model compound [40].

The concept of the lymphatic system as an effective pharmacological compartment has enormous potential for improving the treatment outcomes of a number of diseases with pathophysiology that is associated in one way or another with the lymphatics. Examples include autoimmune diseases, human immunodeficiency virus (HIV) infection, metastatic processes, and lymphatic system-associated cancers such as NHL with mesenteric or retroperitoneal lymph node involvement. Targeting drugs to the lymphatic system for treatment of these conditions has the potential to maximise their therapeutic benefits by creating high concentrations at abdominal lymph nodes before the drug arrives to the systemic circulation. At the same time, the systemic chemotherapy dose can be decreased, resulting in reduced side effects associated with systemic exposure.

Bexarotene (BEX) is an orally bioavailable synthetic rexinoid that selectively binds to retinoid X receptors [107]. It was the first selective retinoid that entered clinical trials [108] and it is currently approved for treatment of cutaneous T-cell lymphoma (CTCL) in patients whose disease is refractory to at least one systemic chemotherapy [109]. Following the approval, the efficacy and safety of BEX was shown in refractory early-stage CTCL [110] and other related conditions such as panniculitis-like T-cell lymphoma [111]. Therefore, targeting bexarotene to the intestinal lymphatics by a lipophilic prodrug approach to take advantage of the intestinal lymphatic transport could be beneficial for lymphoma patients with the lymphadenopathy in the mesentery (as described in Section 1.2.2.).

1.3. Pharmacokinetic optimisation of cyclin-dependent kinase inhibitors

1.3.1. Pharmacokinetic optimisation in discovery and development of orally bioavailable anticancer agents

Drug discovery and development processes are time-consuming and expensive [21, 67, 68]. This is primarily associated with the high attrition rates of drug candidates, mostly due to undesirable pharmacokinetic and safety profiles [23, 69, 70]. *In silico* prediction of drug-likeness of compounds has made substantial improvements but challenges still remain and experimental testing of compounds is necessary to assist decision making processes [71, 72]. Therefore, *in vitro* biopharmaceutical screening of drug candidates is implemented from early stages of drug discovery and development process [20, 73, 74]. Traditional *in vitro* biopharmaceutical screening integrated with the modern *in silico* simulation tools can narrow down the list of potential drug candidates and promote development of most promising compounds [68, 74]. This can also provide guidance to medicinal chemists for further optimisation of the structural design of the molecules [23, 70].

Conventional chemotherapeutic agents have been mainly relying on intravenous route of administration [75, 76]. However, due to recent advancements in drug discovery and development process, increasing number of orally bioavailable anticancer agents have been developed and are available on the market [75, 77]. Oral administration offers multiple advantages. Oral dosing allows self-administration by the patients and avoids the inconvenience of intravenous injections which needs hospitalisation [78,

79]. Therefore, it improves patient compliance and reduces costs of therapy. It also prevents risk of infection that might be caused as a complication of injectable routes of administration. Most importantly, it makes treatment of chronic diseases more practical [75, 79].

However, many anticancer agents possess unfavourable properties that make sufficient systemic exposure following oral administration challenging. These properties are mainly physicochemical characteristics that result in low solubility, poor permeability, high efflux and rapid pre-systemic metabolism [76]. Additionally, cancer patients often have had surgeries or radiation therapies and usually have other concomitant medications, which increases the variability in pharmacokinetics [13]. Therefore, biopharmaceutical optimisation of anticancer agents is needed during discovery and development of anticancer agents intended for oral administration.

1.3.2. Development of cyclin-dependent kinase inhibitors

Cyclin-dependent kinases (CDKs) are essential in cell growth as they control progression of cell cycles and regulate transcription [80]. CDK inhibitors have been discovered and developed on this premise to seek inhibition of unsuppressed cancer cell proliferation. The potential of CDK inhibitors in clinic was shown with flavopiridol in patients with chronic lymphocytic leukaemia (CLL) [81]. Flavopiridol exerts its inhibitory effects on several CDKs but the key mechanism responsible for the anticancer efficacy in CLL correlates mostly with CDK9 inhibition [82, 83].

Among the CDK family, CDK9 is particularly related to regulation of RNA transcription [80]. High expression of CDK9 and cyclin T1, corresponding cyclin partner of CDK9, is observed in CLL, indicating their key roles in pathologic mechanism of the disease [81]. CDK inhibitors that inhibit not only CDK9 but also other CDKs have shown narrow therapeutic window and unfavourable adverse effect profiles [83]. Therefore, anticancer agents that specifically target CDK9 are desired for improved efficacy and reduced toxicity.

Recently, potent and selective CDK9 inhibitors have been synthesised and proved to trigger apoptosis in primary cells from patients with CLL [82, 84, 85]. Identification of bioavailable CDK9 inhibitors and research aimed to enhance their bioavailability will lead to development of efficient treatment for CLL.

1.4. Project hypotheses and aims

Biopharmaceutics and pharmacokinetics are often considered as an observational aid tool in drug discovery which means that the data is more used to describe the characteristics of compounds, rather than being used for optimisation in drug discovery. However, the main hypothesis of this research project was that optimisation of treatment based on pharmacokinetic principles is on its own a powerful approach in improvement of treatment outcomes. This work therefore focused on optimisation of treatment of cancer based on principles of pharmacokinetics using two main approaches 1) lipophilic prodrug approach to specifically target the intestinal lymphatic system following oral administration and 2) identification of orally

bioavailable candidate anticancer agents and biopharmaceutical development to increase the bioavailability for sufficient systemic exposure to the drug.

1.4.1. Intestinal lymphatic system targeting of anticancer agents by lipophilic prodrug approach

As explained in Section 1.2.3., intestinal lymphatic uptake of drug molecules following oral administration relies on the association of the molecule with CM in the enterocytes. Therefore, by designing prodrugs of anticancer agents so that they possess the necessary physicochemical properties for enhanced association with CM, we will be able to target anticancer agents to the intestinal lymphatic system. Specific objectives for this approach include the following:

- Design and synthesis of prodrugs to enhance association with CM by alteration of physicochemical properties of log P, log $D_{7.4}$, polar surface area, hydrogen donor, hydrogen acceptor, etc.
- Evaluation of chemical and enzymatic conversion of the prodrugs to their corresponding active entities
- Evaluation of intestinal lymphatic system targeting potential using *in vitro* association with artificial emulsion and *ex vivo* association with natural chylomicrons
- *In vivo* evaluation of the prodrugs to assess plasma pharmacokinetic profiles and biodistribution into the intestinal lymphatic system, including mesenteric lymph nodes and lymph fluids

- *In vitro* efficacy evaluation to elucidate pharmacodynamic effects of cell growth inhibition that can be potentially expected at concentrations observed within the lymphatic system *in vivo*.

Chapter 3 will describe method development and validation for determination of bexarotene (BEX) in biological matrices. Chapter 4 will discuss the prodrug approach for intestinal lymphatic targeting.

1.4.2. Pharmacokinetic development of CDK9 inhibitors

As explained in Section 1.3.1., development of orally bioavailable anticancer agents is important as oral delivery of drugs is the most preferred route of administration. Therefore, it is crucial to identify orally bioavailable compounds during drug discovery and development processes. High oral bioavailability is desired to ensure drug exposure is at sufficient levels for the therapeutic effects with acceptable dosage, which will also contribute in mitigating unnecessary side-effects in the GI tract [86]. In addition, higher oral bioavailability will result in lower inter-subject variability which is critical for anticancer agents that are likely to have narrow therapeutic windows [22, 87, 88]. Specific objectives for this approach include the followings:

- *In vitro* biopharmaceutic evaluation of candidate CDK9 inhibitors in terms of solubility in water and biorelevant media, permeability using Caco-2 cells and metabolic stability using liver microsomes
- Integration of *in vitro* biopharmaceutic evaluation data into *in silico* simulation by GastroPlus^{TM} to predict pharmacokinetic properties such as oral bioavailability and identify the most promising candidates

- *In vivo* confirmation of oral bioavailability of selected lead candidates in rats by plasma pharmacokinetic studies
- Biopharmaceutical development of promising candidates to enhance further the oral bioavailability including *in silico-in vitro-in vivo* approaches

Chapter 5 will describe Caco-2 permeability studies and the lab-to-lab variability in the assays. Chapter 6 will discuss pharmacokinetic optimisation of CDK9 inhibitor candidates.

2. MATERIALS AND METHODS

2.1. Materials

Bexarotene (BEX, CAS: 153559-49-0) was purchased from LC Laboratories (Woburn, MA, USA). Δ^9-Tetrahydrocannabinol (CAS: 1972-08-3) was from THC Pharm GmbH (Frankfurt, Germany)). CDK9 inhibitor candidate compounds DF030263, FS90-263, HMKII-90, HMKII-101, HMKIII-17, HMKIII-41, HS-47, HS3-72, HS3-77, S3-68 and S3-138 were synthesised by researcher in the Fischer Group at School of Pharmacy, University of Nottingham (Nottingham, UK). Rat and mouse plasma were purchased from Sera Laboratories (West Sussex, UK) and human plasma from TCS Biosciences (Buckingham, UK). Dulbecco's modified eagle medium [DMEM, supplemented with GlutaMAX™, 4.5 g/L D-glucose and 25 mM 4-2-hydroxyethyl-1-piperazineethanesulfonic acid (HEPES)] was purchased from Gibco (Paisley, UK). Caco-2 cells of passage number 47 were purchased from Cell Culture Collections, Public Health England (Salisbury, UK). Diffuse large B-cell lymphoma (DLBCL) cell lines of DOHH2 and Vallois (VAL) were obtained from the Gene Regulation and RNA Biology group in University of Nottingham. Hank's balanced salt solution (HBSS), HEPES buffer, fetal bovine serum (FBS), antipyrine, cetirizine, chlorpromazine, cimetidine, desipramine, dexamethasone, diclofenac, furosemide, hydrochlorothiazide, ketoprofen, metoprolol, naproxen, piroxicam, propranolol, ranitidine, sildenafil, terbutaline, verapamil, Intralipid®, sodium taurocholate (NaTc), NaCl, NaF, retinoic acid (RA, *all-trans*), lecithin and porcine liver esterase were obtained from Sigma (Gillingham, UK). Thiazolyl blue tetrazolium bromide (MTT), Corning 24-well Transwell®, Costar Spin-X Centrifuge Tubes, sesame oil, polyethylene glycol 400

(PEG400) and all solvents (HPLC grade or higher) were purchased from Fisher Scientific (Loughborough, UK). All solvents were of HPLC grade or higher.

2.2. Chemical synthesis of prodrugs

2.2.1. General synthetic scheme for esterification

Ester prodrugs of BEX and RA were synthesised by adding 2.87 mmol of the desired alcohol to 0.287 mmol of BEX or RA. 1-Ethyl-3-(3-dimethylaminopropyl)carbodiimide (0.431 mmol) and 4-dimethylaminopyridine (0.057 mmol) were added as catalysts, and dichloromethane (15 mL) was used as the solvent. The mixture was stirred using a magnetic stirrer overnight at room temperature. Purification was performed by flash chromatography using a 200-400 mesh silica gel-packed glass column and hexane:ethyl acetate, 50:2 (v/v) as the mobile phase. Specific details for compounds that had different synthetic schemes are described in Appendix 1. The chemical synthetic schemes used in this study were not from previously reported studies.

2.2.2. Characterisation of synthesised prodrugs

^{1}H NMR and ^{13}C NMR spectra were obtained using Bruker 400 Ultrashield Spectrometer at 400 and 100 MHz, respectively. Bruker TOPSPIN 2.1 software was used to analyse the spectra. Chemical shifts were reported as parts per million (ppm) relative to the tetramethylsilane (internal standard) to the nearest 0.01 ppm and coupling constants (*J*) to the nearest 0.1 Hz. High resolution mass spectrometry (HR-

MS) was performed using Bruker MicroTOF operated with electrospray ionisation in positive mode.

2.3. Chylomicron and artificial lipid particle association assay

2.3.1. Preparation of artificial lipid particle emulsion

To prepare the artificial lipid particle emulsion, Intralipid® 20% (Sigma, Gillingham, UK) was diluted using phosphate buffered saline (PBS) to yield 100 mg/dL of triglyceride (TG) concentration [61, 64]. A TG enzymatic kit (Sigma Aldrich, Dorset, UK) was used to monitor the TG concentration by following manufacturer's instructions.

2.3.2. Preparation of human plasma-derived chylomicron emulsion

The protocol for preparation of human plasma-derived CM emulsion was approved by the Faculty of Medicine and Health Sciences Research Ethics Committee, Queens Medical Centre, Nottingham University Hospitals (BT12102015 CBS SoP). Healthy volunteers (five) of 19-40 years old and with body mass index of 18.5-25 were enrolled in the study after providing informed consent. The participants were excluded if any medication was used within one week prior to enrolment. On the morning of the study, participants received a high-fat meal (equivalent to a full English breakfast). Between 3-4 h following breakfast, 30 mL of blood was collected using heparinised tubes

(Vacutainer® Blood Collection Tubes) and centrifuged (800 *g*, 10 min, 15 °C) to obtain plasma.

CM separation was performed as previously reported with minor modifications [39, 64]. Briefly, KBr (0.57 g) was mixed with 4 mL of plasma to yield density of 1.1 g/mL. PBS with densities of 1.006, 1.019, and 1.063 g/mL were prepared by adding appropriate amounts of KBr, monitoring the density by measuring the weight of the solution. These PBS of different densities were layered on top of the plasma to build density gradient layers in polyallomer ultracentrifuge tubes. The samples were then centrifuged at 268,350 *g* for 35 min at 15 °C using an ultracentrifuge (SORVALL® TH-641 Rotor, Thermo Fisher Scientific, UK). Following ultracentrifugation, approximately 1 mL of the upper layer containing CM was collected. TG concentration of CM emulsion was assessed using the TG enzymatic kit (Sigma Aldrich, Dorset, UK). TG concentration of the emulsion was adjusted to 100 mg/dL by diluting with PBS of 1.006 g/mL density. The CM emulsion was stored at 4 °C until the association assay (<24 h).

2.3.3. Association assay procedure

The association of the compounds with artificial lipid particle emulsion and human CM was assessed using previously reported methodology with minor modifications [39]. Briefly, 1 mL of artificial lipid particle or CM emulsions (TG concentration 100 mg/dL) was used for the association assay. The emulsion was spiked with stock solutions of tested compounds (BEX, RA and their prodrugs in acetonitrile) to give a final concentration of 1.755 μM. The reaction mixtures were incubated at 37 °C for 1

h with magnetic stirring at 300 rpm. Following the incubation, density gradient ultracentrifugation was applied as described in Section 2.3.2. to isolate the artificial lipid particles or CM associated with the tested compounds from the rest of the experimental medium. The amount of the tested compound residing in this isolated layer compared to the spiked amount was used to calculate the association %. All experiments were conducted in quintuplicate or above.

2.4. Prodrug conversion assay

The prodrugs were tested for their stability and conversion into their corresponding active drug using fasted state simulated intestinal fluid (FaSSIF), fed state simulated intestinal fluid (FeSSIF), FaSSIF with added esterase enzyme activity (20 IU/mL), rat plasma, and postprandial rat lymph [89]. The FaSSIF and FeSSIF were prepared as described in Section 2.8.1. The medium was pre-heated to 37 °C prior to the assay for 5 min. The experiment was initiated by spiking stock solutions of prodrugs to give a final concentration of 10 μM of the prodrugs in the medium. When the stability of the artificial emulsion-associated prodrugs was tested in plasma, the association of compounds with artificial emulsion was performed prior to stability experiments (according to Section 2.3.3.) and the concentrations of the compounds in the associated emulsion were measured. The emulsion was then spiked to give a concentration of 10 μM of the prodrugs in plasma. The reaction mixtures were incubated at 37 °C and shaken at 200 rpm on a temperature-controlled orbital shaker (Thermo Scientific MaxQ4000, Waltham, MA, USA) for 4 h. Samples were withdrawn at pre-determined time points, and the reaction was terminated by addition of acetonitrile. The samples were then subjected to sample preparation as described in Section 2.11. The natural

log percentage of the prodrug concentration was plotted against incubation time, and the slope (k) was obtained from the plot. Half-life ($t_{1/2}$) was calculated by the following equation: $t_{1/2} = -0.693/k$. All experiments were conducted in triplicate.

2.5. Triglyceride solubility measurement

Compounds of BEX, BGA2 and RA were dissolved in fresh aliquots of sesame oil in excessive amounts in glass vials (in triplicate) and stirred using a magnetic stirring bar at 37 °C for 72 h. The mixture was then filtered by centrifugation in a Costar Spin-X Centrifuge Tube (Fisher Scientific, Loughborough, UK) at 2400 *g* for 5 min. The filtrates were analysed for concentration of the tested compounds by means of HPLC.

2.6. Cell growth inhibition assay

Cell growth inhibition was assessed by MTT assay with a minor modification from previously reported methods using DOHH2 and VAL cell lines [90-92]. Cells were seeded at a density of 2000 cells/well and allowed to adapt overnight. Test compounds of BEX and RA were serial-diluted with dimethyl sulfoxide (DMSO) and spiked on the next day to yield 0.1% (v/v) DMSO. Control wells were treated with 0.1% DMSO vehicle alone. At the time of drug addition, separately prepared wells were processed for T_{zero} readings as previously described [92]. The treated cells were incubated further for 72 h at 37 °C and processed for cell growth assessments.

2.7. Permeability assay

2.7.1. Cell culture

Caco-2 cells of passage numbers 51-54 were used in the study. Caco-2 cells were passaged in 75 cm^2 cell culture flasks (Corning Inc, Corning, NY) at 1×10^4 cells/cm^2 at least twice before seeding in Transwell® plates (Cat 351181 Corning Inc, Corning, NY). DMEM cell culture medium supplemented with 10% FBS and 1% penicillin-streptomycin was used and the cells were maintained at 37 °C, 95% relative humidity and 5% CO_2. Cells were seeded at a density of 3.75×10^4 cells/cm^2 in the Transwell® plates. Medium was replaced on the next day following seeding and every other day thereafter for 21 days before permeability assay. Transepithelial electrical resistance (TEER) values were measured using an EVOM2 instrument (World Precision Instruments, Sarasota, FL). Caco-2 monolayers with TEER values between 280-500 Ωcm^2 were used in the permeability assay.

2.7.2. Caco-2 permeability assay

On the day of the experiment, the Caco-2 monolayers were washed twice with transport buffer (HBSS buffer supplemented with 10 mM HEPES and pH adjusted to 7.4 using HCl or NaOH). The cells were then allowed to equilibrate for 30 min at 37 °C with the transport buffer. Donor solutions were prepared to yield 50 or 200 μM of the test compound. For assessment of apical-to-basolateral permeability, the donor solution (300 μL) was added to the apical side of the monolayer and samples (350 μL) were collected from the basolateral side. Basolateral-to-apical permeability was assessed by adding the donor solution (1 mL) to the basolateral side of the membrane

and collecting samples (120 µL) from the apical side. The samples were withdrawn at 30, 60, 90 and 120 min and fresh transport buffer of equal volume to the samples was replaced each time. At the end of the assay, TEER was measured again to assess any unknown pharmacological or toxicological effect of compounds on the monolayers. All experiments were performed in triplicates.

The apparent permeability coefficient (P_{app}) was obtained using the following equation:

$$P_{app} = (dQ/dt) \cdot (1/(AC_0))$$

where *dQ/dt* is the steady-state flux (µmol/s) from 30 to 120 min, *A* is the effective filter area of each well in the Transwell® (cm^2) and C_0 is concentration of the donor solution (µM) [93, 94]. Efflux ratio was calculated by the ratio of P_{app} from basolateral-to-apical permeability to P_{app} from apical-to-basolateral permeability.

2.8. Solubility assay

2.8.1. Preparation of biorelevant media

Three different types of fluids simulating the GI environment were prepared according to previously reported preparation methods [95-97]: FaSSGF, FaSSIF and FeSSIF. The composition of these three simulated fluids were as described in Table 2-1. Prior to the assay, the pH of FaSSGF was adjusted to 1.6 and 3.0 using HCl and the pH of FaSSIF and FeSSIF was adjusted to be between 5.0-7.8 with interval of 0.2 using HCl

or NaOH. All fluids were prepared on the day before the assay and stored at 4 °C until use.

Table 2-1. Composition of the simulated fluids (mM)

	FaSSGF	FaSSIF	FeSSIF
NaTc	0.08	3	15
Lecithin	0.02	0.75	3.75
NaCl	34.2	105.9	203.3
NaOH	-	8.7	102
NaH_2PO_4	-	28.65	-
Acetic acid	-	-	144

FaSSGF, fasted state simulated gastric fluid; FaSSIF, fasted state simulated intestinal fluid; FeSSIF, fed state simulated intestinal fluid.

2.8.2. Solubility assay procedure

On the day of assay, 198 µL of test medium (FaSSGF, FaSSIF, FeSSIF and water) was aliquoted into centrifugal tubes (Costar Spin-X Centrifuge Tube, Fisher Scientific, Leicestershire, UK). A volume of 2 µL of 20 mM stock solution in DMSO was then spiked into each tube to yield 200 µM of test concentration. The tubes were incubated at 37 °C shaking at 250 rpm for 2 h using a shaking incubator (Thermo Scientific MaxQ4000, Thermo Scientific, OH, USA). After the incubation, the samples were immediately centrifuged for 5 min at 2400 *g* (Heraeus Fresco 17 Centrifuge, Thermo Electron, MA, USA). The filtrate was collected and subjected to analysis as described below (Section 2.11.). The assay was performed in triplicate.

After obtaining the aqueous solubility results, the pH of the solubility test medium was measured for each compound. The compounds were spiked in (deionised-distilled water) DDW at 200 µM to yield a saturated condition. The mixture was stirred at 250 rpm for 2 h at 37 °C and the pH was measured using a pH meter (T50 Graphix, Mettler Toledo Inc., Leicester, UK).

2.9. Liver microsomal stability assay

2.9.1. Stability assay procedure

Human or rat liver microsomes were used for *in vitro* liver microsomal stability assay and the assay was conducted as previously reported with minor modifications [98]. Briefly, the reaction mixture was composed of the following: 84.7 mM of potassium phosphate buffer (pH 7.4), 10 mM of $MgCl_2$, 0.5 mg protein/mL of microsomes and 1.0 µM of test compounds of CDK9 inhibitor candidates. The reaction was initiated with addition of 1 mM NADPH. Samples (100 µL) were withdrawn from the reaction mixture at 0, 10, 20 and 30 min and the reaction was terminated by acetonitrile (300 µL). The experiment was performed in triplicate.

2.9.2. Calculations of stability results

The concentration-time profiles from microsomal stability results were plotted in semi-log plot. Half-life ($t_{1/2}$) was calculated from the plot using the following equation:

$$t_{1/2} = -\frac{0.693}{k}$$

where *k* represents the slope from the plot of natural log percentage of test compound remaining versus time. The $t_{1/2}$ was then converted into *in vitro* intrinsic clearance (CL_{int}, mL/min/kg) by the following equation [99, 100]:

$$CL_{int} = \frac{0.693}{t_{1/2}} \cdot \frac{mL\ incubation}{mg\ microsomes} \cdot \frac{mg\ microsomes}{g\ liver} \cdot \frac{g\ liver}{kg\ body\ weight}$$

where the *mg microsomes/g liver* and *g liver/kg body weight* values were 48.8 and 25.7 for humans and 44.8 and 40.0 for rats, respectively [99, 101]. The hepatic clearance (CL_h) was predicted using the CL_{int} values in each species by the commonly employed models of well-stirred model and parallel-tube model [100, 102]:

Well-stirred model: $CL_h = Q \cdot CL_{int} / (Q + CL_{int})$

Parallel-tube model: $CL_h = Q \cdot (1 - e^{(-CL_{int} / Q)})$

where Q is blood flow rate. Hepatic extraction ratio (E_h) was then calculated with the CL_h values using the following equation [102]:

$$E_h = \frac{CL_h}{Q}$$

where *Q* represents hepatic blood flow rate, which was 20.7 and 55.2 mL/min/kg for humans and rats, respectively [101]. The fraction of the compound that enters the liver and passes through it unchanged (F_h) was obtained from the E_h values using the equation: $F_h = 1 - E_h$ [102]. This F_h also refers to the fraction of the compound that escapes first-pass metabolism of the liver after intestinal absorption following oral administration.

2.10. *In silico* simulations of pharmacokinetics

2.10.1. Simulation of absorption

In silico simulation of fraction absorbed in humans (F_a) was performed using GastroPlus™ version 9.0.0007. The physicochemical properties of simulated compound were used as predicted by the built-in ADMET Predictor™ version 7.2.0.0 (Simulations Plus, Inc, Lancaster, CA, USA). Built-in pharmacokinetic model and physiological parameters for a 30 year-old American male were used as default settings, and "Human – Physiological – Fasted" settings were applied for the gut physiology. Paracellular permeability was turned on and logD model was set as Structure-based version 6.1.

P_{app} values of compounds (training set compounds) with known effective permeability in human (P_{eff}) (training set compounds) were used as an input to calibrate the permeability model in GastroPlus™ and as a result a "user-defined permeability model" was established. The same permeability value can result in different simulation results depending on how the "user-defined permeability model" is determined. Therefore establishing a "user-defined permeability model" represents calibrating the permeability model. In other words, the "user-defined permeability model" plays a role as a calibration curve that can correlate P_{app} values to P_{eff} values. A detailed description of the "user-defined permeability model" in GastroPlus™ is in the Appendix 2. The training set compounds included antipyrine, furosemide, hydrochlorothiazide, ketoprofen, metoprolol, naproxen, propranolol, ranitidine, terbutaline and verapamil. P_{app} values from our laboratory and also the results from six different sets of literature values were used to produce seven "user-defined

permeability models". Log-linear model was selected for all datasets as it was the one suggested by GastroPlus™ after solving the correlation for all datasets. These established models were used to quantitatively evaluate the lab-to-lab variability in Caco-2 permeability models.

The experimental P_{app} values of application set compounds (desipramine, dexamethasone, sildenafil, chlorpromazine, diclofenac, piroxicam, cetirizine, cimetidine and pravastatin) obtained from our laboratory were then applied for F_a simulation in GastroPlus™. For each compound, all input parameters of permeability were fixed and only the "user-defined permeability model" was changed for each simulation. Each P_{app} value of the application set compounds obtained from this study was applied to the seven different "user-defined permeability models" and P_{eff} values were separately predicted. These P_{eff} values were then used to simulate seven different F_a values for each compound. All other physicochemical input parameters except permeability were used as predicted by the ADMET Predictor™. Other input parameters such as particle size, precipitation time, *etc*., were used as provided by default. The dose and formulation were according to the experimental conditions used in literatures and the information used for simulation are shown in Table 2-2.

Table 2-2. Dose and formulation input parameters of application set compounds for GastroPlus™ simulation

Compounds	Dose (mg)	Formulation
Desipramine	50	Tablet
Dexamethasone	1.5	Tablet
Sildenafil	50	Tablet

Chlorpromazine	50	Tablet
Diclofenac	50	Tablet
Piroxicam	20	Capsule
Cetirizine	10	Tablet
Cimetidine	100	Tablet
Pravastatin	40	Tablet

The root mean square error (RMSE) was used to assess the differences in values from different sets. The RMSE was calculated using the following equation:

$$\mathrm{RMSE} = \sqrt{\frac{\sum_{t=1}^{N}(\hat{y}_t - y_t)^2}{N}}$$

where y_t represents values obtained from different sets or laboratories for compound *t*.

2.10.2. Simulation of oral bioavailability

The results from solubility, permeability and liver microsomal stability assays were incorporated into GastroPlus™ for *in silico* simulation of pharmacokinetic properties. GastroPlus™ setup was as described in Section 2.10.1. Paracellular permeability was turned on and logD model was set as Structure based version 6.1. A user-defined permeability model was established as described in Section 2.10.1. using P_{app} values of 13 compounds obtained in this project (antipyrine, cimetidine, desipramine, furosemide, hydrochlorothiazide, ketoprofen, metoprolol, naproxen, piroxicam, propranolol, ranitidine, terbutaline and verapamil) from the reference compounds list provided by GastroPlus™ [93]. Built-in advanced compartmental absorption and transit (ACAT) model and physiologically-based pharmacokinetic (PBPK) model were applied for the simulation. All other input parameters were as predicted by the

ADMET Predictor™ or as provided by default. Simulations were performed for fasted state of the rat and the human.

2.10.3. Simulation of absorption sites

Intestinal absorption of DF030263 compound in different compartments of the GI tract was simulated *in silico* using GastroPlus™ setup described in Section 2.10.1. The input parameters are listed in Table 2-3. Parameters and settings not mentioned in the Table 2-3 were used as predicted by the ADMET Predictor™ or as given by software default. The physiology setting was selected as "Rat-Fasted" or "Rat-Fed" and paracellular permeation option was turned on. Percentages of the dose absorbed at different compartments of the GI tract were simulated at both fasted and fed states for rats.

Table 2-3. Input parameters for *in silico* simulation of DF030263 compound

Parameters	Value
Molecular weight (g/mol)	435.6
Log P	3.1[a]
pK_a	10.7[a]
Human jejunal permeability ($\times 10^{-4}$ cm/s)	1.37[b]
Diffusion coefficient ($\times 10^{-5}$ cm^2/s)	0.6288[b]
Drug particle density (g/mL)	1.2[c]
Mean precipitation time (sec)	900[c]
Reference solubility (mg/mL)	0.03846[d]
Biorelevant solubilities (mg/mL)	
FaSSGF (pH 1.6)	0.6737[d]
FaSSIF (pH 6.6)	0.04935[d]

FeSSIF (pH 5.0)	0.06529[d]

[a] Predicted by ACD/Labs

[b] Predicted by GastroPlus™

[c] GastroPlus™ default values

[d] Experimental results

2.10.4. Deconvolution of plasma concentration-time profiles

Deconvolution of plasma concentration-time profiles obtained in rats following oral and intravenous administration of DF030263 was conducted using Phoenix WinNonlin version 6.3 (Pharsight, Mountain View, CA, USA). The mean plasma concentration-time profiles following oral and intravenous administrations were used for the deconvolution. The results of deconvolution were expressed by cumulative input vs time and input rate vs time.

2.11. Analytical methods for determination of concentration

2.11.1. Sample preparation

The general sample preparation scheme consisted of a combination of protein precipitation and liquid-liquid extraction applied to samples prior to HPLC injection. To 100 µL sample, 10 µL of internal standard solution was added and 10 µL of working stock solution of 10 times higher concentration was added for calibration curve samples. Acetonitrile (300 µL) was then added for protein precipitation and 300 µL of pH modifier was added when necessary. Liquid-liquid extraction was achieved with extraction solvent (volume specified below) and the samples were then vortex-mixed for 10 min and centrifuged at 1160 *g* for 10 min. The organic layer was

transferred and evaporated to dryness under N_2 gas at 40 °C. Reconstitution solvent (100 µL) was then added and vortex-mixed for 10 min before being transferred to HPLC vial for analysis. Specific conditions of pH modifier, extraction solvent and reconstitution solvent are detailed in Tables from 2-4 to 2-7.

Table 2-4. Sample preparation conditions for compound studied in Chapter 3

Compound	pH modifier	Extraction solvent[a]	Reconstitution solvent[b]	Internal standard
BEX	0.1 M HCl	Hexane:ethyl acetate = 10:1	50%	THC

THC, Δ^9-Tetrahydrocannabinol

a Total volume of 3.3 mL used

b Reconstitution solvent expressed as % of acetonitrile in water

Table 2-5. Sample preparation conditions for compounds studied in Chapter 4

Compounds	pH modifier	Extraction solvent[a]	Reconstitution solvent[b]	Internal standard
BEX, BME, BET, BPR, BBU, BIP, BIB, BHE, BOT, B22, B24, B25, B26, B27, BAM1, BAM2	0.1 M HCl	Hexane	90%	DDT
RA, RAE, RAC	0.1 M HCl	Hexane	50%	Probucol
BDH	0.1 M HCl	Hexane	50%	DDT
BAE1	None	Hexane	50%	DDT
BAE2	None	Hexane	80%	DDT
BGA1	0.1 M HCl	Hexane	50%	DDT
BGA2, BCY1	0.1 M HCl	Hexane	50%	DDT
BUN, BOC, BOL	0.1 M HCl	Hexane	100%	Probucol
BTG	0.1 M HCl	Hexane	100%	Probucol

DDT, dichlorodiphenyltrichloroethane

a Total volume of 3 mL used

b Reconstitution solvent expressed as % of acetonitrile in water

Table 2-6. Sample preparation conditions for compound studied in Chapter 5

Compounds	pH modifier	Extraction solvent[a]	Reconstitution solvent[b]	Internal standard
Antipyrine	-	DCM	40%	Verapamil
Cetirizine	-	DCM	40%	Chlorpromazine
Chlorpromazine	0.1 M NaOH	MTBE	40%	Verapamil
Cimetidine	-	MTBE	40%	Verapamil
Desipramine	-	MTBE	40%	Dexamethasone
Dexamethasone	0.1 M HCl	MTBE	40%	Ketoprofen
Diclofenac	0.1 M HCl	MTBE	40%	Dexamethasone
Furosemide	0.1 M HCl	MTBE	20%	Dexamethasone
Hydrochlorothiazide	-	MTBE	20%	Dexamethasone
Ketoprofen	0.1 M HCl	MTBE	40%	Dexamethasone
Metoprolol	0.1 M NaOH	EA	20%	Atenolol
Naproxen	0.1 M HCl	MTBE	40%	Dexamethasone
Piroxicam	0.1 M HCl	MTBE	40%	Furosemide
Propranolol	0.1 M NaOH	MTBE	40%	Dexamethasone
Ranitidine	0.1 M NaOH	DCM	40%	Verapamil
Sildenafil	-	MTBE	40%	Verapamil
Terbutaline	0.1 M NaOH	EA	20%	Metoprolol
Verapamil	-	MTBE	40%	Desipramine

DCM, dichloromethane; MTBE, methyl-*tert*-butyl ether; EA, ethyl acetate

a Total volume of 2 mL used

b Reconstitution solvent expressed as % of acetonitrile in water

Table 2-7. Sample preparation conditions for compound studied in Chapter 6

Compounds	pH modifier[a]	Extraction solvent[c]	Reconstitution solvent[d]	Internal standard
S3-138	HCl	MTBE	40%	Piroxicam
HMKII-90	NaOH	MTBE	40%	Dexamethasone

HS-47	NaOH	MTBE	40%	Chlorpromazine
S3-68	NaOH	MTBE	40%	Chlorpromazine
HMKII-101	NaOH	MTBE	40%	Chlorpromazine
HMKIII-17	Potassium phosphate buffer, pH 7.4[b]	MTBE	40%	Dexamethasone
FS90-263	NaOH	MTBE	40%	Dexamethasone
DF030263	NaOH	MTBE	40%	Dexamethasone
HS3-77	NaOH	MTBE	40%	Dexamethasone
HMKIII-41	Potassium phosphate buffer, pH 7.4[b]	MTBE	40%	Dexamethasone
HS3-72	NaOH	MTBE	40%	Dexamethasone

MTBE, methyl-tert-butyl ether

[a] 1 M of HCl or NaOH was used for solubility assay samples and 0.1 M of HCl or NaOH was used for samples from all other assays

[b] 1 M of potassium phosphate buffer (pH 7.4) was used for only solubility assay samples

[c] Total volume of 2 mL used

[d] Reconstitution solvent expressed as % of acetonitrile in water

2.11.2. Analytical conditions

Two different HPLC-UV systems were utilised in the current project. One consisted of a Waters Alliance 2695 separations module coupled with a Waters 996 photodiode array detector and the other consisted of a Waters 600 Pump, Waters 717 Autosampler and Waters 2996 Photodiode Array Detector. In each HPLC-UV setup, column oven was used to maintain column temperature at 40 °C and the samples in the autosampler were maintained at 4 °C. Injection volume was 40 µL for all samples. Empower™ 2 software was used for data processing. Specific analytical conditions are detailed in Tables from 2-8 to 2-12.

Table 2-8. Analytical method conditions for compounds studied in Chapter 3 (Waters Alliance module used)

Compound	Mobile phase		Flow rate (mL/min)	Column[b]	UV wavelength (nm)
	Acetonitrile	Buffer[a]			
BEX	75%	25%	0.2	C18	259

a 10 mM ammonium acetate, pH 4.1 (pH adjusted with glacial acetic acid)

b Waters Atlantis C18 2.1 × 150 mm, 5 µm particle size column (Milford, MA, USA) equipped with a SecurityGuard 2 × 4 mm, 3 µm particle size (Phenomenex, Macclesfield, UK)

Table 2-9. Analytical method conditions for compounds studied in Chapter 4 (Waters Alliance module used)

Compounds	Moblie phase (%)		Flow rate (mL/min)	Column[b]	UV wavelength (nm)
	Acetonitrile	Buffer[a]			
BEX, BME, BET, BPR, BBU, BIP, BIB, BHE, BOT, B22, B24, B25, B26, B27, BAM1, BAM2	85	15	0.4	C18	259
RA, RAE, RAC	85	15	0.4	C18	357
BDH	60	40	0.4	C18	259
BAE1	60	40	0.4	C18	259
BAE2	80	20	0.4	C18	259
BGA1	60	40	0.4	C18	259
BGA2, BCY1	80	20	0.4	C18	259
BUN, BOC, BOL	Gradient 1[c]		0.6	Biphenyl	259
BTG	Gradient 2[d]		0.6	Biphenyl	259

[a] 10 mM ammonium acetate, pH 4.1 (pH adjusted with glacial acetic acid)

[b] C18, Gemini C18 2.0 × 150 mm, 3 µm particle size; Biphenyl, Kinetex Biphenyl 2.1 × 100 mm, 5 µm particle size

[c] Gradient 1: Buffer 40% at 0-4 min, decrease to 5% at 4-7 min, 5% at 7-23 min, increase to 40% at 23-26 min, 40% at 26-45 min

[d] Gradient 2: Buffer 40% at 0-4 min, decrease to 5% at 4-7 min, decrease to 0% at 7-10 min, 0% at 10-25 min, increase to 40% at 25-27 min, 40% at 27-50 min

Table 2-10. Analytical method conditions for compounds studied in Chapter 5 (Waters 600 pump and 717 autosampler system used)

Compounds	Mobile phase		Flow rate (mL/min)	Column[b]	UV wavelength (nm)
	Acetonitrile	Buffer[a]			
Antipyrine	40%	60%	0.4	C18	243
Cetirizine	50%	50%	0.5	C18	229
Chlorpromazine	50%	50%	0.5	C18	254
Cimetidine	60%	40%	0.3	CN	221
Desipramine	50%	50%	0.5	C18	252
Dexamethasone	50%	50%	0.5	C18	240
Diclofenac	60%	40%	0.5	C18	278
Furosemide	40%	60%	0.4	C18	229
Hydrochlorothiazide	40%	60%	0.4	C18	271
Ketoprofen	50%	50%	0.5	C18	254
Metoprolol	70%	30%	0.5	CN	223
Naproxen	50%	50%	0.5	C18	229
Piroxicam	50%	50%	0.5	C18	277
Propranolol	40%	60%	0.5	C18	229
Ranitidine	70%	30%	0.3	CN	227
Sildenafil	40%	60%	0.5	C18	222
Terbutaline	70%	30%	0.3	CN	278
Verapamil	40%	60%	0.5	C18	278

[a] 10 mM ammonium acetate, pH 4.1 (pH adjusted with glacial acetic acid)

[b] C18, Gemini C18 4.6 × 250 mm, 5 μm particle size; CN, Luna CN 4.6 × 150 mm, 5 μm particle size

Table 2-11. Analytical method conditions for compounds studied *in vitro* in Chapter 6 (Waters 600 pump and 717 autosampler system used)

Compounds	Mobile phase		Flow rate (mL/min)	Column[b]	UV wavelength (nm)
	ACN	Buffer[a]			
S3-138	50%	50%	0.5	C18	309
HMKII-90	40%	60%	0.5	C18	277
HS-47	50%	50%	0.5	C18	303

S3-68	50%	50%	0.5	C18	303
HMKII-101	50%	50%	0.5	C18	293
HMKIII-17	40%	60%	0.5	C18	298
FS90-263	40%	60%	0.5	C18	274
DF030263	40%	60%	0.5	C18	257
HS3-77	40%	60%	0.5	C18	274
HMKIII-41	40%	60%	0.5	C18	274
HS3-72	40%	60%	0.5	C18	274

[a] 10 mM ammonium acetate, pH 5.0 (pH adjusted with glacial acetic acid)

[b] C18, Gemini C18 4.6 × 250 mm, 5 μm particle size

Table 2-12. Analytical method conditions for compounds studied *in vivo* in Chapter 6 (Waters Alliance module used)

Compounds	Mobile phase			Flow rate (mL/min)	Column[b]	UV wavelength (nm)
	ACN	MeOH	Buffer[a]			
DF030263	30%	20%	50%	0.4	C18	256.5
HS3-77	30%	20%	50%	0.4	C18	274

[a] 10 mM ammonium acetate, pH 5.0 (pH adjusted with glacial acetic acid)

[b] C18, Gemini C18 4.6 × 250 mm, 5 μm particle size

2.12. Animal experiments

2.12.1. Animals

The protocols for plasma pharmacokinetic and biodistribution experiments following oral administration were reviewed and approved by the University of Nottingham

Ethical Review Committee in accordance with the Animals [Scientific Procedures] Act 1986. Male Sprague Dawley rats (Charles River Laboratories, UK) weighing 350-380 g were used and were housed in the Bio Support Unit, University of Nottingham. The procedures of continuous lymph collection and pharmacokinetic experiments following cannulation of the caecum were performed under approved protocol by the Institutional Animal Care and Use Committee at Rutgers, The State University of New Jersey. Male Sprague Dawley rats (Envigo, Inc., NJ, USA) weighing 300-350 g were used for experiments at Rutgers. Free access was given to food and water with controlled temperature and 12 h light/dark cycle and the animals were acclimatised for at least six days prior to any procedures at both institutions.

2.12.2. Pharmacokinetic study

Jugular vein cannulation surgery procedures were conducted under general anaesthesia for blood sampling. The animals were allowed two days to recover following surgery and were fasted up to 12 h prior to experiments with free access to drinking water. For studies in Chapters 3 and 4, formulations were prepared at concentrations equivalent to 2.5 mg/mL and 10 mg/mL of active drug for intravenous and oral administration, respectively. PEG400 was used as the dosing vehicle for intravenous administration. For oral administration, all prodrugs were administered as a solution in sesame oil to stimulate intestinal lymphatic transport [64]. For oral administration of BEX and RA, sesame oil was co-administered with BEX or RA formulated in PEG400 due to low solubility of the two compounds in TG. Oral administration of BEX in the lipid-free group was performed with PEG400. For studies in Chapter 6, the compounds were formulated in PEG400:water (50:50, v/v) at concentrations of 2 and 4 mg/mL for

intravenous and oral administration, respectively. In all pharmacokinetic studies, the formulations were administered by an oral gavage for oral administration or *via* the jugular vein cannula followed by 0.3 mL heparinised saline (50 IU/mL) for intravenous injection. Blood samples of 250 µL volume were collected from the cannula at pre-determined time points following administration. NaF (10 mg/mL) was used as an anticoagulant and inhibitor of esterase activity [103, 104] for prodrug studies or K_3EDTA (20 mM) was used when only an anticoagulant was needed. Blood samples were centrifuged at 3000 *g* for 10 min to obtain plasma.

2.12.3. Biodistribution study

Formulations were prepared as described in Section 2.12.2 and were delivered by an oral gavage. Animals were euthanised at pre-determined time points. Blood was collected from the posterior vena cava and lymph samples were taken from the mesenteric lymph duct. MLNs were dissected and collected as previously described [63, 105]. The MLNs were isolated from surrounding tissue with care not to compromise the integrity of the lymph nodes. The MLNs were homogenised (POLYTRON® PT 10-35 GT, Kinematica AG, Luzern, Switzerland) with 10 mg/mL NaF in water (1:2, w/v) on an ice bath prior to sample preparation for HPLC analysis.

2.12.4. Postprandial continuous lymph collection

Surgical and experimental procedures for lymph collection were performed as previously described with minor modifications [106]. Peanut oil (2 mL) was orally administered to the animals 1-2 h prior to surgery. The thoracic duct was cannulated

and the cannula was exteriorised under the skin to the back of the neck under general anaesthesia. The rats were allowed to recover for 24 h before collection and gel-based food and water were provided during recovery and lymph collection. Postprandial lymph was collected continuously through the extension tubing into a tube kept on ice.

2.12.5. Colonic administration

Colonic administration was performed with the formulation of 4 mg/mL DF030263 at 3 mL/kg delivered via the cannula inserted into the caecum in freely moving animals. The formulation was infused using a syringe pump (PHD Ultra, Harvard Apparatus, Holliston, MA, USA) at a constant rate for 1 h for colonic administration. Following the administration, blood samples (250 μL) were collected from the jugular vein cannula at pre-determined time points. Blood samples were centrifuged (3000 *g*, 10 min) and plasma samples were stored in -80 °C until analysis.

2.13. Statistical analyses

Data were presented as mean ± standard deviation (SD) unless stated otherwise. Assessment of statistical significance in differences between two groups was conducted by two-tailed unpaired *t*-test. Statistical significance among three or more groups was determined by a one-way ANOVA followed by Tukey's multiple comparisons test. Statistical significance was declared when a *p*-value was lower than 0.05. The analyses were performed on GraphPad Prism version 7.01 (GraphPad Software, Inc., La Jolla, CA, USA). The concentrations that inhibited cell growth by 50% (GI_{50}) were also calculated using GraphPad Prism. Pharmacokinetic parameters

were calculated by non-compartmental analysis using Phoenix WinNonlin 6.3 software (Pharsight, Mountain View, CA, USA). Non-compartmental analysis was applied because compartmental analysis was not uniformly applicable to all individual data.

3. DEVELOPMENT AND VALIDATION OF SIMPLE AND SENSITIVE BIOANALYTICAL METHOD FOR DETECTION OF BEXAROTENE IN RAT PLASMA

This Chapter has been published in the literature as Lee JB, Zgair A, Kim TH, Kim MG, Yoo SD, Fischer PM, Gershkovich P, Simple and sensitive HPLC-UV method for determination of bexarotene in rat plasma, *J Chromatogr B Analyt Technol Biomed Life Sci.* 2017 Jan 1;1040:73-80.

3.1. Introduction

In addition to the effectiveness of BEX in lymphoma, described in Section 1.2.3., it also showed certain promise in non-small cell lung cancer [112-115]. Furthermore, clinical trials are currently ongoing for efficacy in acute myeloid leukaemia [116, 117] and other tumours such as aerodigestive tract cancer [118], breast cancer [119], metastases of differentiated thyroid carcinoma [120] and keratoacanthomas [121].

In the past few years, additional attention was drawn to BEX as it was reported to have neuroprotective effects [122, 123]. Preclinical studies have shown that BEX reverses cognitive and neuronal impairments and improves neural circuit function with a mechanism related to apolipoprotein E, therefore providing a new strategy for treatment of Alzheimer's disease [124, 125]. These results were followed by additional

studies which showed neuroprotective effects of BEX in Parkinson's disease [126]. Although some debate on its effectiveness in neurodegenerative diseases still remains [127, 128], a clinical trial of BEX in Alzheimer's disease is ongoing and a clinical trial in healthy volunteers to elucidate its neuroprotective mechanism is also being conducted [123]. Other clinical trials investigating potential indications of BEX include trials in chronic severe hand dermatitis [129], lymphomatoid papulosis [130], psoriasis [131], alopecia areata [132], schizophrenia [133] and Cushing's disease [134].

In response to the extensive clinical research of BEX, interest in mechanistic preclinical studies to explore its benefits in cancer and other diseases persists. Apart from the already known anticancer effects such as inhibition of cell cycle progressions and induction of apoptosis [135], studies have demonstrated that BEX induces differentiation of cells, which can lead to treatment of cancer [136, 137]. It also prevents multidrug resistance, which is a major problem in chemotherapies [138] and other studies have shown that it has anticancer effects by inhibition of angiogenesis and metastasis [139]. Preventive effects of BEX have also been elucidated in lung cancer [140, 141], breast cancer [142] and intestinal cancer [143]. Other preclinical studies include research in neurodegenerative diseases as previously mentioned [144, 145], and also research in cholesterol homeostasis [146, 147] and pharmacokinetic studies to interpret relationships between exposure and effects [112]. Additionally, recent pharmaceutical research of nano-crystalisation of BEX has been reported with bioanalysis of plasma samples for pharmacokinetics [148, 149]. Unfortunately, these studies have not included a validation of the analytical methods used.

Previously published analytical methods for quantification of BEX in biological matrices include an assay that involves HPLC with fluorescence detection [150]. This method achieved good sensitivity with lower limit of quantification (LLOQ) of 0.5 ng/mL and has been applied to clinical pharmacokinetic studies. However, it is limited by the fact that it requires a high volume of plasma (1 mL) to achieve this sensitivity. This could be a major limitation for preclinical studies in rodents as sample volume is usually substantially lower in these studies. Furthermore, the calibration curve of this method was separated into a low-range and a high-range, and the two ranges utilised different instruments for analysis. Additionally, there was no full validation of that analytical method to meet the guidelines proposed by the US Food and Drug Administration (FDA) [151]. Another published method employed gas chromatography-mass spectrometry to achieve LLOQ of 1 ng/mL, but requires a chemical derivatisation step which makes the method time-consuming, complicated and expensive [152]. A more simple analytical method using HPLC-UV has been reported but this study was focused on the metabolic pathway of BEX [153]. Therefore it did not report specific details on the analytical procedure such as LLOQ, quantification range, use of an internal standard and validation.

Therefore, the aim of this study was to develop a simple, sensitive and cost-efficient bioanalytical method for determination of BEX in rat plasma, utilising low-volume samples and a high-range calibration curve. The assay was developed using HPLC coupled with ultra-violet (UV) detection and full validation of the method was performed to meet the regulations of the FDA. The developed and validated method

was applied to a pharmacokinetic study of intravenous bolus administration in rats. The suitability of the method for mouse and human plasma was also assessed in this study.

3.2. Scheme of work

Sample preparation and analytical conditions described in Table 2-4 and Table 2-8, respectively, were applied in this chapter. Plasma pharmacokinetic study described in Section 2.12.2. was performed and the scheme of work is shown in Figure 3-1.

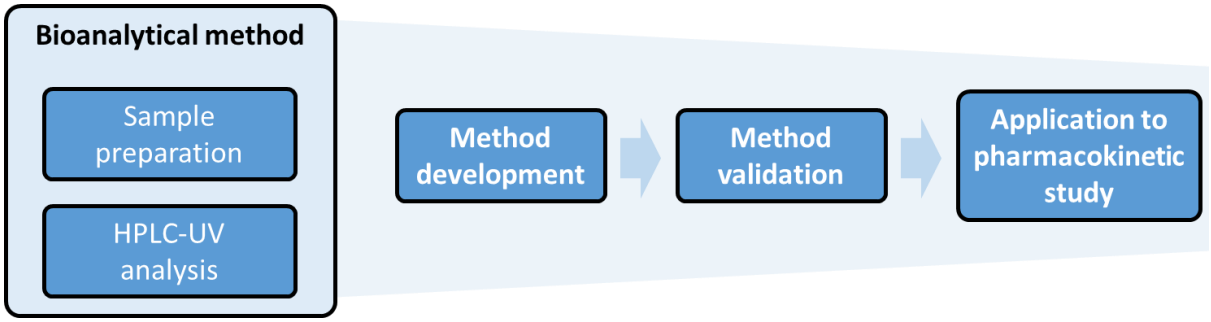


Figure 3-1. Schematic diagram of workflow for development, validation and application of bioanalytical method for BEX in rat plasma.

3.3. Validation criteria

Full validation of the bioanalytical method was conducted in accordance with the guideline established by the FDA [151].

3.3.1. Selectivity

The selectivity of the developed bioanalytical method was assessed by comparing the chromatograms of plasma samples spiked with BEX (n = 6) at the LLOQ with the

chromatograms of blank plasma samples. It was also assessed in plasma samples obtained from the pharmacokinetic experiment in rats [151].

3.3.2. Accuracy and precision

Accuracy was the bias from nominal concentration and was expressed as relative error (RE). Precision was the coefficient of variation and was expressed as relative standard deviation (RSD). The intra-day accuracy and precision were validated by preparing and analysing six replicates of quality control (QC) samples [LLOQ, low QC (LQC), medium QC (MQC) and high QC (HQC)] on the same day. The inter-day accuracy and precision were validated by preparing and analysing six replicates of QC samples on six different days. The acceptable values for accuracy and precision were RE within ±15% and RSD ≤15%, respectively, with the exception of RE within ±20% and RSD ≤20%, respectively, for the LLOQ.

3.3.3. Sensitivity

The LLOQ was determined as the lowest tested concentration of BEX in spiked plasma that had acceptable accuracy and precision of RE within ±20% and RSD ≤20%, respectively, from intra-day and inter-day analyses [151].

3.3.4. Linearity

Calibration curves were constructed at the range of 10 – 10000 ng/mL as described above with 10 ng/mL as LLOQ. A double blank sample (unspiked plasma) and a blank

sample (plasma spiked with IS solution only) were included in each calibration curve. The peak ratio between BEX and the IS was plotted against nominal concentration to obtain calibration curves. Calibration curves with correlation coefficient (r^2) values of >0.99 and accuracy of ±15% (except for LLOQ where ±20% was applied) were considered to be acceptable.

3.3.5. Recovery

The recovery of BEX was determined by comparing the peak areas of processed samples with peak areas of solutions of equivalent concentration in the reconstitution solvent mixture [151]. It was expressed as the mean ± SD from three concentrations tested (LQC, MQC and HQC). The recovery of IS was determined in the same manner at a concentration of 10 µg/mL.

3.3.6. Freeze and thaw stability

Three freeze-thaw cycles (freezing at -80 °C for 24 h and thawing at room temperature) were applied to six replicates of QC samples (LQC, MQC and HQC). Following the third freeze-thaw cycle the samples were processed and a freshly prepared set of calibration curve was used for quantification.

3.3.7. Bench-top, short-term and long-term stability

Sample stability studies were performed with six replicates of QC samples (LQC, MQC and HQC). Bench-top stability was assessed by preparing the QC samples and

storing them at room temperature for 6 h. The QC samples for short-term stability were prepared and stored at -20 °C for 24 h. Long-term stability was tested by storing the QC samples for 2, 4 and 8 weeks at -80 °C. After desired storage time, the samples underwent sample preparation procedure as described in Section 2.3.2. Quantification was performed using a calibration curve freshly prepared each time.

3.3.8. Autosampler stability

Six replicates of QC samples (LQC, MQC and HQC) were prepared and processed according to the sample preparation procedure described above. These processed samples were stored at 4 °C for 24 h to mimic the condition inside the autosampler of HPLC-UV system. After 24 h, the analysis was performed and the samples were quantified using a freshly prepared calibration curve.

3.3.9. Stock solution stability

Working standard solutions for QC samples were prepared at concentrations of 0.25, 4 and 80 µg/mL and were stored in room temperature for 6 h. These solutions were then used to prepare six replicates of QC samples (LQC, MQC and HQC) and they were submitted for sample preparation procedure. Calibration curve samples used for quantification of these QC samples were prepared at the time of sample preparation procedure.

3.4. Results and discussion

3.4.1. Method development

As BEX is a weak acid (pK_a = 4.08, predicted by ACD/Labs, Toronto, Canada), to improve the extraction efficiency, the pH of plasma samples was modified using 0.1 M HCl following protein precipitation with acetonitrile. When 0.1 M HCl was not added to plasma, major fraction of BEX stayed in the ionised form, resulting in poor recovery. After acidification of the samples, BEX was easily extracted. Since BEX is a highly lipophilic compound (Log P = 8.55, predicted by ACD/Labs, Toronto, Canada), non-polar organic solvents were considered to be suitable for the extraction step [40, 154, 155]. Extraction using n-hexane was attempted initially, but interestingly addition of ethyl acetate, a relatively polar extraction solvent, improved recovery of BEX. However, increasing the ratio of ethyl acetate further decreased the recovery and finally n-hexane-ethyl acetate with the ratio of 10:1 (v/v) was selected as the extraction solvent.

For the mobile phase mixture, water was initially tried as the aqueous component. However, BEX was not efficiently retained in the C18 column as it had an ionised form in water. Therefore 10 mM ammonium acetate buffer was used instead of water and 10 mM of buffer was deemed to have sufficient buffer strength for concentrations of BEX tested. The pH of the buffer was tested at a range of 4.0-5.5 and from the shift of retention time, it was found that BEX was better retained at lower pH. The final pH of the buffer (pH 4.1) and the composition ratio with acetonitrile were selected to provide optimal selectivity and sensitivity.

3.4.2. Method validation

3.4.2.1. Selectivity

The selectivity of the method was demonstrated as interference peaks from blank rat plasma samples were effectively separated from the peak of BEX (Figure 3-2). It is also shown in Figure 3-2D that endogenous peaks that originate from plasma of rats used in pharmacokinetic experiments did not interfere with the peaks of interest. Therefore the current method provides selective determination of BEX in rat plasma. The inability of UV-based analytical methods in detecting metabolites can be a limitation to the current study.

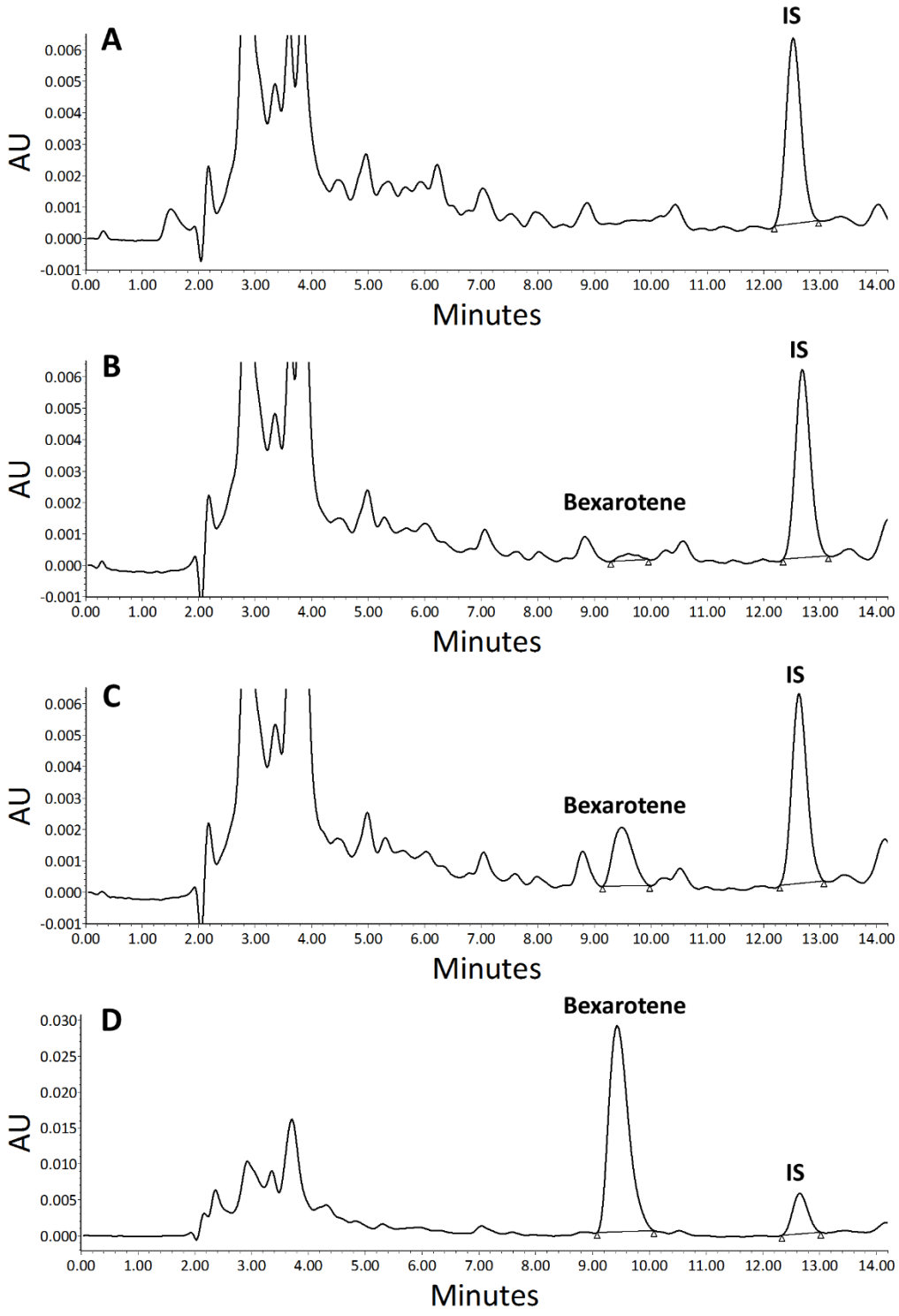


Figure 3-2. Representative chromatograms from rat plasma. A, Rat plasma spiked with 10 µg/mL of IS; B, rat plasma spiked with 10 ng/mL BEX and 10 µg/mL of IS (LLOQ sample); C, rat plasma spiked with 100 ng/mL BEX and 10 µg/mL of IS (calibration curve sample); D, rat plasma sample obtained in pharmacokinetic study 1 h following intravenous bolus administration of 2.5 mg/kg BEX. All observed at λ = 259 nm.

3.4.2.2. Accuracy and precision

Accuracy and precision, expressed as RE and RSD, respectively, for intra- and inter-day validations are shown in Table 3-1. The values for all QC samples (LQC, MQC and HQC) were within the acceptable range (RE within ±15% and RSD <15%). The values for LLOQ samples were also within the criteria (RE within ±20% and RSD <20%), indicating that the developed method was able to quantify BEX with appropriate accuracy and precision [151].

Table 3-1. Intra- and inter-day validation results of the analytical method of BEX in rat plasma using HPLC-UV (n = 6)

	Intra-day		**Inter-day**	
Concentration levels	**Accuracy (RE, %)**	**Precision (RSD, %)**	**Accuracy (RE, %)**	**Precision (RSD, %)**
LLOQ (10 ng/mL)	4.67	6.10	-2.73	14.30
LQC (25 ng/mL)	-5.06	10.00	-0.27	7.57
MQC (400 ng/mL)	7.57	3.00	-0.82	12.27
HQC (8000 ng/mL)	7.93	3.50	0.54	9.63

LLOQ, lower limit of quantification; LQC, low quality control; MQC, medium quality control; HQC, high quality control.

3.4.2.3. Sensitivity and linearity

As mentioned in the Section 3.4.2.2., the LLOQ samples had acceptable accuracy and precision in intra- and inter-day validations and therefore 10 ng/mL was determined to be the LLOQ for the developed method (Table 3-1). The linearity of the calibration curves was established over a range of 10-10000 ng/mL as all the points within the calibration curve, except LLOQ, were within the criteria of RE within ±15% and RSD

<15% and the correlation coefficient (r^2) values were >0.99. The LLOQ of 10 ng/ml is sufficiently sensitive to support preclinical pharmacokinetic studies in rats.

3.4.2.4. Recovery

The absolute recoveries (mean ± SD) of BEX from rat plasma were 96.2 ± 0.6%, 97.2 ± 1.1%, and 96.0 ± 2.8% for the LQC, MQC and HQC samples, respectively. Such high recovery was reached by optimising the extraction solvent. The high recovery of this method contributed to achieving good sensitivity. The recovery of the IS was 89.4 ± 2.7%.

3.4.2.5. Stability

The stability of spiked rat plasma samples under different storage conditions is shown in Table 3-2. The RE and RSD values were within acceptable limits for all conditions tested. The bench-top stability and stock solution stability ensures that the samples and stock solutions are stable during sample preparation procedures, respectively. Short- and long-term stability results indicate that these samples can be stored under these conditions without compromising the accuracy and precision. Samples that had undergone freeze-thaw cycles have demonstrated that stability is not affected up to three cycles. Also, autosampler stability indicates that processed samples can be stored in the autosampler for up to 24 h. Although some stability data in human plasma samples with BEX has been previously reported, it only included bench-top, freeze-thaw cycles and autosampler stabilities [150]. To the best of our knowledge, the present study is the first report of full validation in rat plasma, including all the stability tests required by the FDA [151].

Table 3-2. Stability results of rat plasma samples of BEX under various storage conditions (n = 6)

	Benchtop stability (25 °C, 6 h, n = 6)		Short term stability (-20 °C, 24 h, n = 6)		Autosampler stability (4 °C, 24 h, n = 6)		Freeze-thaw stability (3 cycles, n = 6)	
Concentration levels	**RE (%)**	**RSD (%)**	**RE (%)**	**RSD (%)**	**RE (%)**	**RSD (%)**	**RE (%)**	**RSD (%)**
LQC (25 ng/mL)	0.14	7.05	-3.99	3.78	7.88	4.27	-2.86	13.14
MQC (400 ng/mL)	7.81	4.84	-2.41	10.46	12.20	2.69	-1.83	12.17
HQC (8000 ng/mL)	7.58	6.07	-1.67	6.63	-5.83	5.75	-3.30	8.78

RE, relative error; RSD, relative standard deviation; LQC, low quality control; MQC, medium quality control; HQC, high quality control.

Table 3-2. ***(continued)***

	Stock solution stability (25 °C, 6 h, n = 6)		Long term stability (-80 °C, 2 wks, n = 6)		Long term stability (-80 °C, 4 wks, n = 6)		Long term stability (-80 °C, 8 wks, n = 6)	
Concentration levels	**RE (%)**	**RSD (%)**	**RE (%)**	**RSD (%)**	**RE (%)**	**RSD (%)**	**RE (%)**	**RSD (%)**
LQC (25 ng/mL)	-4.14	4.08	-10.18	6.78	-8.21	4.07	-3.73	6.49
MQC (400 ng/mL)	-2.48	1.68	-13.94	5.72	-7.91	5.52	-8.32	2.64
HQC (8000 ng/mL)	-8.53	11.56	-11.39	9.79	-1.65	6.54	-7.61	2.50

RE, relative error; RSD, relative standard deviation; LQC, low quality control; MQC, medium quality control; HQC, high quality control.

3.4.3. Pharmacokinetic study in rats

The applicability of the analytical method was demonstrated in a pharmacokinetic study in rats following IV bolus administration. The plasma concentration-time profiles of BEX are shown in Figure 3-3 and pharmacokinetic parameters obtained by non-compartmental analysis are shown in Table 3-3. The plasma concentration profiles showed consistency across the animals (Figure 3-3) which is also reflected in the variability of the obtained pharmacokinetic parameters (Table 3-3). The selectivity,

sensitivity and range of the calibration curve of the developed method are sufficient to be utilised in pharmacokinetic studies in rats.

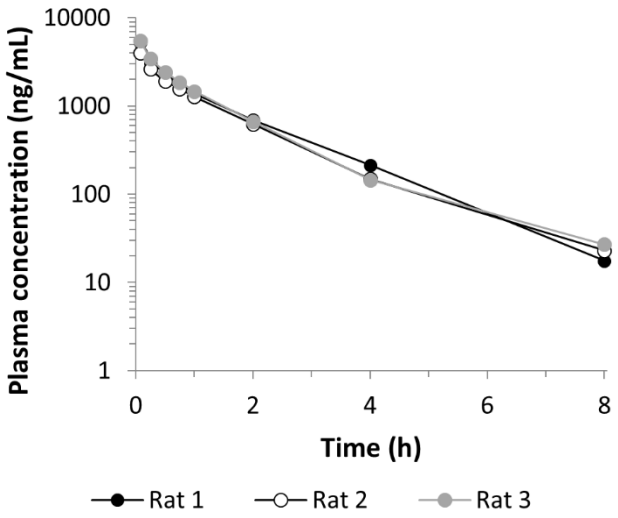


Figure 3-3. Plasma concentration-time profiles of BEX following intravenous bolus administration at 2.5 mg/kg in rats (n = 3).

Table 3-3. Pharmacokinetic parameters of BEX obtained following intravenous bolus administration of 2.5 mg/kg BEX in rats (n = 3)

Parameters	**Mean**	**SD**
$AUC_{0\rightarrow t}$ (h·ng/mL)	4631	453
AUC_{inf} (h·ng/mL)	4668	452
C_0 (ng/mL)	6219	1068
$t_{1/2}$ (h)	1.15	0.02
V_{ss} (mL/kg)	734	104
CL (mL/h/kg)	539	55

AUC_{inf}, area under the curve from time zero to infinity; $AUC_{0\rightarrow t}$, area under the curve from time zero to the last sampling time point; C_0, concentration extrapolated to time zero; $t_{1/2}$, half-life; V_{ss}, volume of distribution at steady state; CL, clearance.

3.4.4. Assessment of the suitability of the analytical method to human and mouse plasma.

Following the development and validation of the bioanalytical method for rat plasma, it was further applied to human and mouse plasma to assess the potential suitability of the methodology for studies in additional species. The same sample preparation method was applied to both human and mouse plasma for the levels of LQC, MQC and HQC. The validity was assessed by inter-day validation and the accuracy and precision are shown in Table 3-4. Good selectivity was also exhibited by comparing chromatograms of spiked samples and blank plasma samples for both human and mouse plasma (Figures 3-4 and 3-5, respectively). The only remarkable point was that for human plasma, an interference peak appeared at the retention time of IS (Figure 3-4). The problem was solved by observing the IS peak at 220 nm for human plasma only (Figure 3-4). These results show that the current method has good potential to be utilised in studies involving both human subjects and mice. A bioanalytical method for determination of BEX in mouse plasma has not been previously reported.

Table 3-4. Intra-day validation results of the analytical method of BEX in human and mouse plasma using HPLC-UV (n = 6)

	Human plasma		**Mouse plasma**	
Concentration levels	**Accuracy (RE, %)**	**Precision (RSD, %)**	**Accuracy (RE, %)**	**Precision (RSD, %)**
LQC (25 ng/mL)	-2.67	8.52	5.59	7.08
MQC (400 ng/mL)	-1.69	13.04	10.75	5.87
HQC (8000 ng/mL)	-5.49	14.65	6.96	3.54

RE, relative error; RSD, relative standard deviation; LQC, low quality control; MQC, medium quality control; HQC, high quality control.

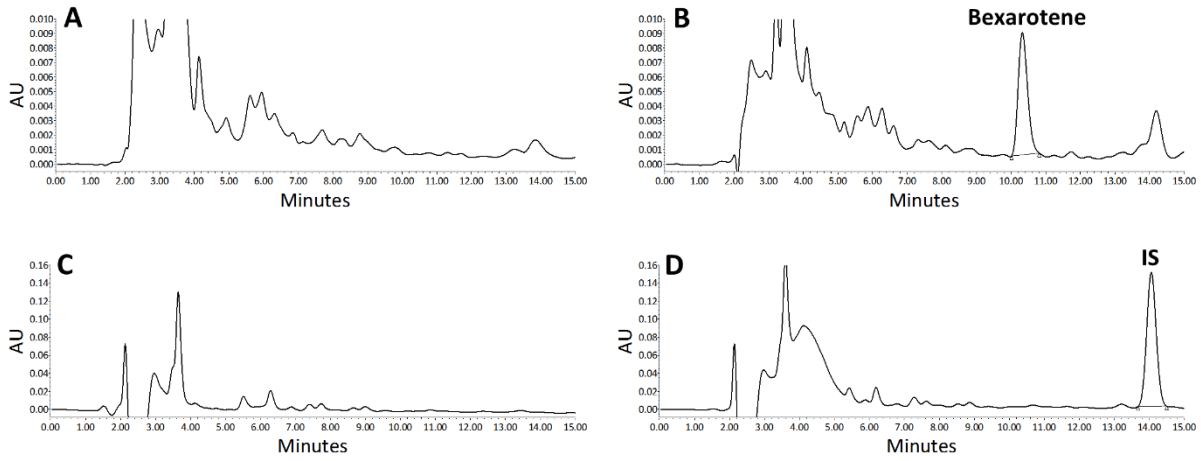


Figure 3-4. Representative chromatograms from human plasma. A, blank human plasma observed at λ = 259 nm; B, human plasma spiked with 400 ng/mL BEX observed at λ = 259 nm (MQC sample); C, blank human plasma observed at λ = 220 nm; D, human plasma spiked with 10 µg/mL of IS observed at λ = 220 nm.

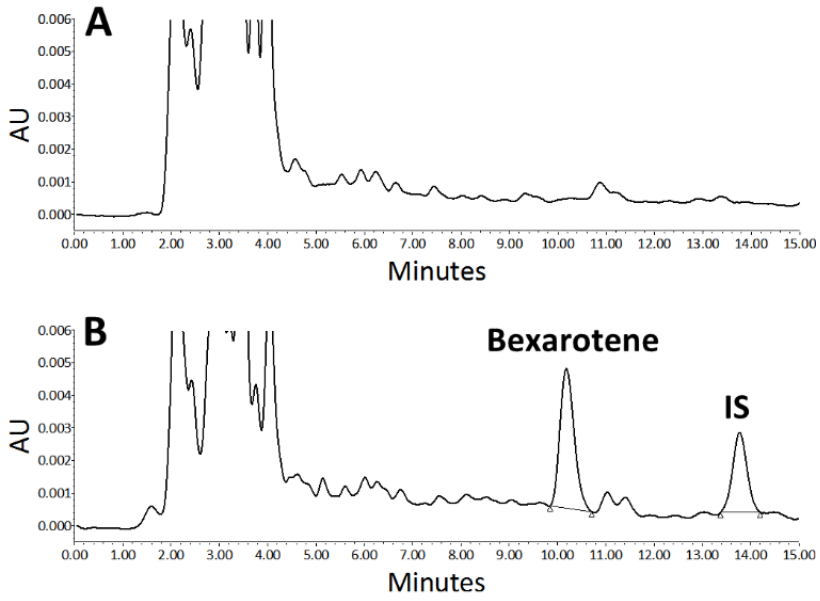


Figure 3-5. Representative chromatograms from mouse plasma. A, blank mouse plasma; B, mouse plasma spiked with 400 ng/mL BEX and 10 µg/mL of IS (MQC sample). All observed at λ = 259 nm.

3.5. Conclusion

The present study describes development and full validation of a simple, sensitive and cost-efficient bioanalytical method using HPLC-UV for the determination of BEX in rat plasma. This method utilises 100 µL volume of samples to achieve LLOQ adequate to support preclinical pharmacokinetic studies. A full validation of a bioanalytical method for BEX in rat plasma is reported here for the first time. It was also shown that the method can be applied to studies involving human subjects and mice. In the current PhD project, this method was used for quantification of BEX and its prodrugs with modifications when needed.

4. INTESTINAL LYMPHATIC SYSTEM TARGETING BY LIPOPHILIC PRODRUG APPROACH

4.1. Introduction

Intestinal lymphatic system is an important organ of the immune system as it accommodates more than half of the body's lymphocytes [156, 157]. In addition, the intestinal lymphatic system is important in pathophysiology of lymphomas, HIV infection and metastasis of some solid tumours. Therefore, efficient targeting of drugs to the intestinal lymphatic system has potential to improve treatment of lymphatic system-associated cancers and cancer metastasis, as well as diseases such as autoimmune disorders and HIV infections [29, 47, 48, 158-162].

Lipophilic prodrug approach has been employed in the past to take advantage of the intestinal lymphatic transport of drug molecules that otherwise would not have the necessary physicochemical properties (log P, log $D_{7.4}$, polar surface area, number of hydrogen donors, number of hydrogen acceptors, molar volume, freely rotatable bonds, density) required for association with chylomicrons. However, previously suggested approaches were mainly based on glyceride mimetic or very bulky prodrug moieties [59, 62, 66, 159, 163]. It has been proposed, and there indeed seems to be a long-standing belief, that simple ester prodrug approach would not be suitable for this purpose because of its instability during absorption phase [59]. It should also be noted that these previous studies were mainly to increase systemic exposure of the drug and

not to specifically target the intestinal lymphatics for the pharmacological effects within the lymphatic system.

Herein, however, a study where lipophilic prodrug approach was used to target BEX and RA efficiently to the intestinal lymphatic system by activated ester prodrug approach is reported. Drugs with a wide list of indications and mechanisms of action could potentially benefit from targeting to the intestinal lymphatic system by the proposed approach. However, this work was focused on targeting BEX and RA to improve the treatment outcomes of non-Hodgkin's lymphoma (NHL) in patients with substantial involvement of mesenteric lymph nodes (MLN) in the disease. In this study, 25 prodrugs of BEX were synthesised and assessed, and the activated ester prodrug has been shown as the most promising approach for targeting the intestinal lymphatic system. This successful approach was further applied to RA. It is also shown that the two drugs exert synergism towards treatment of the DLBCL at concentrations which are realistically achievable in the lymph nodes when suggested targeting approach is utilised.

4.2. Scheme of work

Chemical synthesis was performed according to Section 2.2. and *in vitro/ex vivo* experiments were conducted as described in Sections from 2.3. to 2.6. Procedures for *in vivo* studies followed methods of Sections from 2.12. Scheme of work is shown in Figure 4-1.

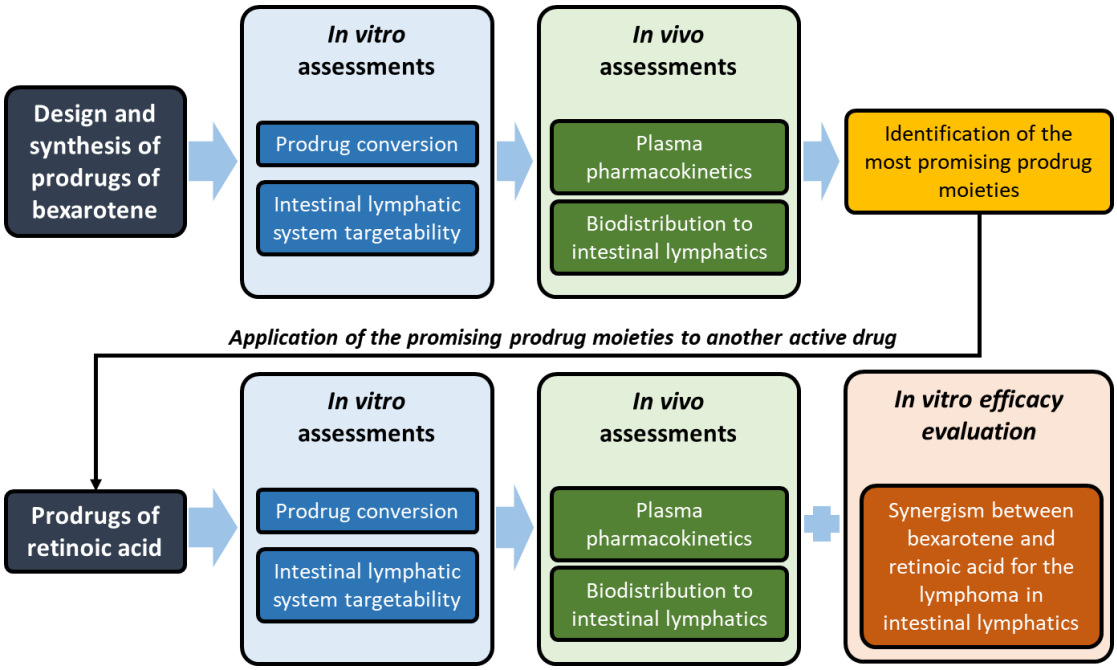


Figure 4-1. Schematic diagram of lipophilic prodrug approach for BEX and RA to target the intestinal lymphatic system.

4.3. Results

4.3.1. Preparation of prodrugs of BEX

A total of 25 prodrugs of BEX were designed *in silico* to possess the necessary physicochemical properties needed for association with CM and therefore high potential for the intestinal lymphatic transport following oral administration [61, 164]. All prodrugs were then successfully synthesised and purified. The structures of the prodrugs are shown in Figure 4-2 and physicochemical properties are listed in Table 4-1; characterisation of these molecules can be found in Appendix 1.

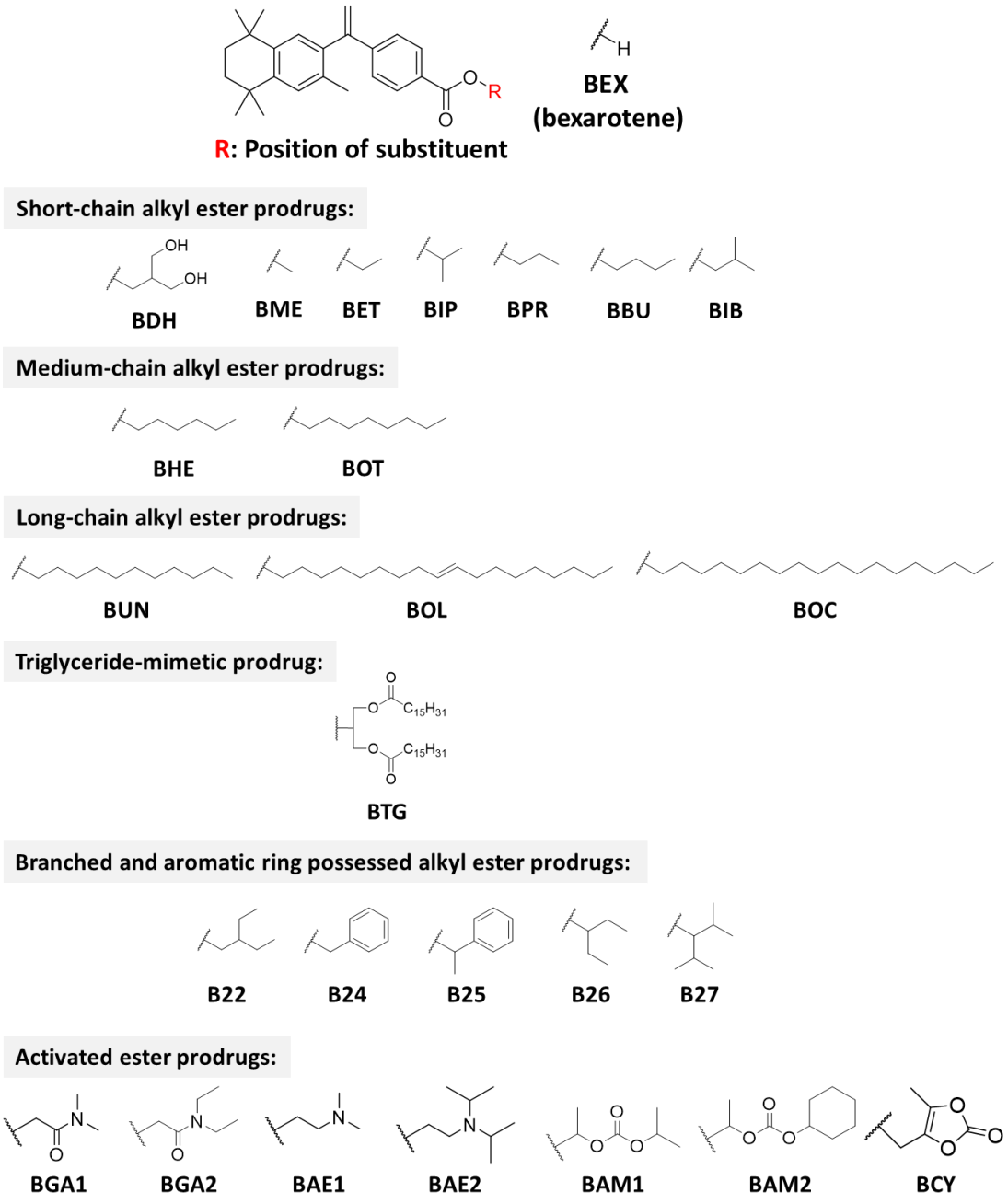


Figure 4-2. Chemical structures of BEX and its prodrugs.

Table 4-1. Physicochemical properties of BEX and its prodrugs

	Log $D_{7.4}$	Log P	Polar surface area ($Å^2$)	H-Acceptors	Non-terminal rotatable bonds	Density (g/cm^3)	Molar volume (cm^3)	H-Donors
BEX	4.04	8.55	37.3	2	3	1.042	334.2	1
BME	7.67	7.67	26.3	2	4	1.007	359.6	0
BET	7.98	7.98	26.3	2	5	1.000	376.1	0
BPR	8.24	8.24	26.3	2	6	0.994	392.6	0
BBU	8.40	8.40	26.3	2	7	0.988	409.1	0
BIP	8.25	8.25	26.3	2	5	0.993	393	0
BIB	8.54	8.54	26.3	2	6	0.987	409.5	0
BDH	5.76	5.76	66.8	4	8	1.079	404.5	2
BHE	10.00	10.00	26.3	2	9	0.978	442.1	0
BOT	10.88	10.88	26.3	2	11	0.969	475.2	0
BUN	12.45	12.45	26.3	2	14	0.958	524.7	0
BOC	14.74	14.74	26.3	2	21	0.938	640.2	0
BOL	14.18	14.18	26.3	2	20	0.944	633.8	0
BTG	19.66	19.66	122.3	9	45	1.002	1011.3	0
B22	9.17	9.17	26.3	2	8	0.977	442.5	0
B24	9.13	9.13	26.3	2	6	1.043	420.3	0
B25	9.43	9.43	26.3	2	6	1.034	437.6	0
B26	8.91	8.91	26.3	2	7	0.982	426	0
B27	9.67	9.67	26.3	2	7	0.971	459.8	0
BGA1	6.91	6.91	46.61	4	6	1.048	413.5	0
BGA2	7.69	7.69	46.61	4	8	1.033	446.5	0
BAE1	6.76	7.62	29.54	3	7	1.007	416.4	0
BAE2	7.18	8.77	29.54	3	9	0.984	483.2	0
BAM1	7.73	7.73	61.83	5	9	1.057	452.7	0
BAM2	8.41	8.41	61.83	5	9	1.12	460.6	0
BCY	6.83	6.83	61.83	5	6	1.117	412.2	0

4.3.2. Association with lipoproteins

As shown in Figure 4-3, all prodrugs possessed higher associations than BEX with artificial emulsion prepared from Intralipid® *in vitro* and with natural human CM *ex vivo* (p <0.05), indicating improved potential to target the intestinal lymphatic system. The affinity of tested compounds for the artificial emulsion and natural human CM did not differ statistically for most prodrugs except for compounds BGA2 and BAE2. The correlation between the *in vitro* and *ex vivo* assessments demonstrated an R^2 value of 0.694 (Figure 4-4).

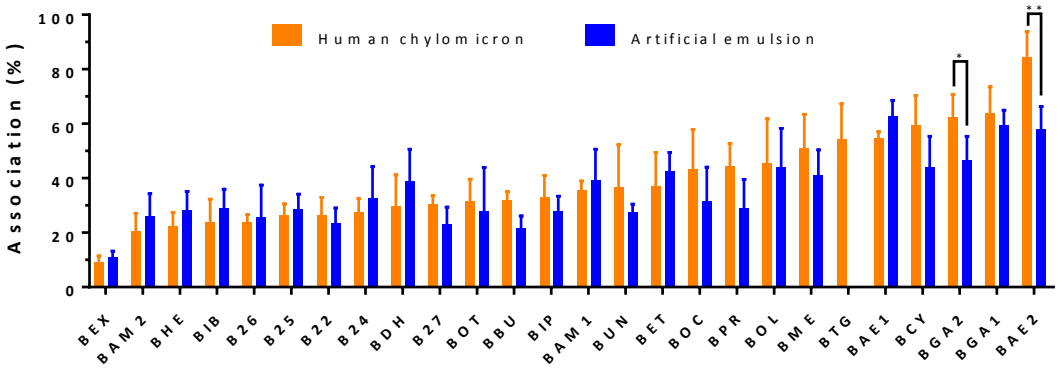


Figure 4-3. Association % of compounds with human chylomicron and artificial emulsion prepared from Intralipid®, representing potential of intestinal lymphatic system targetability. *, p<0.05; **, p<0.01 (mean ± SD, n = 5 or 6). Association of BTG with artificial emulsion could not be measured due to constraints in analytical methods.

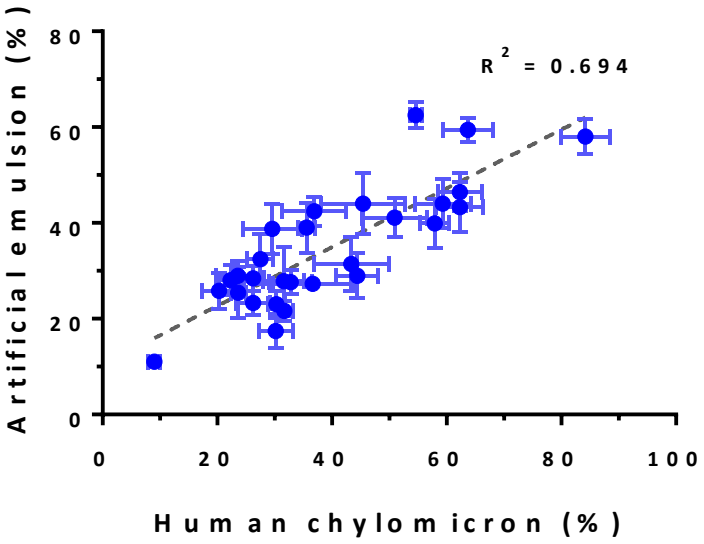


Figure 4-4. Correlation graph between association (%) of compounds with human chylomicron and artificial emulsion prepared from Intralipid® (mean ± SD). Moderate correlation with coefficient of correlation (R^2) of 0.694 was found between the two test media.

4.3.3. Conversion of BEX prodrugs to BEX

The prodrugs were tested for their stability and convertibility *in vitro* to the active drug (BEX) in rat plasma and FaSSIF with added esterase enzyme activity (Figure 4-5). In this project, conversion of the prodrugs in the lymphatic system would be the most desired information. However, due to practical limitations and high similarities of plasma with lymph, plasma was selected as a surrogate test medium instead of lymph fluid (detailed explanation can be found in Discussion section). All prodrugs had an ester bond which can be cleaved by esterases to release BEX. The degradation of prodrugs corresponded to generation of BEX and no other peaks were apparent in the HPLC-UV chromatograms at wavelength of 259 nm, indicating direct biotransformation of the prodrugs to BEX. Therefore, the half-lives shown in Figure 4-5 represent the stability and convertibility of the prodrugs to BEX. These half-lives

were proportionally prolonged with the increase in the chain length or the bulkiness of the prodrug moieties. Compounds BOT and B27 were converted to BEX in rat plasma but not in the simulated intestinal fluid. Compounds BUN, BOL, BOC and BTG did not degrade and they did not release BEX in either media. To test the chemical stability of the prodrugs, compounds BET and BDH were representatively tested in FeSSIF and FaSSIF without enzyme. BET was selected because it was the least stable in enzymatic stability tests and BDH because it had –OH groups which other prodrugs did not possess. As a result, they were found to be stable and half-lives were unobtainable.

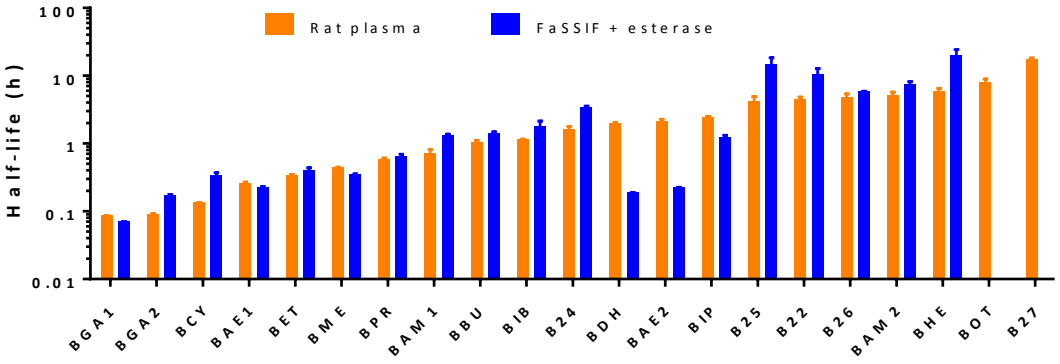


Figure 4-5. Half-lives of prodrugs in rat plasma and FaSSIF with added esterase activity (20 IU/mL), representing their converting rate to BEX (mean ± SD, n = 3). Half-lives of BOT and B27 in FaSSIF + esterase were not obtainable because no prodrug cleavage was observed.

Based on their relatively high affinity for CM, which represents high potential for lymphatic system targetability, and short half-life in rat plasma, which represents rapid enzymatic convertibility, BET and BCY were selected as the most promising prodrug candidates for additional studies. Therefore, prodrug conversion was then studied in further detail for compounds BET and BCY in an environment that would more closely mimic *in vivo* situations (Figure 4-6). The compounds were associated with artificial

emulsion prior to spiking the rat plasma, as it is the associated form of drug with lipoproteins that would be delivered to the intestinal lymphatics. The conversion of the prodrugs was significantly delayed when they were in the associated form (half-lives increased 2.7- and 4.5-fold for BET and BCY, respectively). Control groups in which the plasma was pre-treated with artificial emulsion prior to addition of prodrugs were employed to determine whether this delay was caused by an interaction between the artificial emulsion and enzymes in plasma. It can be seen that the delayed conversion only occurs when prodrugs are associated with the artificial emulsion prior to being introduced to the plasma. The conversion of BET and BCY was also tested in postprandial lymph collected from rats. The half-lives in lymph were comparable to those obtained in plasma in which the prodrugs were in lipoprotein-associated forms.

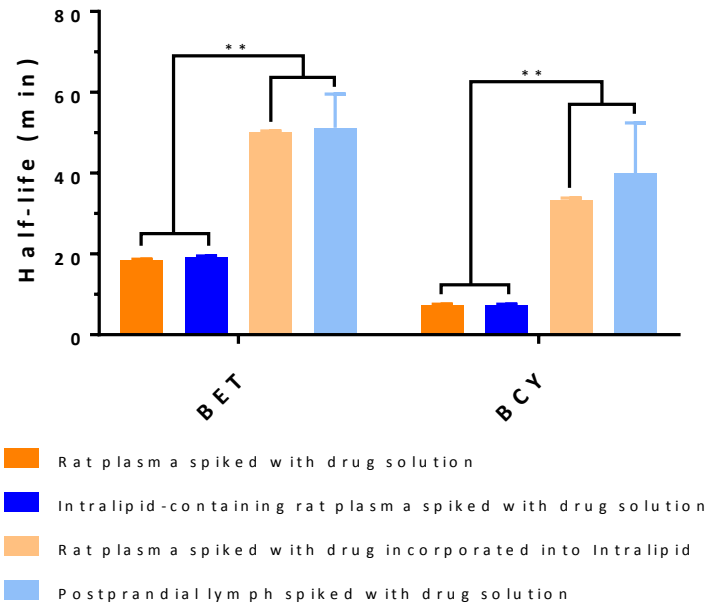


Figure 4-6. Detailed bio-relevant assessment of stability of BET and BCY mimicking various *in vivo* situations (mean ± SD, n = 3). Bars in light orange represent stability of prodrugs when they are spiked in the form of drug-chylomicron (CM) complex as it would be the associated form that reaches intestinal lymphatics. Bars in dark blue were tested to evaluate if the presence of Intralipid® was inhibitory towards the enzymatic activity. Bars in light blue

represent stability tested *ex vivo* with postprandial lymph where CM is present in abundant amount. **, p<0.01.

4.3.4. TG solubility of BEX and its prodrugs

Accurate TG solubility results were obtained for BEX and BGA2, for which the solubility was relatively low, at 1.77 ± 0.10 and 2.67 ± 0.06 mg/mL, respectively (mean ± SD, n = 3). BET, BCY and BTG were all soluble in sesame oil at concentrations ≥10 mg/mL active drug (BEX), which was the concentration of formulation used in *in vivo* studies. Further concentration escalation of these compounds to determine the maximal solubility in TG would require excessive amounts of material and therefore was not performed due to limited availability of the synthesised compounds.

4.3.5. Plasma pharmacokinetics of BEX and selected prodrugs

BEX, BET, BCY and BTG were tested *in vivo* for pharmacokinetic profiles (Figure 4-7 and Table 4-2). Selection of these prodrugs was based on the fact that BET had the fastest conversion rate among first-generation prodrugs before the activated ester BCY was synthesised and BTG is the TG mimetic prodrug commonly applied in prodrug approaches targeting intestinal lymphatics. Figure 4-7A shows plasma pharmacokinetic profiles following intravenous administration. Prodrugs were rapidly converted to BEX in plasma and there was no statistically significant difference between elimination half-lives ($t_{1/2}$) of BEX following administration of BEX and the prodrugs (Table 4-2). Figure 4-7B shows plasma concentration-time profiles of BEX and BEX prodrugs following oral administration. Neither the plasma concentration-

time profiles nor the pharmacokinetic parameters (Table 4-2) differed for BEX between lipid-free and lipid-coadministered groups following oral administration. The oral bioavailability values (F_{oral}) of BEX following administration of each prodrug was calculated based on the intravenous administration profile obtained previously [165]. The bioavailabilities did not differ significantly compared to administration of BEX itself with lipid (p>0.05) (Table 4-2). For the compound BTG, only BEX was detected while the intact form of BTG was not detected in plasma at any time point.

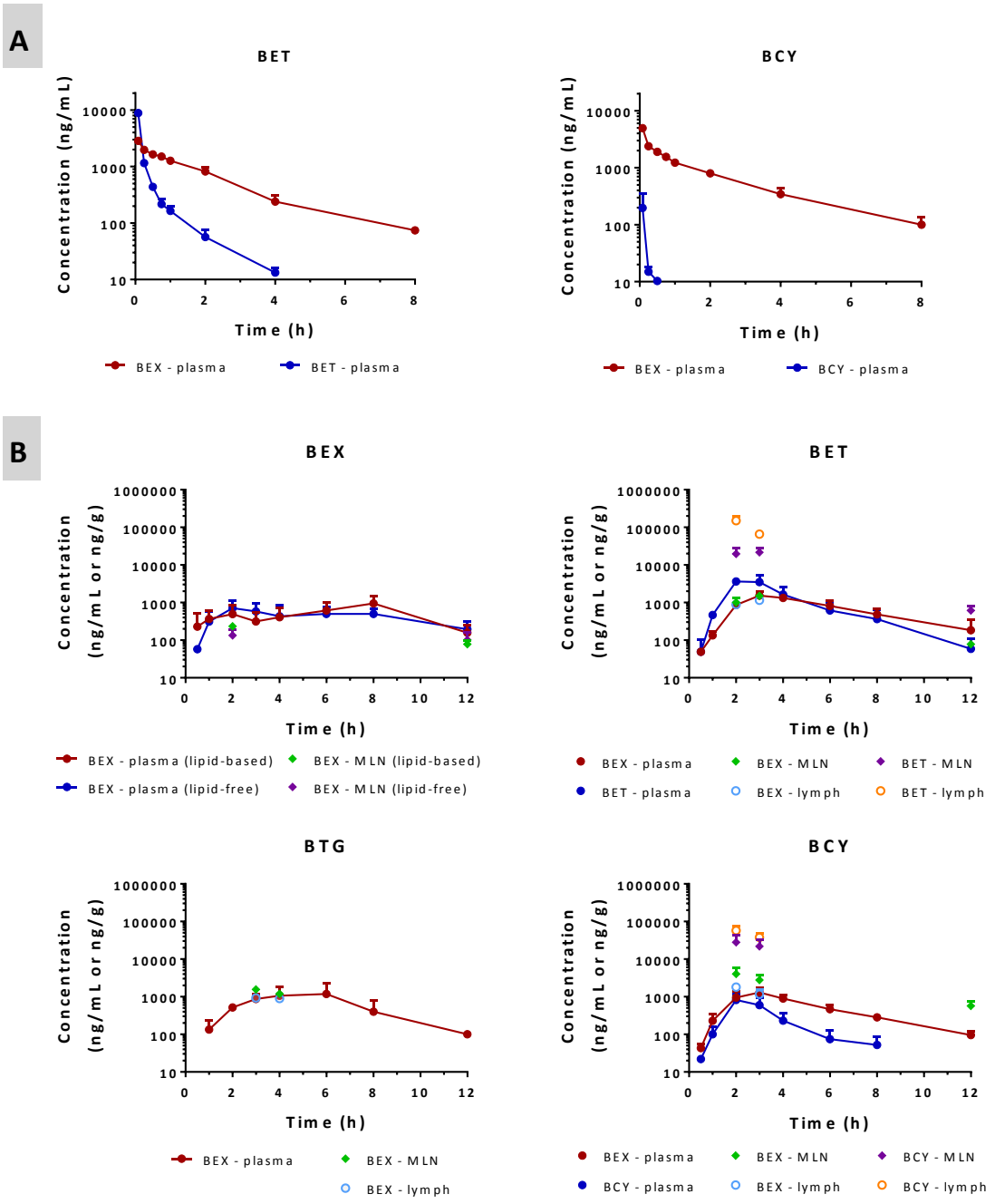


Figure 4-7. *In vivo* pharmacokinetic profiles of BEX and their prodrugs. A, BEX (2.5 mg/kg) and its prodrugs (equivalent to 2.5 mg/kg of BEX) following i.v. administration in rats (mean ± SD, n = 3). B, BEX (10 mg/kg) and its prodrugs (equivalent to 10 mg/kg of BEX) following oral administration in rats (mean ± SD, n =4 to 6). For both A and B, administered compounds are mentioned as the title of each graph. Symbols represent the compound quantified and the medium of samples, as specified in the legends below each graph. Concentrations in plasma and lymph are presented in ng/mL. Concentrations in mesenteric lymph nodes (MLN) are presented in ng/g.

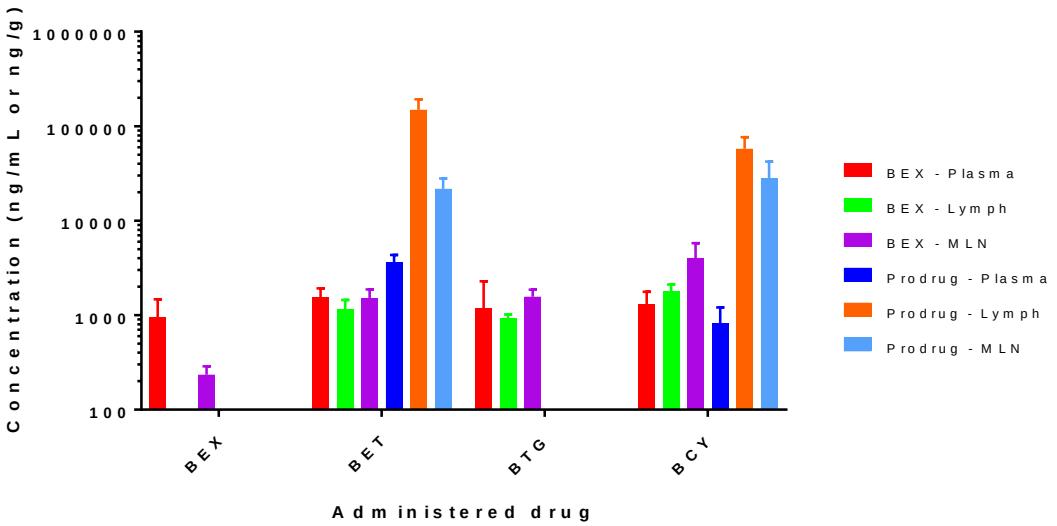


Figure 4-8. Maximum achievable concentration of BEX and its prodrugs in plasma, lymph and mesenteric lymph nodes (MLN) following oral administration in lipid-coadministration conditions in rats. Concentrations in plasma and lymph are presented in ng/mL. Concentrations in MLN are presented in ng/g.

Table 4-2. Plasma pharmacokinetic parameters of BEX following administration of BEX or its prodrugs by i.v. and p.o. administration (mean ± SD).

Compound dosed	**BEX**		**BET**		**BCY**		**BTG**
Route of administration	**p.o. (lipid-free)**	**p.o. (lipid-based)**	**i.v.**	**p.o.**	**i.v.**	**p.o.**	**p.o.**
AUC_{inf} (h·ng/mL)	5836 ± 2140	6618 ± 1312	4614 ± 653	8645 ± 2598	5448 ± 301	5976 ± 1407	6887 ± 3821
$AUC_{0\rightarrow t}$ (h·ng/mL)	4907 ± 1787	5664 ± 1763	4443 ± 628	7751 ± 1552	5178 ± 182	5610 ± 1394	6538 ± 3956
C_0 or C_{max} (ng/mL)	899 ± 338	1099 ± 432	2860 ± 189	1589 ± 360	4953 ± 614	1306 ± 464	1502 ± 1026
$t_{1/2}$ (h)	3.0 ± 0.7	3.7 ± 1.2	1.6 ± 0.1	2.7 ± 1.0	1.8 ± 0.3	2.6 ± 0.4	2.5 ± 1.2
F_{oral} (%)[1]	26.5 ± 9.6	30.6 ± 9.5	-	41.8 ± 8.4	-	30.3 ± 7.5	35.3 ± 21.4

[1] Calculated based on the $AUC_{0\rightarrow t}$ obtained following intravenous administration of BEX at 2.5 mg/kg [165]. AUC_{inf}, area under the curve from time zero to infinity; $AUC_{0\rightarrow t}$, area under the curve from time zero to the last sampling time point; C_0, concentration extrapolated to time zero; C_{max}, maximum observed concentration; $t_{1/2}$, half-life; F_{oral}, oral bioavailability.

4.3.6. Biodistribution of BEX and selected prodrugs to the intestinal lymphatics

The biodistribution of BEX, BET, BCY and BTG was assessed in lymph collected from the mesenteric lymph duct and in MLNs (Figure 4-7B). The two sampling time points were considered as the most important for each compound in assessment of lymphatic transport: T_{max} observed in plasma and 1 h before T_{max}. This was based on our previous reports showing that the concentration of drugs in the intestinal lymphatics could actually be higher prior to the T_{max} observed in plasma [63]. Concentrations of BEX prodrugs BET and BCY in lymph fluid were 50- to 130-fold higher than those found in plasma, indicating substantial intestinal lymphatic transport of the tested prodrugs. Similar to plasma results above intact BTG was not detected in lymph and MLNs.

The concentrations of active drug BEX in MLNs were substantially higher than those found in plasma when BTG and BCY were administered (1.5- and 3.5-fold, respectively). This MLN/plasma concentration gradient was not as high as that exhibited by levels of prodrugs as seen in Figure 4-8 (6.8- to 49-fold). However, the prodrug approach still resulted in efficient and targeted delivery of BEX to MLNs. The maximal observed concentration of BEX in MLNs following BEX, BET and BCY administrations is depicted in Figure 4-9. Oral administration of BCY in condition which facilitate lymphatic transport resulted in 17-fold higher concentration of BEX in MLNs compared to administration of BEX itself at equivalent BEX dose.

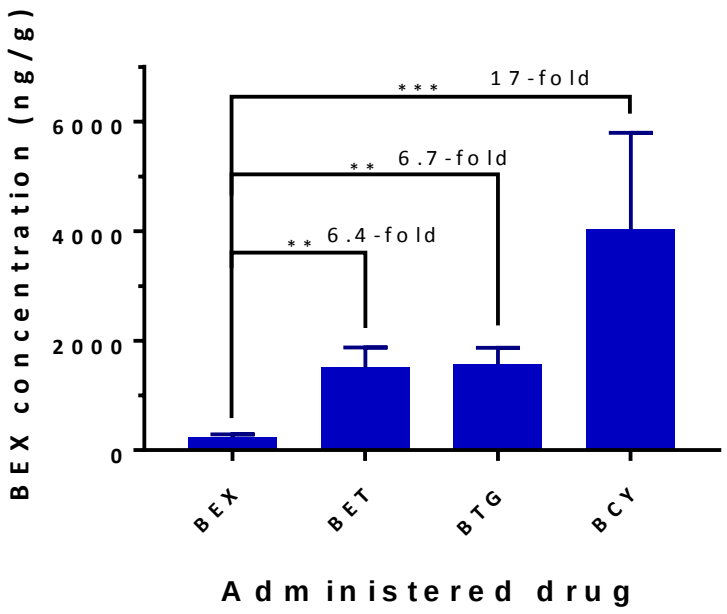


Figure 4-9. Maximal observed concentration of BEX achieved in mesenteric lymph nodes (MLN) (ng/g) following oral administration of BEX, BET, BTG and BCY (mean ± SD). **, p<0.01; ***, p<0.001.

4.3.7. Application of the prodrug approach to intestinal lymphatic targeting of RA

The prodrug approaches which resulted in successful intestinal lymphatic transport of BEX were applied to another drug, RA. Two lead candidates were synthesised: ethyl ester, RAE and cyclic ester, RAC (Figure 4-10A). Both RAE and RAC showed improved association with artificial emulsion and natural human CM compared with RA (Figure 4-10B). The conversion rate of RAC to RA was faster than that of RAE, which was consistent with BET and BCY prodrugs of BEX (Figure 4-10C), and therefore RAC was selected as the lead RA prodrug for subsequent *in vivo* studies. RA and RAC were tested *in vivo* for plasma pharmacokinetics and biodistribution to the intestinal lymphatics following oral administration in conditions which facilitate lymphatic transport (Figure 4-10D). The plasma concentration-time profiles of RAC

resembled the profiles observed with BCY and the maximum concentration of RA achieved in MLNs following administration of RAC was 2.4-fold higher compared to administration of RA itself at equivalent dose (Figure 4-10E). On the other hand, similar to the case of BEX and its prodrugs, the plasma AUCs of RA obtained following administration of RA and RAC did not differ significantly (3313 ± 1846 and 2541 ± 540 h·ng/mL, respectively, p>0.05).

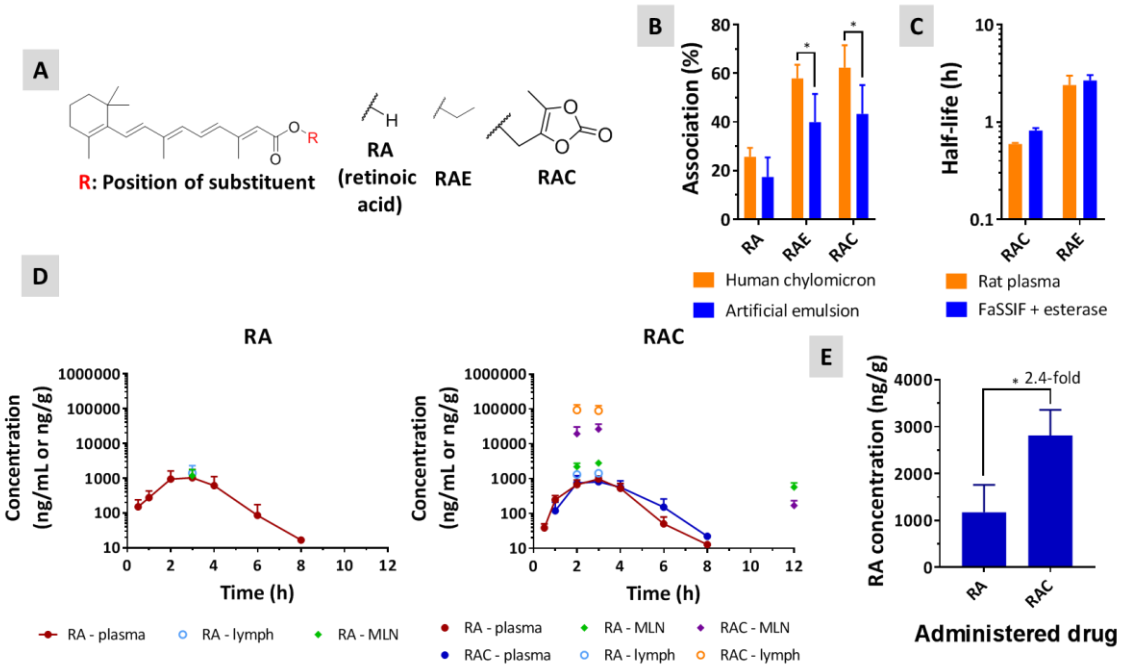


Figure 4-10. Application of the prodrug approach to RA (retinoic acid). A, chemical structures of RA and its prodrugs; B, association with human chylomicrons and artificial emulsion (mean ± SD, n = 6); C, half-life in rat plasma and fasted state simulated intestinal fluid (FaSSIF) with esterase (mean ± SD, n = 3); D, *in vivo* pharmacokinetic profiles in plasma and intestinal lymphatics following oral administration of RA (10 mg/kg) or RAC (at equivalent to 10 mg/kg RA) in rats (mean ± SD, n = 5 or 6); E, maximum concentration of RA achieved in mesenteric lymph nodes (MLN) (ng/g) following oral administration of RA and RAC (mean ± SD). *, p<0.05.

4.3.8. *In vitro* efficacy and synergism

The anticancer effects of BEX and RA were assessed by MTT assay using DLBCL cell lines. The GI_{50} of each drug was firstly determined in each cell line. Subsequently, cells were co-treated with different doses of RA and a range of BEX concentrations in order to obtain the GI_{50} of BEX in the presence of RA. Cell growth was significantly and synergistically inhibited by BEX in conjunction with RA at low doses in both cell lines (0.625% × GI_{50} of RA: 0.425 and 0.400 μM for DOHH2 and VAL, respectively), which is shown by the shift in dose-response curves (Figure 4-11A). The effective synergy in cell growth inhibition between the two drugs is shown as isobole plots following a previously reported method [166] (Figure 4-11B). Synergy is demonstrated by the GI_{50} values of BEX in the presence of RA (orange dots) all of which are significantly lower than the 'expected' concentrations equivalent to an additive effect (blue line). Significantly reduced GI_{50} values of BEX when RA is co-administered also demonstrates improved potency and synergy of BEX and RA in DLBCL (Figure 4-11C).

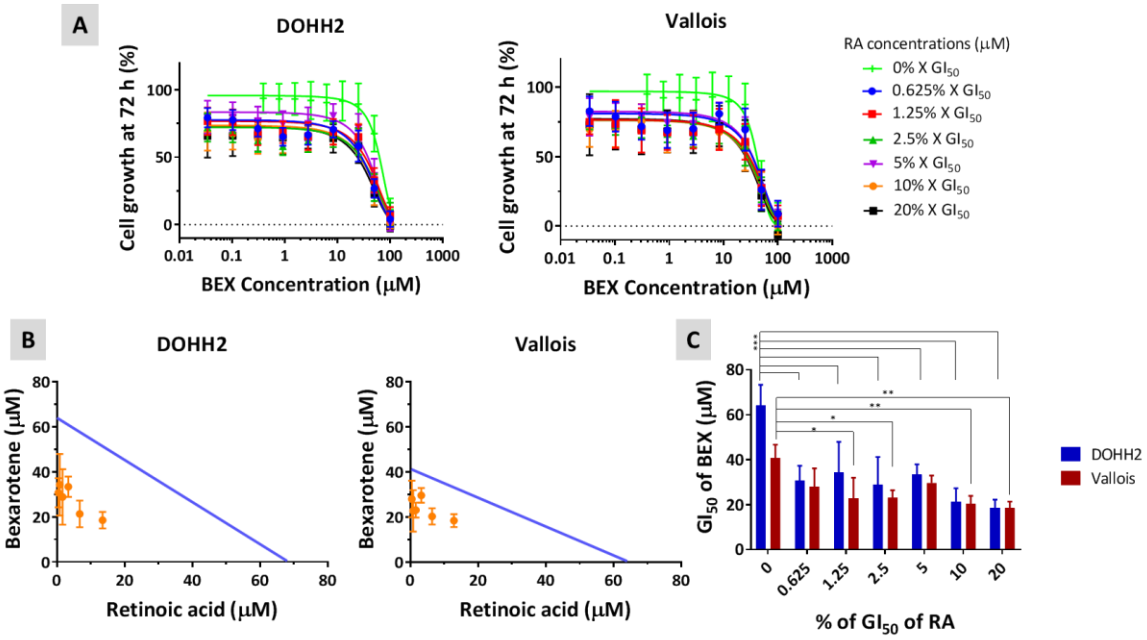


Figure 4-11. Assessment of cell growth inhibition and synergism of BEX and RA using MTT assay in DLBCL cell lines of DOHH2 and VAL. A, dose-response curves showing cell growth inhibition of BEX in presence of various concentration of RA; B, isobolograms indicating effective synergism between BEX and RA. Blue lines represent expected effectiveness when the two drugs are additive, where the *y*-intercept is GI_{50} of BEX and *x*-intercept is GI_{50} of RA. Orange dots represent GI_{50} observed with synergism (mean ± SD); C, synergism expressed by reduced GI_{50} of BEX in presence of RA. All MTT assay results shown from 4 trials of n = 6 (mean ± SD). *, p<0.05; **, p<0.01; ***, p<0.001.

4.4. Discussion

In this study, the lipophilic ester prodrug approach was applied to target drugs selectively to the intestinal lymphatics. Systemic treatment usually struggles to deliver sufficiently high concentration of drugs into the intestinal lymphatics where many immune system-related diseases prevail [27, 58, 167, 168]. The concept underlying the lipophilic prodrug approach for efficient and selective lymphatic targeting was to take advantage of the physiological process of intestinal lymphatic absorption of dietary lipids from the GI tract. Lipophilic prodrugs of BEX had substantially higher

association with CM compared with BEX. This was crucial for the current study as the association of drugs with CM in the enterocytes is the key process that determines whether lipophilic compounds can be delivered *via* the intestinal lymphatic transport pathway or not. The difference between log P and log $D_{7.4}$, therefore the ionisability of compounds at pH 7.4, has been previously discussed as the most critical physicochemical property affecting the affinity to CM [61]. The BEX prodrugs studied in this study have their prodrug moieties attached to the carboxylic acid group of BEX hence minimising the ionisability and resulting in significantly improved association (Figure 4-1 and Table 4-1).

It should be noted that the lipophilic prodrug approach to target intestinal lymphatics has been utilised in a limited number of previous studies [33]. However, much of the previous research employed TG-mimetic or long-chain fatty acid prodrug moieties in order to maximise lymphatic transport [59, 62, 66, 159, 163]. In the current work, TG-mimetic and long-chain fatty acid prodrug moieties (BUN, BOC, BOL and BTG) were also included which indeed resulted in high association with CM (Figure 4-3). However, it was remarkable that prodrugs with short-chain prodrug moieties (BME, BET and BPR) exhibited equally high affinity to CM, which indicated comparable potential for selective delivery to the intestinal lymphatics. The association was also tested with artificial emulsion (Intralipid®) which resulted in similar affinity as natural CM for most compounds. Intralipid® is a lipid emulsion mostly consisting of TG, and therefore the similarity in association suggests that the affinity to TG is the most important factor in the association of compounds with CM. However, some compounds showed significantly different association levels between artificial

emulsion and natural human CM (Figure 4-3), which indicates that surface apolipoproteins play a role in association with CM for at least some molecules [61].

Prodrugs need to release their active drug molecule in order to exert their pharmacological effects. Since the main interest of this study is delivery of active drug to the intestinal lymphatic system, it would be ideal to assess release of the active moiety directly in intestinal lymph fluid for all prodrug candidates. However, there are drawbacks to using the lymph fluid due to the practical limitations of lymph volume which could be collected which would result in excessive number of animals required and technical difficulties associated with lymphatic cannulation surgeries. Therefore, the initial screening of all prodrugs was performed by means of stability in plasma, while the most promising prodrugs were selected to assess their stability directly in the postprandial lymph. Plasma has very similar properties to lymph fluid with respect to enzymatic conversion of compounds. Although slightly lower protein binding has been observed in lymph compared to plasma for some drugs, it is known that the composition and levels of enzymes in the lymph fluid is similar to those in blood [169, 170]. Therefore, rat plasma was chosen as a surrogate model to initially screen candidate prodrugs for the enzymatic release of the active moiety.

The stability of the prodrugs tested using rat plasma showed that hydrolysis of the ester bond was the main metabolic pathway. The decrease of prodrug concentration directly corresponded to the increase of active drug (BEX) concentration and no other metabolites of the prodrugs were observed in the chromatograms. A range of half-lives were obtained from various prodrug moieties (Figure 4-5) which revealed structure-

activity relationships: 1) the length and bulkiness of prodrugs correlated with prolonged half-lives which was consistent with previous reports [171]; 2) comparison between BET vs BIP, B24 and B25 showed that the methyl group at position 1 of the prodrug moiety increased prodrug stability which is also consistent with previous reports [126].

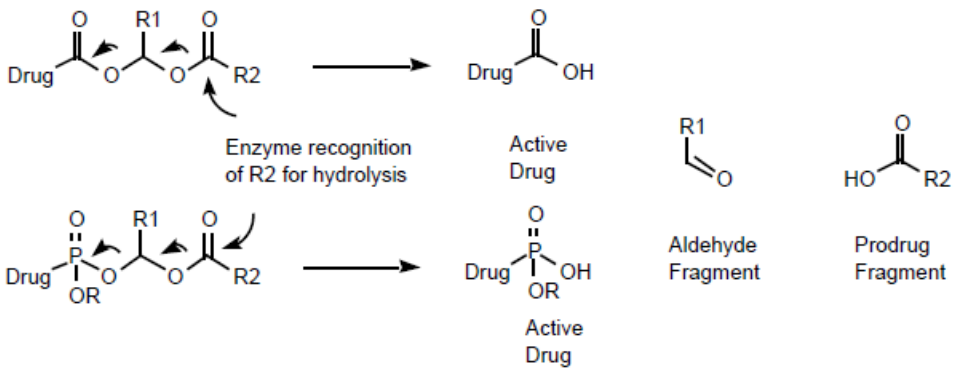
Prodrug conversion studied in FaSSIF with esterase represented degradation of the prodrugs in the GI environment prior to absorption. Only esterase was added to the FaSSIF because all prodrugs had ester bonds and the purpose of the experiment was to assess the conversion of the prodrugs by the esterase in the GI environment (pH, solubilising factors, absence of protein and temperature). An ideal prodrug for the current study would be one that is stable in the GI tract but readily releases the active drug once it reaches the intestinal lymphatics. Therefore a prodrug with a long half-life in FaSSIF with esterase and a short half-life in rat plasma would be preferred for subsequent *in vivo* studies. That being said, it has been reported that a relatively short half-life in GI fluids might not be always a significant issue in prodrug absorption [172]. In addition, lipid-based formulations can hinder enzymatic reactions in the GI tract [173]. Therefore, BET was selected as the initial candidate prodrug for subsequent *in vivo* studies as it was the most readily converting prodrug with relatively high association with CM among the first generation of prodrugs.

The plasma pharmacokinetic profiles and biodistribution of BEX to MLNs following oral administration of BEX itself were not affected by presence of lipids and the concentrations in MLNs were lower than that in plasma (Figure 4-7B). This indicates

that BEX itself had no intestinal lymphatic transport when it was administered orally in conditions which facilitate lymphatic absorption. BET (a short-chain alkyl ester prodrug) has significantly higher association with CM than BEX and therefore resulted in substantially higher concentration in the intestinal lymphatics (MLNs and lymph) compared to plasma. Successful targeting of BET to the intestinal lymphatics was achieved: the obtained concentrations were 41- and 6.0-fold higher in lymph and MLNs, respectively, than in plasma. On the other hand, the concentration of BEX, the active drug, was comparable between the three matrices of MLNs, lymph and plasma. It was demonstrated that the affinity of BET with CM was sufficient to deliver considerable concentrations of the prodrug to the lymphatics but the conversion rate was not rapid enough to yield high concentrations of BEX in the lymphatic system.

BTG (a triglyceride mimetic prodrug) was also assessed for *in vivo* pharmacokinetics and showed, comparable to BET, intestinal lymphatic targeting of BEX (Figure 4-7B). The fact that intact BTG was not found in all *in vivo* samples is consistent with a previous study which showed that TG-mimetic prodrugs are hydrolysed in the intestine before absorption and subsequent re-synthesis occurs in the enterocytes to yield TG-related molecules [159]. Conversion of BTG was not observed in rat plasma *in vitro*, but still *in vivo* it yielded levels of BEX in the intestinal lymphatics comparable to that in plasma (Figure 4-7B). This likely indicates that conversion of BTG to BEX would rely on lipase enzymes in the intestinal lumen that can recognise it as TG, rather than esterase-mediated release of BEX in plasma. The FaSSIF with added esterase activity was not able to facilitate this enzymatic reaction because of the absence of specific lipase enzymes. The lipase was not added in order to maintain simplicity of the experimental setup.

Following the *in vivo* results of BET and BTG, second generation activated ester prodrugs of BEX were designed (BCY, BGA1, BGA2, BAE1, BAE2, BAM1 and BAM2). The recognition sites for the enzymes are away from the main scaffold for these prodrugs, thereby reducing steric hindrance of the enzymatic cleavage [174]. Examples of these enzymatic reactions are depicted in Figure 4-12. Indeed, most of these molecules showed higher rates of release of active drug (BEX) compared to the first generation prodrugs (Figure 4-5). Among these activated ester candidates, BCY was selected to proceed to *in vivo* studies due to its high affinity for CM combined with the large difference between half-lives in rat plasma and FaSSIF with esterase (Figures 4-3 and 4-5). Although BGA2 was also considered as a possible candidate, its low TG solubility precluded progress to *in vivo* studies.



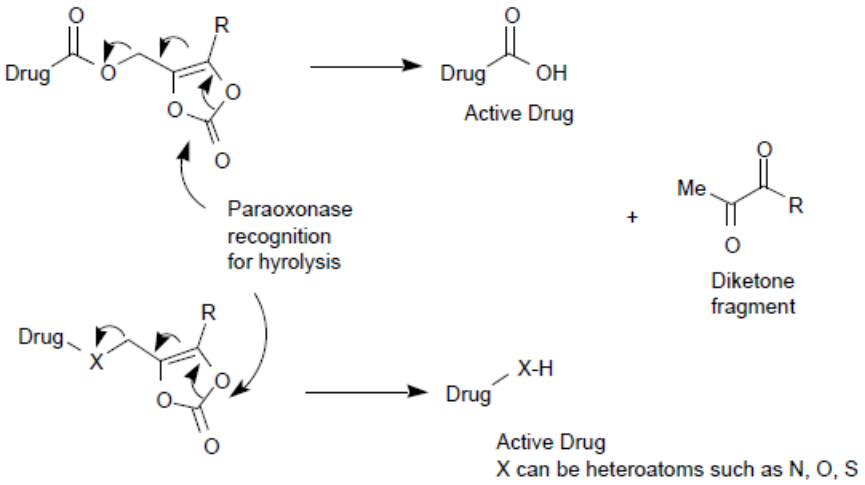


Figure 4-12. Examples of enzymatic hydrolysis of activated esters. Adapted with permission of the publisher [174].

In vivo studies with BCY showed that it indeed released higher amounts of free BEX in the lymph nodes compared to BET and BTG following intestinal lymphatic transport of the prodrug. The concentration of BEX in MLNs was 3.1-fold higher than that in plasma when BCY was administered (Figure 4-7B). The concentration of BEX in MLNs achieved by administration of BCY was 17-fold higher than that achieved by administration of BEX (Figure 4-8). It clearly demonstrated that enhanced release of BEX from the activated ester prodrug significantly improved targeting of BEX to the MLNs. It should be emphasised that the MLNs are the physiological compartment of interest as this is where the relevant cancerous cells reside, HIV hides and replicates, and lymphadenopathy persists [27, 47, 49, 52, 54, 58, 63].

It was noted that there was apparent discrepancy between the release of BEX by the prodrugs in rat plasma *in vitro* and intestinal lymphatics *in vivo*. In rat plasma *in vitro*,

the half-lives of BET and BCY were 20 and 8 min, respectively, but contrary to this rapid conversion, the release of BEX in the intestinal lymphatics *in vivo* seemed to be slower. From the *in vivo* profiles (Figure 4-7), it is evident that the prodrug resides in the intestinal lymphatics for >1 h, but the conversion to BEX was not at the level observed *in vitro* (Figure 4-5). Therefore, it was thought that the release of BEX in the intestinal lymphatic system *in vivo* was slower than the release *in vitro* in rat plasma. It was hypothesised that association of the prodrugs with lipoproteins would hinder their conversion, as the associated form would be passed on to the intestinal lymphatics. It was indeed observed that lipoprotein-associated forms of the prodrugs exhibited delayed conversion in plasma (Figure 4-6). The half-lives obtained in postprandial lymph were prolonged similarly to the lipoprotein-associated forms in plasma, which could be due to association of the prodrugs with the very high number of CM present in the postprandial lymph. This was further confirmed by the TG measurements in each test medium (Appendix 3). Taken together, it likely indicates that association with CM delays enzymatic conversion of the prodrugs in the intestinal lymphatics *in vivo* but does not prevent the release completely.

The activated ester prodrug approach was then applied to another active drug, RA. The *in vitro* and *ex vivo* CM association results of ethyl ester, RAE, and cyclic ester, RAC, confirmed that the trend of improved association was consistent with BEX prodrugs (Figure 4-10B). Similar to BEX, RA also possesses a carboxylic acid group and derivatisation of this group results in minimal ionisability of the compound. Therefore, it can be proposed that the current prodrug approach could be applied to parent drug molecules that possess carboxylic acid groups that can be easily masked and result in minimal difference between log P and log $D_{7.4}$.The activated cyclic ester prodrug was

again found to release the active moiety (RA) more rapidly than the ethyl ester prodrug (Figure 4-10C). The *in vivo* pharmacokinetics also showed similar profiles to BEX and BCY as the concentration of RA in MLNs was 2.9-fold higher than that in plasma (Figure 4-10D). The successful targeting of the prodrug to the intestinal lymphatics and the release of RA resulted in 2.4-fold higher concentration of RA in MLNs compared to when RA itself was administered orally (Figure 4-10E). This difference was not as high as that achieved for BEX by BCY, and it is thought to be due to relatively slow release of RA from the prodrug, even when the activated ester prodrug moiety was applied. This can be seen from the difference of half-lives between BCY and RAC (Figures 4-5 and 4-10).

In addition, the synergistic anticancer effects of BEX and RA were demonstrated in DLBCL cell lines (Figure 4-11). BEX is a known specific agonist for retionid X receptor (RXR) and all-*trans* RA is a specific agonist for the RA receptor (RAR) [175]. These receptors need to dimerise in order to exert their pharmacological effects and RXR can hetero-dimerise with RAR or peroxisome proliferator-activated receptor (PPAR) to regulate cell proliferation and differentiation [176]. Hetero-dimerisation between RXR-PPAR leads to cell proliferation whereas RXR-RAR hetero-dimers can evoke anti-proliferative effects and apoptosis [175]. The synergism between BEX and RA has not been reported previously and herein, it is demonstrated that such synergism between the two drugs exists. Therefore, delivering both BEX and RA efficiently and selectively to the intestinal lymphatic system adopting an activated ester approach can potentially result in better treatment for people affected by DLBCL, especially when there is significant involvement of MLNs in the disease.

In this study, specific and targeted delivery of drugs to the intestinal lymphatics utilising the lipophilic prodrug approach is reported. It had been previously stated that simple ester prodrugs would not be very efficient in enhancing intestinal lymphatic transport [59]. Indeed, lymphatic transport of BEX and RA prodrugs did not alter the overall bioavailability of the respective active drugs. However, the aim of the project was to change the paradigm of targeting intestinal lymphatics from increasing bioavailability to delivering high concentrations of the active drug to the intestinal lymphatic compartments. For this purpose, the suitable prodrugs proved to be ones that modify the physicochemical properties to increase the affinity to CM, while also readily releasing the active drug upon reaching the lymphatics. This was effectively accomplished by simple esterification, but required activated esters for enhanced release of the active moiety within the intestinal lymphatic system. The lack of change in the overall bioavailability of the active drug is in fact a substantial benefit for anticancer agents, as increased systemic exposure could lead to increased toxicity and side effects. It highlights the significance of BCY, since it increased exposure of the MLNs to BEX by 17-fold while maintaining the overall systemic bioavailability. It should be noted that in previous studies when TG mimetics or long chain fatty acids were used as prodrug approaches to deliver the drug into the intestinal lymphatics, the fold-increase in concentration achieved in MLNs was comparable to the BTG in this study, and substantially lower than what has been achieved by the activated ester approach (BCY) [159].

4.5. Conclusion

This study reports an activated ester lipophilic prodrug approach to deliver efficiently and selectively BEX and RA to the intestinal lymphatics. These two drugs have been demonstrated to exert synergistic growth inhibitory effects *in vitro* if delivered simultaneously. Prodrugs of a various range of physicochemical properties with different chain lengths and bulkiness were synthesised and assessed for targeting the active drug to the intestinal lymphatics. The findings indicate that commonly used long-chain fatty acid prodrugs and TG mimetic prodrugs might not be the most efficient in delivering the active drug to the intestinal lymphatic system. However, it was found that activated esters which promote conversion are very efficient for the purpose of delivery to and release of the active drug within the intestinal lymphatic system. The approach of activated ester prodrugs could benefit patients affected by a large number of pathological conditions with involvement of the intestinal lymphatics in the disease.

5. PERMEABILITY OF DRUGS: QUANTITATIVE ANALYSIS OF LAB-TO-LAB VARIABILITY IN CACO-2 PERMEABILITY ASSAYS

In the current PhD project, Caco-2 cell-based permeability assay was applied for testing permeability and predicting oral absorption of drug candidates, which is to follow in Chapter 6. During the establishment of the Caco-2 assay, it was noted that lab-to-lab variability can be significant in the results from the assay and that it could substantially affect prediction of oral absorption. Therefore, further research in this lab-to-lab variability was conducted and it is described in this Chapter. This Chapter has been published in the literature as Lee JB, Zgair A, Taha DA, Zang X, Kagan L, Kim TH, Kim MG, Yun HY, Fischer PM, Gershkovich P, Quantitative analysis of lab-to-lab variability in Caco-2 permeability assays, *Eur J Pharm Biopharm*. 2017 May; 114:38-42.

5.1. Introduction

The extent of gastro-intestinal absorption is one of the key properties for drugs intended for oral administration [177-182]. Of many factors that govern intestinal absorption of a compound, permeability is often tested *in vitro* by means of cell-based assays such as the Caco-2 assay [94, 178-183]. While the Caco-2 assay is the gold

standard for *in vitro* permeability assessment, interpretation of the results from such assays needs careful attention due to high lab-to-lab variability [94, 182].

This variability can be attributed to factors such as cell passage number, cell culture conditions, number of cells, cell monolayer integrity, *etc*., and can potentially mislead decisions if permeability results from different laboratories are directly compared [182]. The lab-to-lab variability itself is a known phenomenon in the field, but the extent of variability and the consequences of direct comparison of results from different laboratories have not been explicitly shown before. Therefore, the aim of this study is to compare Caco-2 permeability results between different laboratories and to evaluate potential implications of the direct use of permeability results from different laboratories for predicting oral drug absorption.

5.2. Scheme of work

Permeability studies were performed as described in Section 2.7. *In silico* simulation was conducted by procedures of Section 2.10.1. Scheme of work is shown in Figure 5-1.

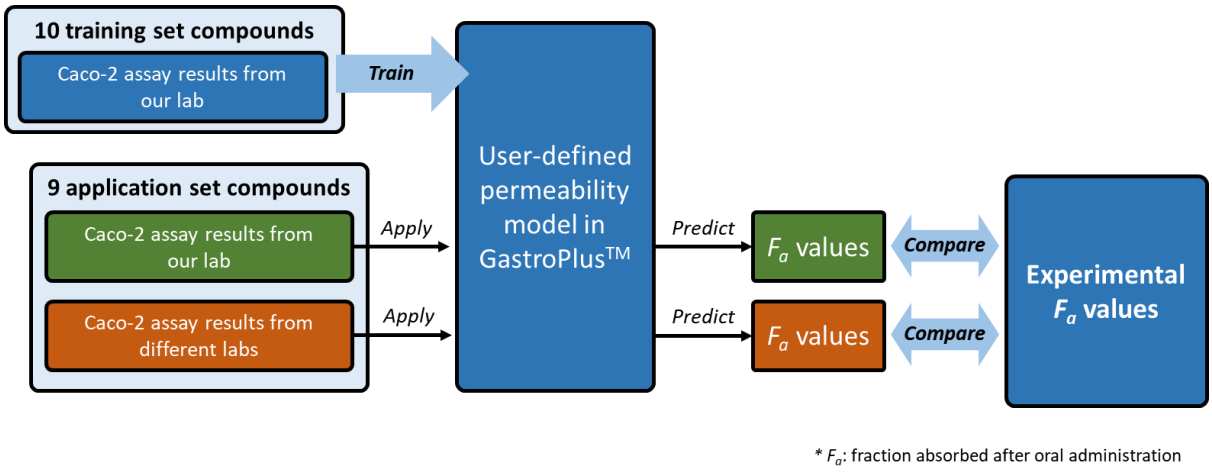


Figure 5-1. Schematic diagram of analysing lab-to-lab variability in Caco-2 assay and investigating potential impact of the variability in prediction of oral absorption.

5.3. Results and discussion

5.3.1. Permeability assay

The P_{app} values obtained from the permeability study in our laboratory are listed in Table 5-1. Human P_{eff} or F_a values plotted against Caco-2 P_{app} values from our laboratory are shown in Figure 5-2. These trends in Figure 5-2 are in agreement with previously reported results [177-180, 183]. However, substantial differences were found across the datasets from different laboratories for absolute P_{app} values for each individual compound (Table 5-1). This was demonstrated by the root mean square error (RMSE) value, which was as high as 0.581 between the P_{app} values in our laboratory and Irvine *et al.* In this particular case, the P_{app} of antipyrine was different by as much as 13-fold. Therefore it is clear that Caco-2 permeability results (P_{app}) should not be directly compared across different laboratories.

Table 5-1. P_{app} values of training set compounds from our laboratory and six different literature datasets

	Apparent permeability coefficient ($P_{app,}$ × 10^{-6} cm/s)						
Compounds	**Our laboratory**	**Alsenz *et al*[a]**	**Irvine *et al*[a]**	**Li *et al*[a]**	**Zhu *et al*[a]**	**Skolnik *et al*[a]**	**Kerns *et al*[a]**
Antipyrine	11.32	54.3	150	35.7	28.2	-	12
Furosemide	0.25	0.31	0.14	1.3	0.12	1.29	0.086
Hydrochlorothiazide	0.37	0.42	0.92	1.5	0.51	1.81	0.75
Ketoprofen	10.53	24.36	93	34.7	-	18.49	20
Metoprolol	8.19	31.77	140	33.2	23.7	17.74	2.3
Naproxen	12.71	53.07	-	33.8	39.5	31.07	28
Propranolol	11.28	47.2	110	39.4	41.9	21.29	3.3
Ranitidine	0.37	0.67	-	2.1	0.49	2.51	0.47
Terbutaline	0.27	1.71	0.41	0.8	0.38	2.38	-
Verapamil	9.67	44.67	-	45.7	-	22.68	2.4
RMSE[b]	-	0.480	0.581	0.459	0.395	0.301	0.260

[a] Values from references [177-181, 183]

[b] Root mean square error between each set of P_{app} values and experimental results from our laboratory

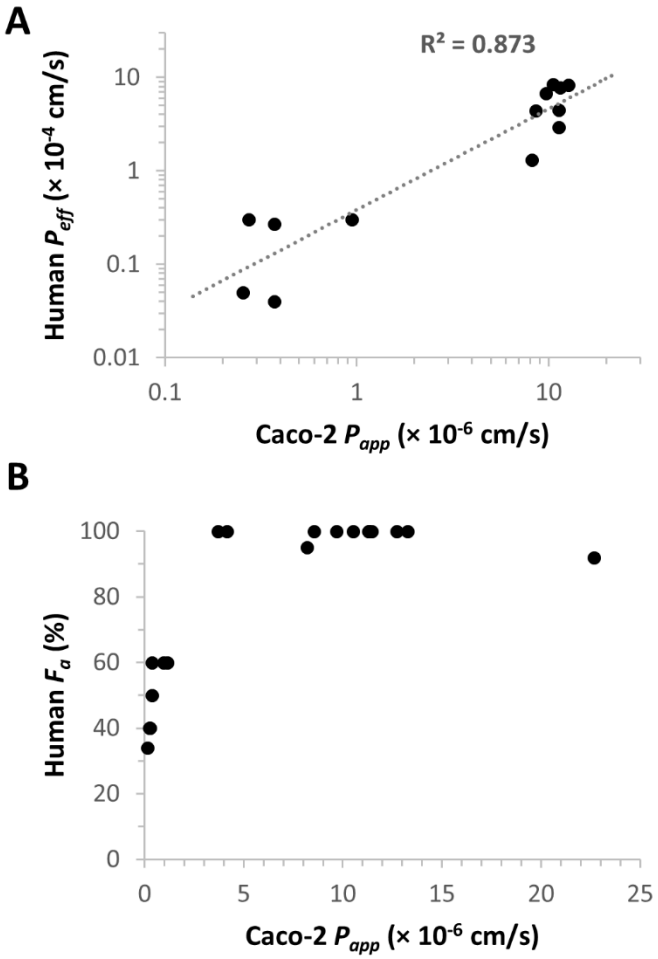


Figure 5-2. Correlation between Caco-2 P_{app} values from experimental results (i.e. our laboratory) and human P_{eff} values from the literature (A) and human F_a values from literature (B). P_{eff} values are from reference [183] and F_a values are from references [177-180, 184-187].

5.3.2. Simulation of F_a

In order to demonstrate the potential consequence of directly comparing P_{app} values across laboratories, F_a was simulated using GastroPlus™ for the application set compounds (Table 5-2). It was thought that F_a is a more informative parameter than P_{eff} for drug discovery scientists of different disciplines and also F_a values are more available in the literature compared to P_{eff} values. The simulation was performed by applying the P_{app} values obtained from our laboratory to permeability models

calibrated with different datasets. The RMSE values were calculated to assess the differences between the simulated F_a values and F_a values reported in the literature. The RMSE for F_a of the application set compounds simulated after calibration using P_{app} of the training set compounds from our laboratory was 0.128. When calibration using P_{app} of the training set compounds from other literature datasets were applied, the RMSE values for F_a across all of the application set compounds were higher in all except one case (0.119-0.275). This shows that Caco-2 Papp values cannot be related across labs due to the high lab-to-lab variability. Based on these high RMSE values, it can be seen that direct comparison of Caco-2 permeability results measured experimentally to those reported by a different laboratory can mislead interpretation and the subsequent predictions.

Table 5-2. Caco-2 P_{app} values and simulated F_a values of application set compounds

Compounds	Caco-2 P_{app} ($\times 10^{-6}$ cm/s)[a]	Intestinal absorption (F_a, %)							
		Our labor-atory[b]	Alsenz *et al.*[b]	Irvine *et al.*[b]	Li *et al.*[b]	Zhu *et al.*[b]	Skolnik *et al.*[b]	Kerns *et al.*[b]	Literature values[c]
Biopharmaceutics classification system class 1									
Desipramine	8.55	100.0	98.2	88.7	95.8	98.8	97.8	100.0	100
Dexamethasone	4.14	99.7	94.9	88.6	88.4	97.0	85.0	99.8	100
Sildenafil	22.68	100.0	99.9	98.5	99.9	99.9	100.0	100.0	92
RMSE		0.046	0.055	0.100	0.084	0.049	0.099	0.046	
Biopharmaceutics classification system class 2									
Chlorpromazine	3.7	100.0	98.3	94.2	92.8	99.3	84.9	100.0	100
Diclofenac	13.28	100.0	99.8	98.3	99.7	99.9	99.9	100.0	100
Piroxicam	11.45	99.9	98.2	91.5	97.1	98.5	98.8	99.9	100
RMSE		0.001	0.014	0.060	0.045	0.009	0.087	0.001	
Biopharmaceutics classification system class 3									
Cetirizine	1.14	87.0	59.7	58.2	36.3	74.2	16.6	93.6	60
Cimetidine	0.95	41.3	12.2	12.3	6.3	21.1	2.8	60.0	60
Pravastatin	0.14	15.8	9.8	16.4	3.3	19.3	0.2	24.7	34
RMSE		0.217	0.309	0.293	0.382	0.254	0.458	0.201	

Overall RMSE[d]	-	0.128	0.182	0.182	0.228	0.149	0.275	0.119	-

[a] Values experimentally obtained from current study

[b] GastroPlus™ simulated F_a values based on user-defined permeability models established using datasets from our laboratory, Alsenz *et al*, Irvine *et al*, Li *et al*, Zhu *et al*, Skolnik *et al* and Kerns *et al*, respectively

[c] Experimental values of intestinal absorption in humans from references [177-180, 184-187]

[d] Root mean square error between each set of F_a values and literature values

The RMSE values were further analysed according to biopharmaceutical classification system (BCS) classes (Figure 5-3). BCS class 3 compounds showed higher RMSE values than class 1 or 2, indicating that permeability-limited compounds can be more sensitive to the lab-to-lab variability. Additionally, it should be stressed that P_{app} values of known compounds (such as those in the training set) have to be evaluated before any permeability assessment can be made from a particular experimental setting. The literature dataset of Kerns *et al*. was an exception, where the RMSE was lower (0.119) than for the experimental results obtained in our laboratory.

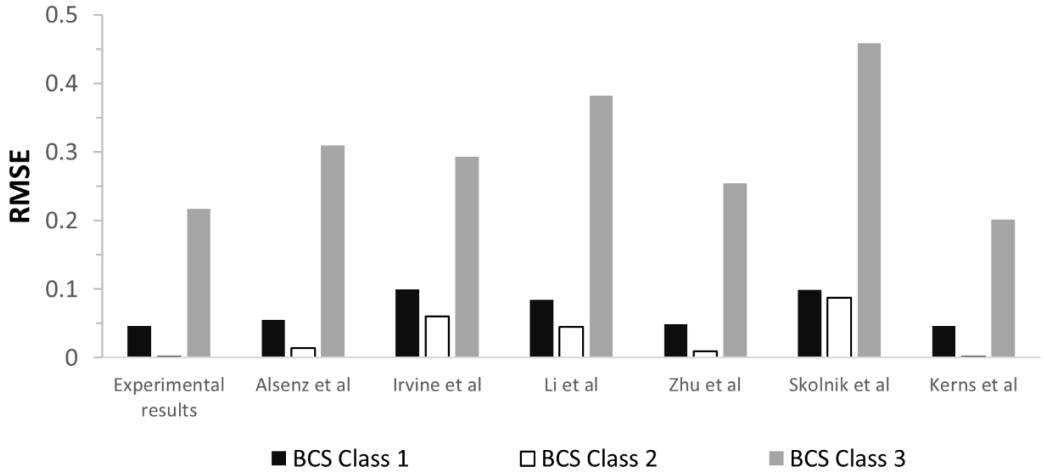


Figure 5-3. Root mean square error (RMSE) for simulated F_a values of application set compounds belonging to different BCS classes.

5.4. Conclusion

In conclusion, Caco-2 cell permeability results for the same compounds can differ substantially between different laboratories. The variability can be caused by multiple factors regarding the experimental setup of the assay including passage numbers, cell seeding density, monolayer formation period, TEER achieved and transport buffer used. Specific experimental setup used in other laboratories are summarised in Table 5-3. These differences can be critical, especially when it comes to application of these results, such as prediction of F_a. This study shows quantitative lab-to-lab variability of Caco-2 permeability results and the potential consequences this can have in application of these results in predicting intestinal absorption of drugs.

Table 5-3. Different experimental settings used in different laboratories for Caco-2 permeability assays

	Passage number	Seeding density ($\times 10^4$ cells/cm^2)	Monolayer formation (days)	TEER ($\Omega \cdot$cm^2)	Transport buffer	
					Apical	Basolateral
Our laboratory	51-54	3.75	21	280-500	HBSS + 10 mM HEPES, pH 7.4	
Alsenz *et al*	103-112	15.625	7	-	40 mM Bis-Tris/120 mM Tris-base buffer, pH 7.4	
Irvine *et al*	31-42	6.3	21-25	>230	HBSS + 10 mM HEPES, pH 7.4	
Li *et al*	32-70	6	21	300-540	DMEM	
Skolnik *et al*	23-37	-	19-23	300-400	HBSS + 10 mM HEPES, pH 7.4	
Kerns *et al*	26-40	-	21-25	-	HBSS + HEPES, pH 6.0	HBSS + HEPES, pH 7.0

The Caco-2 permeability assay established in this Chapter was applied in subsequent studies to predict oral absorption of drug candidates. When GastroPlus™ was used for application of Caco-2 assay results, the calibration by P_{app} values of the training set compounds in this Chapter was applied.

6. PHARMACOKINETIC DEVELOPMENT OF CDK9 INHIBITORS

6.1. Introduction

Oral delivery of chemotherapeutic candidates can often be limited by undesirable pharmacokinetics such as low solubility, poor permeability and rapid clearance, which are the most critical factors that govern the oral bioavailability of drugs [76, 184, 188-191]. Preclinical *in vivo* pharmacokinetic evaluations without any specific information on these parameters would result in excessive amount of time-consuming and expensive experiments. Moreover, rational drug development approach utilising *in silico* and *in vitro* assessments prior to *in vivo* experimentations will lead to more ethical research, and substantially reduce the number of animals used in experiments [20, 23]. This is an important issue, and rational drug development approach would help compliance with current rigorous regulations of animal experiments and promote implementation of the three Rs (replace, reduce and refine) in preclinical research [192-195].

In many published studies, indeed only one or two *in vitro* biopharmaceutical parameters were assessed before proceeding to *in vivo* evaluations [196-204]. However, if only one or two *in vitro* biopharmaceutical parameters are examined, it can mislead the drug discovery processes as oral absorption is an interplay between multiple factors [184, 188]. Therefore, comprehensive *in vitro* biopharmaceutical evaluations of biopharmaceutical properties coupled with *in silico* simulation of the

drug candidates is necessary to facilitate development of the most promising candidates [23, 205].

In this study, a rational drug discovery approach involving an integrated *in vitro* and *in silico* pharmacokinetic evaluation was applied to identify orally bioavailable CDK9 inhibitor candidates. CDKs belong to the serine threonine protein kinases family and are related to regulation of cell cycle and transcription [85]. Deregulated CDKs play a critical role in promoting tumour growth resulting in uncontrolled cell division, and therefore CDKs are potential therapeutic targets for cancer treatment [206, 207]. In particular, CDK9 are involved in the regulation of RNA transcription and apoptosis regulators [208]. Overexpression of CDK9 has been observed in CLL and the efficacy of CDK9 inhibitors on primary CLL cells has been reported [82]. In this study, *in vitro* biopharmaceutical properties of selected candidates were assessed and the results were incorporated into *in silico* simulation. *In vivo* oral bioavailability assessment in rats has also been performed to confirm the predictability of *in vitro* and *in silico* assessments. Further studies were carried out to assess and to optimise the biopharmaceutical properties of DF030263 in order to achieve efficient treatment of CLL following oral administration of this compound. An *in vitro-in vivo-in silico* approach was applied to provide adequate solution towards improvement of the oral bioavailability. Biopharmaceutical optimisation approaches including controlled release in the colon and postprandial conditions have also been assessed for DF030263 in this work in order to enhance systemic exposure of the compound.

6.2. Scheme of work

In vitro biopharmaceutical assessments were performed as described in Sections from 2.7. to 2.9. *In silico* simulations were conducted following Sections from 2.10.2. to 2.10.4. Procedures for *in vivo* experiments were as detailed in Sections 2.12.2. and 2.12.5. Scheme of work is shown in Figure 6-1.

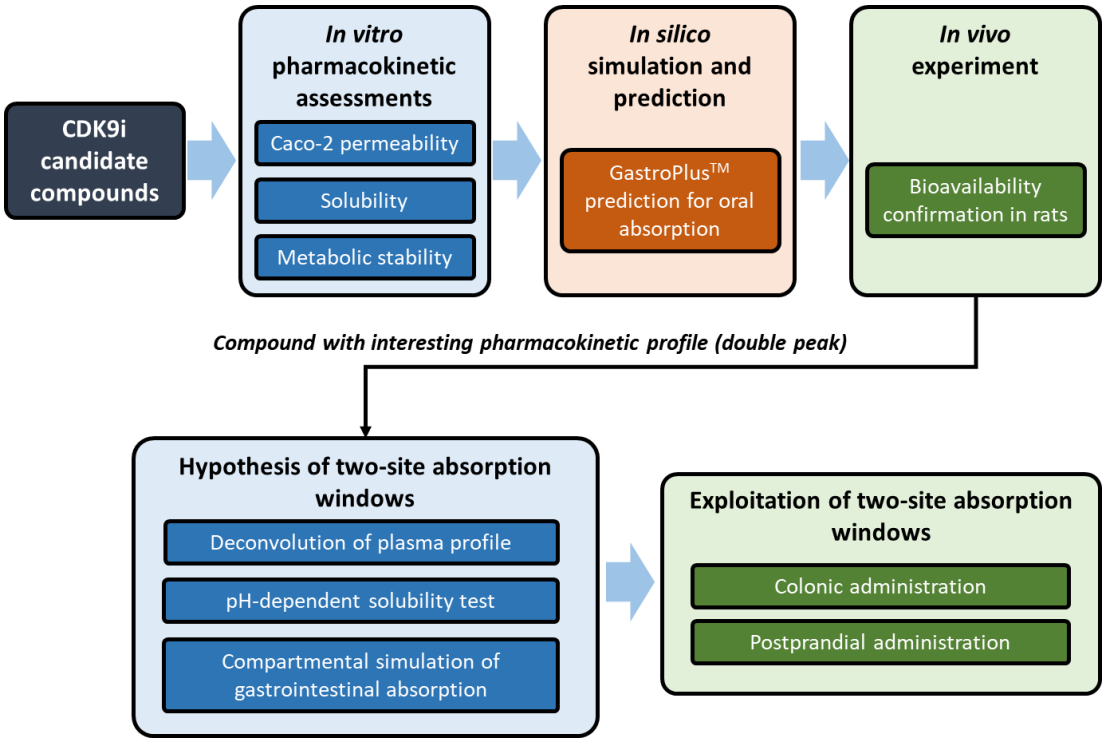


Figure 6-1. Schematic diagram of pharmacokinetic development of CDK9 inhibitors

6.3. Results

6.3.1. *In vitro* biopharmaceutical evaluation of candidate CDK9 inhibitors

Total of 11 CDK9 inhibitor candidate compounds selected based on their CDK9 K_i values and selectivity towards CDK9 compared to other off-target proteins were

assessed for the permeability, solubility and liver microsomal stability (Figure 6-2). The results from Caco-2 permeability assay are shown in Table 6-1. HS-47 showed the highest permeability with the lowest efflux ratio. The apical-to-basolateral P_{app} values for all compounds were lower than that of metoprolol (8.19×10^{-6} cm/s) in this experimental setup [93], which is the reference standard compound for high permeability recommended by the FDA [184]. Therefore none of the candidates were considered as highly permeable. The levels of S3-138 were below the lowest level of quantification (data not shown).

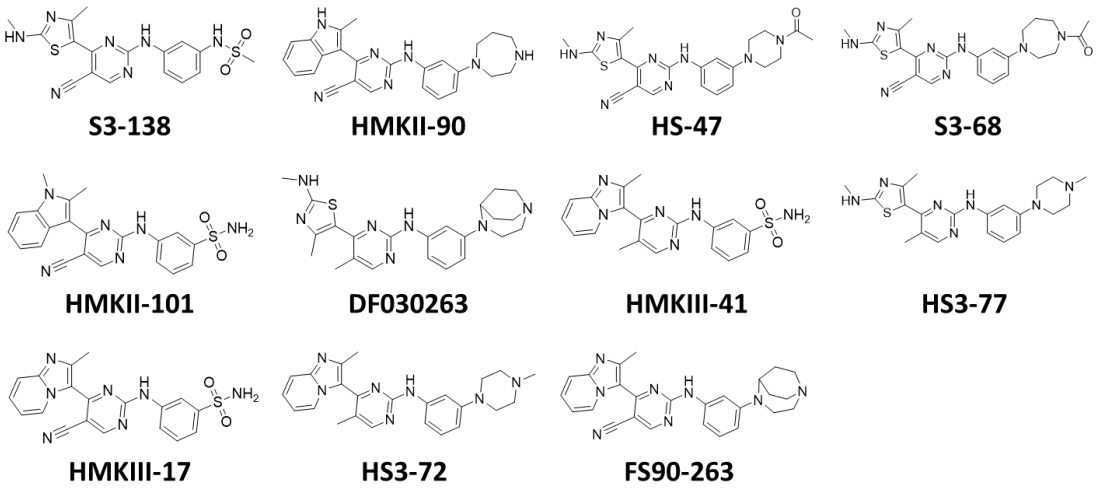


Figure 6-2. Chemical structures of the candidate CDK9 inhibitors.

Table 6-1. Caco-2 permeability results of CDK9 inhibitor candidates (mean ± SD)

Compounds	Molecular weight	CDK9 K_i (nM)[a]	P_{app} (10^{-6} cm/s)		Efflux ratio
			Apical → Basolateral	Basolateral → Apical	
S3-138	415.49	3	-	-	-
HMKII-90	423.52	7	0.3 ± 0.0	1.4 ± 0.4	4.49
HS-47	448.55	7	7.2 ± 3.8	9.6 ± 1.4	1.33
S3-68	462.58	7	4.5 ± 2.4	6.8 ± 0.1	1.49
HMKII-101	418.48	7.5	4.5 ± 0.4	7.2 ± 1.6	1.62
DF030263	435.59	10	2.5 ± 0.2	14.6 ± 0.5	5.71
HMKIII-41	394.45	16.5	0.2 ± 0.1	14.7 ± 2.8	68.73

HS3-77	409.55	20	5.6 ± 1.5	8.1 ± 0.2	1.46
HMKIII-17	405.44	21	0.2 ± 0.0	17.4 ± 1.0	98.09
HS3-72	413.53	27	5.6 ± 1.2	7.7 ± 0.2	1.38
FS90-263	450.55	35	0.2 ± 0.1	4.4 ± 1.1	23.98

[a] Inhibitory constant obtained for CDK9. Adopted from results from Fischer lab, University of Nottingham (unpublished)

Solubility results of the candidate CDK9 inhibitors are listed in Table 6-2. Most compounds showed the highest solubility in FaSSGF. For all compounds, FeSSIF resulted in higher solubility than FaSSIF. When solubility of S3-138 was tested in DDW and FaSSIF, the concentration was below the lowest limit of quantification (50 nM). HS3-77 and HS3-72 were fully solubilised at the initial test concentration (200 µM) in FaSSGF, and were subjected to additional assessment at test concentration of 500 µM with 50 mM in DMSO. Interestingly, they were fully solubilised at higher concentration as well, but further concentration escalation was not feasible due to limitation of solubility in DMSO. Therefore the results were expressed as >500 µM for HS3-77 and HS3-72 in FaSSGF.

Table 6-2. Solubility of CDK9 inhibitor candidates in biorelevant media and DDW (mean ± SD)

	Aqueous		**Solubility (µM)**		
Compounds	**Solubility (µM)**	**pH**	**FaSSGF (pH 1.6)**	**FaSSIF (pH 6.5)**	**FeSSIF (pH 5.0)**
S3-138	<50 nM	8.54	104.1 ± 4.3	<50 nM	6.9 ± 1.6
HMKII-90	100.2 ± 2.7	8.75	63.5 ± 3.7	81.3 ± 1.6	154.5 ± 2.4
HS-47	1.4 ± 0.8	8.44	179.9 ± 8.9	4.8 ± 0.6	42.5 ± 2.3
S3-68	1.6 ± 0.3	8.50	162.5 ± 1.5	7.7 ± 1.3	48.5 ± 2.2

HMKII-101	3.0 ± 0.6	8.55	0.06 ± 0.01	9.7 ± 2.2	29.4 ± 7.1
DF030263	88.3 ± 4.4	8.60	154.7 ± 10.4	109.8 ± 2.8	149.9 ± 7.9
HMKIII-41	21.9 ± 0.8	8.55	178.3 ± 0.9	18.5 ± 0.7	84.8 ± 1.4
HS3-77	56.5 ± 1.4	8.61	>500 μM	90.1 ± 2.9	163.5 ± 1.1
HMKIII-17	6.3 ± 0.4	8.51	163.6 ± 8.9	9.0 ± 0.1	27.3 ± 1.4
HS3-72	83.4 ± 1.3	8.58	>500 μM	115.8 ± 2.9	179.0 ± 4.6
FS90-263	109.3 ± 4.3	8.70	164.4 ± 7.8	109.0 ± 14.4	169.2 ± 5.1

FaSSGF, fasted state simulated gastric fluid; FaSSIF, fasted state simulated intestinal fluid; FeSSIF, fed state simulated intestinal fluid.

Metabolic stability results of the CDK9 inhibitor candidates obtained by means of human and rat liver microsomes are shown in Table 6-3. HMKIII-17 was predicted to be the least affected by the hepatic first-pass metabolism as this compound had the highest F_h values in both species tested. Compounds S3-68 and HMKII-101 showed very fast metabolism and therefore high CL_{int} values, which resulted in $CL_h = Q$ as predicted by the parallel-tube model in both tested species. Concerning the differences between the two species, CL_{int} was consistently higher in the rat but overall the F_h values were comparable. HMKII-90 showed the greatest difference in F_h between the two species by 1.5- and 2.7-fold predicted by the well-stirred and parallel- tube models, respectively.

Table 6-3. Liver microsomal metabolic stability of CDK9 inhibitor candidates in human and rat liver microsomes (mean ± SD)

	Human					
			Well-stirred model		**Parallel-tube model**	
Compounds	**Half-life (min)**	**CL_{int} (mL/min/kg)**	**CL_h (mL/min/kg)**	**F_h (%)**	**CL_h (mL/min/kg)**	**F_h (%)**
S3-138	92.2 ± 24.1	19.6 ± 4.5	10.0 ± 1.3	51.8 ± 6.1	12.6 ± 1.8	39.4 ± 8.9
HMKII-90	36.2 ± 10.8	51.4 ± 16.9	14.5 ± 1.3	29.7 ± 6.5	18.6 ± 1.3	10.1 ± 6.5

HS-47	40.5 ± 8.6	44.4 ± 10.6	14.0 ± 1.0	32.3 ± 4.8	18.1 ± 1.1	12.6 ± 5.4
S3-68	7.2 ± 0.6	242.6 ± 19.7	19.1 ± 0.1	7.9 ± 0.6	20.7 ± 0.0	0.0 ± 0.0
HMKII-101	7.7 ± 0.5	227.3 ± 15.6	19.0 ± 0.1	8.4 ± 0.5	20.7 ± 0.0	0.0 ± 0.0
DF030263	43.9 ± 4.7	39.9 ± 4.1	13.6 ± 0.5	34.3 ± 2.4	17.7 ± 0.6	14.7 ± 3.0
HMKIII-41	86.5 ± 6.3	20.2 ± 1.5	10.2 ± 0.4	50.7 ± 1.8	12.9 ± 0.6	37.8 ± 2.7
HS3-77	44.6 ± 2.8	39.1 ± 2.5	13.5 ± 0.3	34.7 ± 1.4	17.5 ± 0.4	15.2 ± 1.8
HMKIII-17	388.5 ± 78.5	4.6 ± 1.0	3.7 ± 0.6	81.9 ± 3.1	4.1 ± 0.8	80.1 ± 3.7
HS3-72	31.7 ± 3.2	55.2 ± 5.6	15.0 ± 0.4	27.4 ± 2.0	19.2 ± 0.4	7.1 ± 1.8
FS90-263	17.6 ± 1.5	99.0 ± 8.5	17.1 ± 0.2	17.3 ± 1.2	20.5 ± 0.1	0.9 ± 0.3

[a] Well-stirred model [100]: $CL_h = Q \cdot CL_{int} / (Q + CL_{int})$

[b] Parallel-tube model [100]: $CL_h = Q \cdot (1 - e^{(-CL_{int} / Q)})$

Table 6-3. (*continued*)

			Rat			
			Well-stirred model		**Parallel-tube model**	
Compounds	**Half-life (min)**	**CL_{int} (mL/min/kg)**	**CL_h (mL/min/kg)**	**F_h (%)**	**CL_h (mL/min/kg)**	**F_h (%)**
S3-138	75.2 ± 17.1	34.4 ± 9.0	21.0 ± 3.2	62.0 ± 5.9	25.4 ± 4.6	54.1 ± 8.4
HMKII-90	35.1 ± 7.1	72.8 ± 14.6	31.2 ± 2.7	43.5 ± 5.0	40.1 ± 3.9	27.4 ± 7.1
HS-47	25.2 ± 4.8	100.6 ± 17.4	35.5 ± 2.3	35.7 ± 4.2	46.0 ± 3.1	16.7 ± 5.6

S3-68	5.6 ± 0.3	444.7 ± 26.5	49.1 ± 0.3	11.1 ± 0.6	55.2 ± 0.0	0.0 ± 0.0
HMKII-101	3.2 ± 0.4	785.9 ± 109.4	51.5 ± 0.4	6.6 ± 0.8	55.2 ± 0.0	0.0 ± 0.0
DF030263	35.7 ± 1.9	69.7 ± 3.6	30.8 ± 0.7	44.2 ± 1.3	39.6 ± 1.1	28.3 ± 1.9
HMKIII-41	40.7 ± 3.5	61.3 ± 5.4	29.0 ± 1.2	47.5 ± 2.2	36.9 ± 1.7	33.1 ± 3.2
HS3-77	27.1 ± 3.9	92.9 ± 12.4	34.5 ± 1.8	37.5 ± 3.3	44.8 ± 2.5	18.9 ± 4.5
HMKIII-17	254.5 ± 98.6	10.7 ± 3.7	8.9 ± 2.6	83.9 ± 4.8	9.7 ± 3.1	82.5 ± 5.6
HS3-72	15.6 ± 6.8	177.9 ± 62.3	41.3 ± 4.4	25.1 ± 7.9	51.7 ± 4.0	6.3 ± 7.2
FS90-263	11.8 ± 0.1	210.0 ± 2.1	43.7 ± 0.1	20.8 ± 0.2	54.0 ± 0.0	2.2 ± 0.1

	Rat				
		Well-stirred model		**Parallel-tube model**	
Compounds	**CL_{int} (mL/min/kg)**	**CL_h (mL/min/kg)**	**F_h (%)**	**CL_h (mL/min/kg)**	**F_h (%)**
S3-138	34.4 ± 9.0	21.0 ± 3.2	62.0 ± 5.9	25.4 ± 4.6	54.1 ± 8.4
HMKII-90	72.8 ± 14.6	31.2 ± 2.7	43.5 ± 5.0	40.1 ± 3.9	27.4 ± 7.1
HS-47	100.6 ± 17.4	35.5 ± 2.3	35.7 ± 4.2	46.0 ± 3.1	16.7 ± 5.6
S3-68	444.7 ± 26.5	49.1 ± 0.3	11.1 ± 0.6	55.2 ± 0.0	0.0 ± 0.0
HMKII-101	785.9 ± 109.4	51.5 ± 0.4	6.6 ± 0.8	55.2 ± 0.0	0.0 ± 0.0
DF030263	69.7 ± 3.6	30.8 ± 0.7	44.2 ± 1.3	39.6 ± 1.1	28.3 ± 1.9
HMKIII-41	61.3 ± 5.4	29.0 ± 1.2	47.5 ± 2.2	36.9 ± 1.7	33.1 ± 3.2
HS3-77	92.9 ± 12.4	34.5 ± 1.8	37.5 ± 3.3	44.8 ± 2.5	18.9 ± 4.5
HMKIII-17	10.7 ± 3.7	8.9 ± 2.6	83.9 ± 4.8	9.7 ± 3.1	82.5 ± 5.6
HS3-72	177.9 ± 62.3	41.3 ± 4.4	25.1 ± 7.9	51.7 ± 4.0	6.3 ± 7.2
FS90-263	210.0 ± 2.1	43.7 ± 0.1	20.8 ± 0.2	54.0 ± 0.0	2.2 ± 0.1

[a] Well-stirred model [100]: $CL_h = Q \cdot CL_{int} / (Q + CL_{int})$

[b] Parallel-tube model [100]: $CL_h = Q \cdot (1 - e^{(-CL_{int} / Q)})$

6.3.2. *In silico* simulation of pharmacokinetic properties

The results from the permeability, solubility and metabolic stability assays were incorporated into GastroPlus™ for *in silico* simulation of pharmacokinetic properties following oral administration (Table 6-4). The pH measured in DDW was also given as input for simulation because the pH of the DDW might change as compound is added to measure the solubility. Fraction absorbed in the GI tract (F_a), fraction passed to the portal vein (F_{Dp}) and oral bioavailability (F_{oral}) were given as the outputs of simulation. S3-138 was excluded from simulation due to insufficient data available. Solubilities of HS3-77 and HS3-72 in FaSSGF were used as predicted by GastroPlus™ because exact experimental values could not be determined. Out of the ten compounds assessed, HS3-77, HS3-72 and DF030263 were predicted to have the highest oral bioavailability in the rank order of HS3-77>HS3-72>DF030263.

Table 6-4. *In silico* simulation of pharmacokinetic properties of CDK9 inhibitor candidates

	Human			**Rat**		
Compounds	**F_a (%)**	**F_{Dp} (%)**	**F_{oral} (%)**	**F_a (%)**	**F_{Dp} (%)**	**F_{oral} (%)**
HMKII-90	24.32	24.28	19.32	16.58	13.57	11.07
HS-47	17.58	17.58	15.36	29.79	29.78	24.92
S3-68	10.97	10.97	6.27	18.15	18.14	9.99
HMKII-101	3.65	3.65	2.49	18.08	18.08	9.28
DF030263	73.55	73.54	64.61	59.05	58.68	51.31
HMKIII-41	1.59	1.51	1.46	0.67	0.61	0.58
HS3-77	99.92	99.92	93.14	99.33	99.32	90.02
HMKIII-17	0.79	0.79	0.78	0.35	0.35	0.34
HS3-72	99.96	99.96	88.64	99.65	99.65	80.51

FS90-263	4.84	4.70	2.60	2.82	2.77	1.37

F_a, fraction absorbed; F_{Dp}, fraction passed to the portal vein; F, bioavailability

6.3.3. *In vivo* evaluation of pharmacokinetics

In vivo pharmacokinetic experiments were carried out in rats in order to confirm identification of orally bioavailable candidate CDK9 inhibitors. HS3-77 and HS3-72, which had the highest predicted oral bioavailability by *in silico* simulation, were initially tested *in vivo* for oral bioavailability. HS3-72 exhibited a suspected adverse effect of behaviour change (most probably related to neurotoxicity) during preliminary experiments (n = 2) immediately following intravenous administration of a lower dose (1 mg/kg). Therefore the study with HS3-72 had to be immediately terminated and no data have been generated. The plasma concentration-time profiles of HS3-77 following intravenous and oral administration are shown in Figure 6-3. HS3-77 showed rapid absorption following oral administration with T_{max} of 1 h (Table 6-5). HS3-77 was confirmed to be orally bioavailable with bioavailability of 42.7 ± 2.6%.

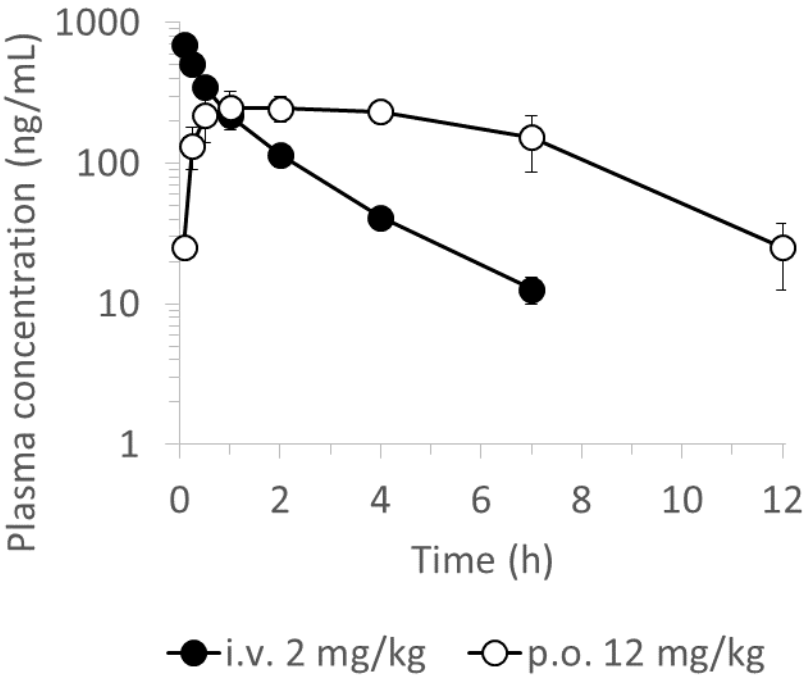


Figure 6-3. Plasma concentration-time profiles of HS3-77 following intravenous and oral administration in rats (n = 3, mean ± SD).

Table 6-5. Pharmacokinetic parameters of HS3-77 obtained from *in vivo* pharmacokinetic experiments in rats

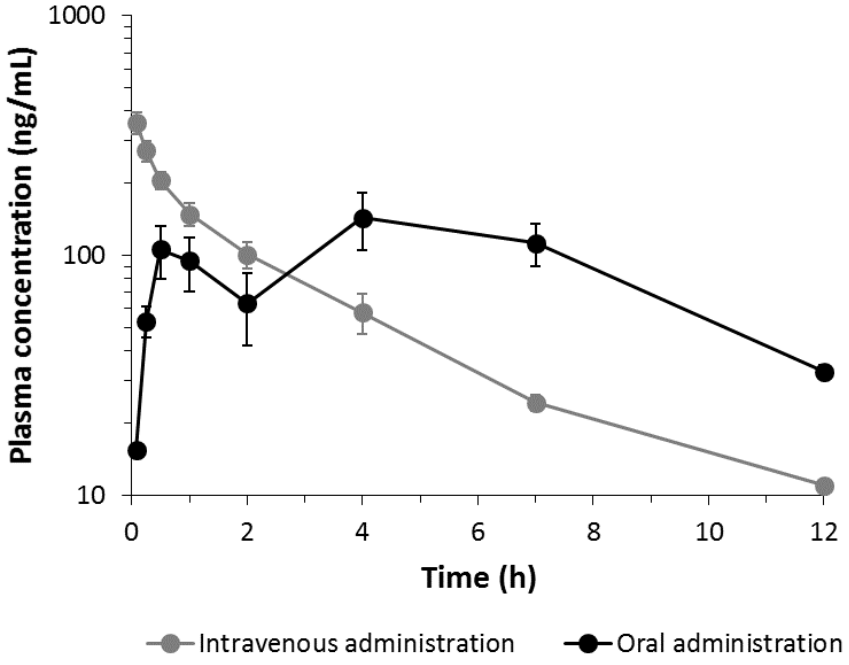
	i.v. administration		p.o. administration	
Parameter	**Mean**	**SD**	**Mean**	**SD**
Dose (mg/kg)	2	-	12	-
$t_{1/2}$ (h)	1.58	0.03	2.36	1.18
C_0 or C_{max} (ng/mL)	804	45	255	62
T_{max} (h)	-	-	1.00	0.00
$AUC_{0\rightarrow t}$	803	101	1967	106
$AUC_{0\rightarrow inf}$	832	108	2134	129
CL (mL/h/kg)	2428	298	-	-
V_{ss} (mL/kg)	4145	382	-	-
Bioavailability (%)	-	-	42.7	2.6

$t_{1/2}$, half-life; C_0, concentration extrapolated to time zero; C_{max}, maximum observed concentration; T_{max}, time of maximum observed concentration; $AUC_{0\rightarrow t}$, area under the curve from time zero to the last sampling time point; $AUC_{0\rightarrow inf}$, area under the curve from time zero to infinity; CL, clearance; V_{ss}, volume of distribution at steady state.

6.3.4. Biopharmaceutical development of compound DF030263

6.3.4.1. *In vivo* oral bioavailability evaluation of DF030263

In vivo oral bioavailability of DF030263 was also evaluated in rats as it was the third-ranked promising candidate from *in silico* simulations (Figure 6-4). The plasma concentration-time profile obtained following oral administration showed a distinct double-peak phenomenon, which was not apparent following intravenous administration. The first peak appeared after rapid absorption of the compound at 0.5 h while the second peak followed a delayed absorption, appearing at 4 h. Although the time between the two peaks varied for individual animals, this double-peak phenomenon was observed in all rats tested for oral administration (n = 4), which warranted further studies described below. The mean oral bioavailability of DF030263 was determined to be 23.8% and other pharmacokinetic parameters obtained from the plasma concentration-time profiles are shown in Table 6-6.



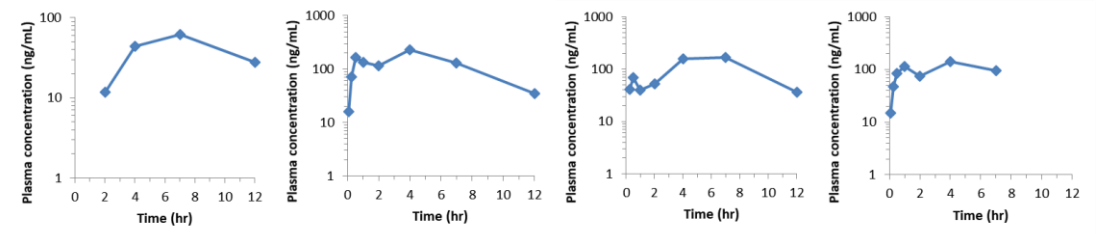


Figure 6-4. *Above*, mean plasma concentration-time profiles of DF030263 in fasted rats following intravenous (2 mg/kg) and oral (12 mg/kg) administration (n = 4, each group). *Below*, individual plasma concentration-time profiles of DF030263 in 4 fasted rats following oral administration (12 mg/kg).

Table 6-6. Plasma pharmacokinetic parameters obtained from *in vivo* pharmacokinetic experiments

	Intravenous administration	**Oral administration at fasted state**
Parameters	**(n = 4)**	**(n = 4)**
Dose (mg/kg)	2	12
C_0 (ng/mL)	410.8 ± 46.4	-
C_{max} (ng/mL)	-	149.9 ± 34.8
T_{max} (h)	-	4
CL (L/h/kg)	2.9 ± 0.4	-
V_{ss} (L/kg)	9.9 ± 1.1	-
$AUC_{0\rightarrow t}$ (h·ng/mL)	673.1 ± 98.1	960.9 ± 231.2
Bioavailability (%)	-	23.8 ± 5.7

* Colonic administration was performed by infusion for 1 h through a cannula inserted to the caecum.

** Significantly different compared to oral administration at fasted state (p <0.05).

C_0, concentration extrapolated to time zero; C_{max}, maximum concentration observed; T_{max}, time of maximum concentration observed; $t_{1/2}$, elimination half-life; CL, clearance; V_{ss}, volume of distribution at steady state; $AUC_{0\rightarrow t}$, area under the curve from time zero to the last observed point.

6.3.4.2. Deconvolution of plasma concentration-time profiles

Deconvolution of the plasma concentration-time profiles obtained from *in vivo* oral bioavailability evaluation was performed in order to understand the absorption or input function of DF030263 following oral administration. The results of cumulative input or input rate vs time are shown in Figure 6-5. It can be seen from Figure 6-5A that the absorption shows a biphasic input function; the first phase between 0-1 h and the second phase between 2-6 h. This becomes more apparent in Figure 6-5B where two peaks are shown from the input rate vs time graph. These results indicated possibility of existence of two absorption windows for DF030263 along the GI tract.

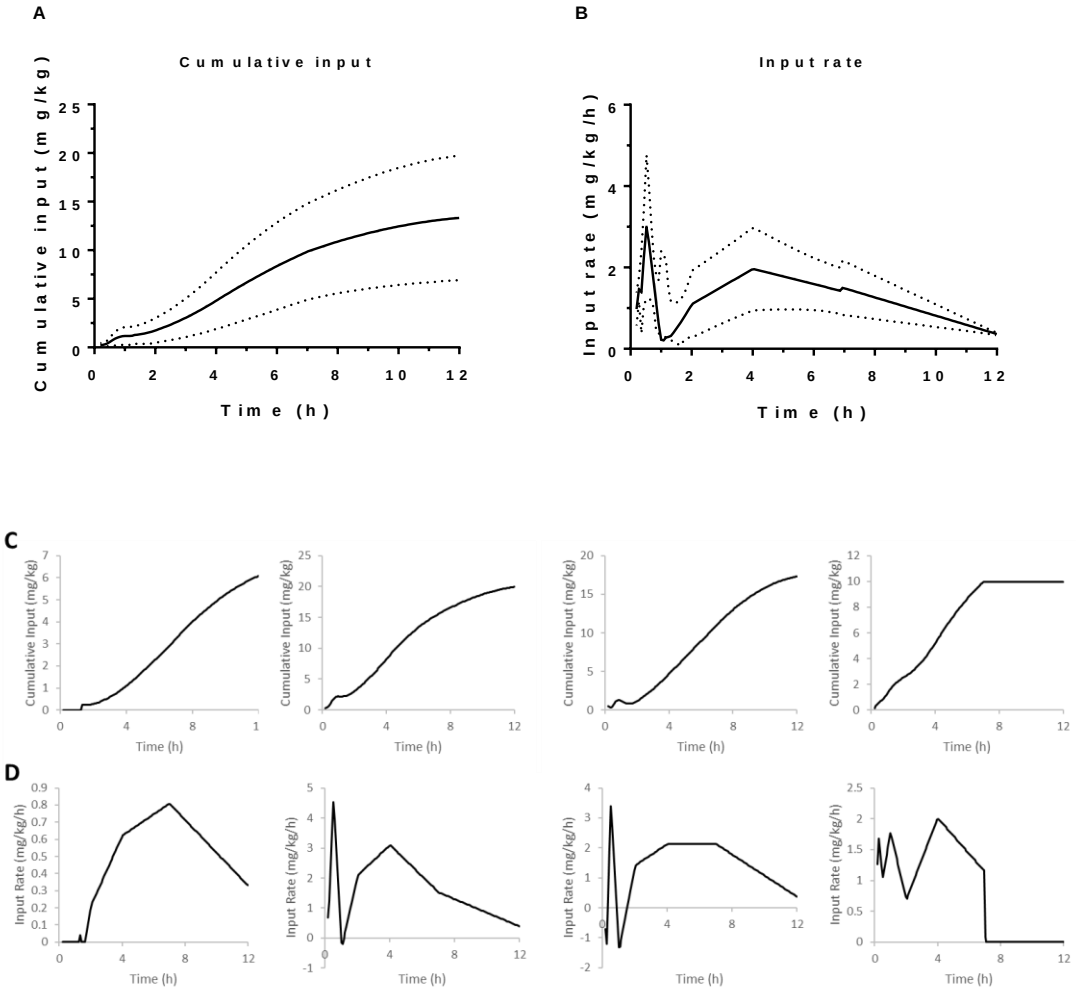


Figure 6-5. Deconvolution results of plasma concentration-time profiles obtained from oral bioavailability evaluation of DF030263. Connected lines represent mean and dotted lines represent SD. A, cumulative input vs time; B, input rate vs time; C, individual graphs for cumulative input vs time; D, individual graphs for input rate vs time.

6.3.4.3. *In vitro* solubility tests

In vitro solubility tests were conducted with simulated fluids of FaSSGF, FaSSIF and FeSSIF to provide information on solubilisation behaviour of DF030263 along the GI tract. The pH values of these simulated fluids are commonly used to represent the mean pH found in the GI tract. However, different pH values are observed in different segments of the GI tract *in vivo* [209-211]. Therefore, in this study, the pH of each simulated fluid was adjusted to represent the pH range found *in vivo* and solubility of DF030263 was tested at each pH level. In general, DF030263 showed higher solubility in acidic environment (Figure 6-6). DF030263 exhibited pH-dependent solubility especially in FaSSIF where the solubility decreased steeply when the pH increased above 6.6. This indicated that there could be high probability of precipitation in segments of GI tract with higher pH levels. This pH-dependent decrease was less apparent in FeSSIF. A limitation of this approach is that the modified pH might had effects on other components of the simulated fluids. In this case, the changes in solubility might be effects from the modified characteristics of the fluid by changes in the other components and not so much the pH. To clarify whether the solubility is purely pH-dependent, the solubility-pH profiles can be tested in buffers (without phospholipids or bile acids) of different pH levels.

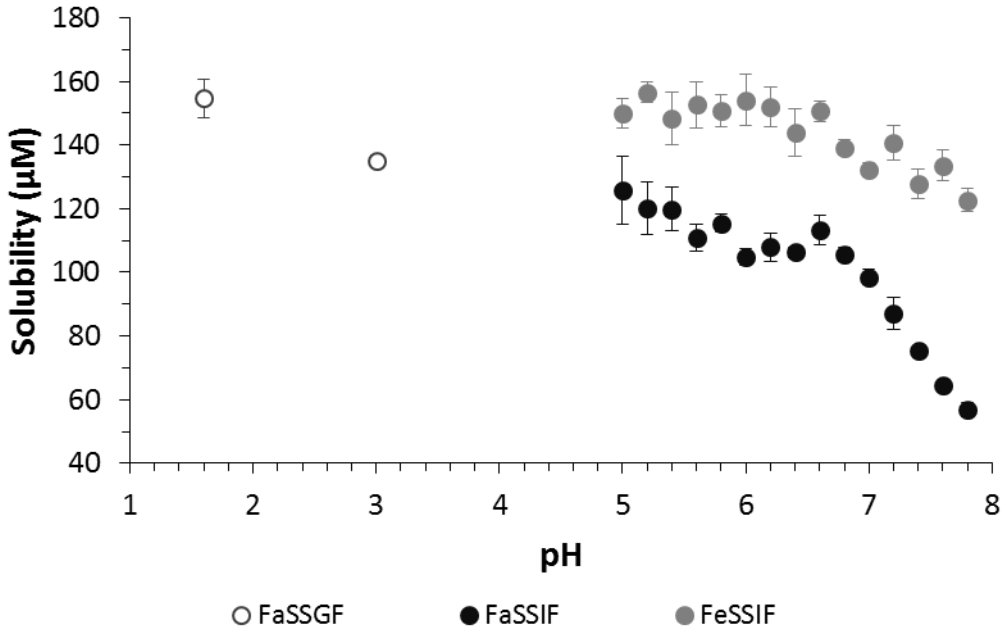


Figure 6-6. Solubility of DF030263 in FaSSGF, FaSSIF and FeSSIF at various pH (n = 3). FaSSGF, fasted state simulated gastric fluid; FaSSIF, fasted state simulated intestinal fluid; FeSSIF, fed state simulated intestinal fluid.

6.3.4.4. *In silico* simulation of intestinal absorption

In silico simulation was performed to predict intestinal absorption of DF030263 *in vivo*. GastroPlus™ utilises ACAT model for their intestinal absorption simulation [212], which compartmentalises the GI tract into nine different compartments. Therefore it was able to predict the fraction of the dose that will be absorbed at the different compartments. The simulation results at both fasted and fed states of the rat are shown in Figure 6-7. The results show that DF030263 is predicted to be firstly absorbed at the proximal regions of the small intestine and then has an additional absorption window in the caecum and colon.

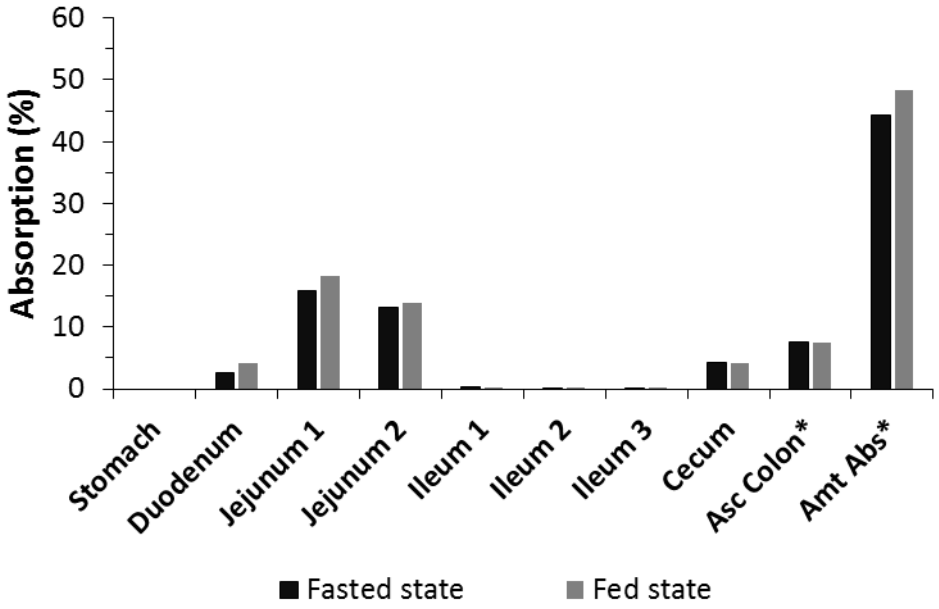


Figure 6-7. *In silico* simulation of intestinal absorption of DF030263 at each compartment of the gastrointestinal tract. *Asc Colon, ascending colon; Amt Abs, total amount absorbed in the gastrointestinal tract.

6.3.4.5. Colonic and postprandial administration of DF030263

Following the above results, colonic and postprandial administration of DF030263 were evaluated in order to improve oral bioavailability of DF030263. Colonic administration was delivered by infusion through the cannula inserted to the caecum for 1 h to mimic controlled release of the drug in the large intestine. Postprandial oral gavage administration was performed on rats that had free access to food and water throughout the experiment. The double-peak phenomenon observed after administration by oral gavage at fasted state was not seen in the case of postprandial administration or colonic delivery (Figure 6-8). Colonic administration resulted in rapid absorption (T_{max} = 1.5 h) but no improvement in bioavailability was noted (Table 6-7). On the other hand, oral administration at fed state resulted in significantly higher C_{max} and bioavailability compared to fasted state.

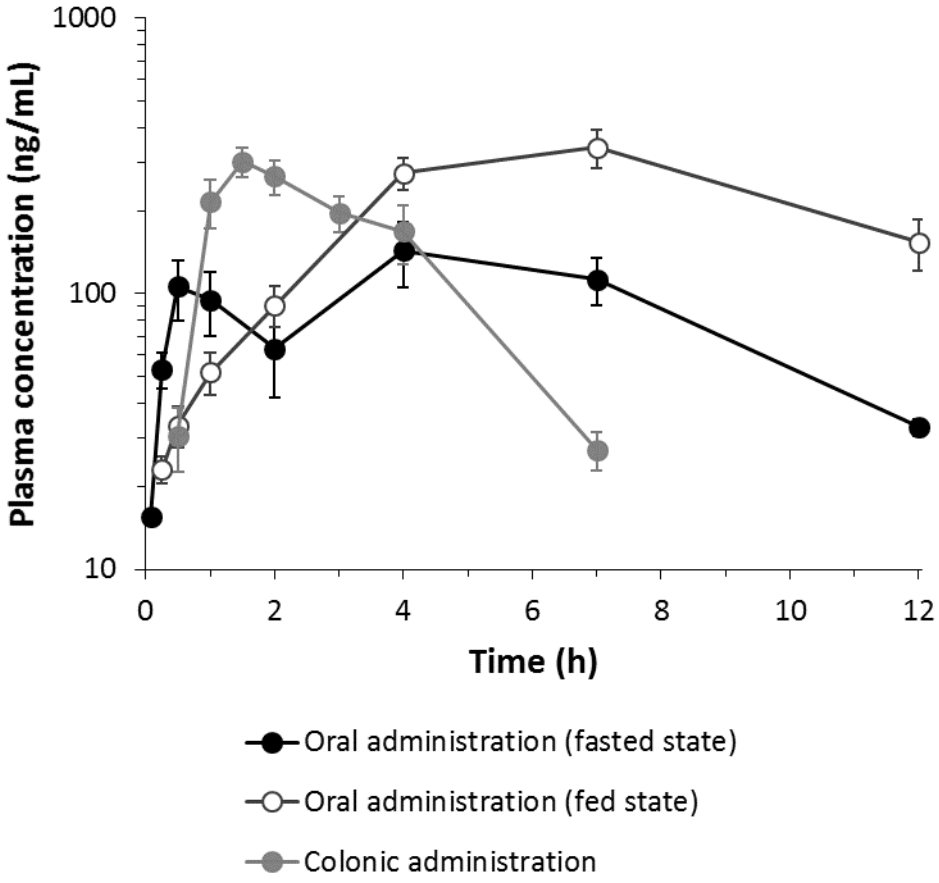


Figure 6-8. Mean plasma concentration-time profiles of DF030263 in rats following oral administration at fed state (12 mg/kg, n = 6) and colonic administration (12 mg/kg, n = 3).

Table 6-7. Plasma pharmacokinetic parameters obtained from *in vivo* pharmacokinetic experiments for fed state and colonic administration

Parameters	Oral administration at fed state (n = 6)	Colonic administration (n = 3)*
Dose (mg/kg)	12	12
C_0 (ng/mL)	-	-
C_{max} (ng/mL)	346.6 ± 50.3**	302.2 ± 37.1
T_{max} (h)	7	1.5
CL (L/h/kg)	-	-
V_{ss} (L/kg)	-	-

$AUC_{0\rightarrow t}$ (h·ng/mL)	2570.2 ± 382.4**	978.9 ± 143.8
Bioavailability (%)	63.6 ± 9.5**	24.2 ± 3.6

* Colonic administration was performed by infusion for 1 h through a cannula inserted to the caecum.

** Significantly different compared to oral administration at fasted state (p <0.05).

C_0, concentration extrapolated to time zero; C_{max}, maximum concentration observed; T_{max}, time of maximum concentration observed; $t_{1/2}$, elimination half-life; CL, clearance; V_{ss}, volume of distribution at steady state; $AUC_{0\rightarrow t}$, area under the curve from time zero to the last observed point.

6.4. Discussion

6.4.1. Rational drug development approach utilising in vitro-in silico-in vivo pharmacokinetic evaluations

Eleven CDK9 inhibitor candidates, selected based on their *in vitro* efficacy and selectivity to the CDK9, were studied for their pharmacokinetic properties using a rational early drug development approach. *In vitro* biopharmaceutics was evaluated in terms of permeability, solubility and metabolic stability and *in silico* simulation was performed using GastroPlus™ to integrate the results from *in vitro* studies. Finally, *in vivo* pharmacokinetic experiments were performed to confirm the identification of an orally bioavailable CDK9 inhibitor candidate. This study shows a demonstration of a rational drug discovery approach utilising *in vitro* and *in silico* pharmacokinetic evaluations prior to *in vivo* studies in order to efficiently identify orally bioavailable drug candidates.

While none of the compounds could be classified as highly permeable, HMKII-90, DF030263, HMKIII-41, HMKIII-17 and FS90-263 demonstrated efflux ratio>2

(Table 6-1) in Caco-2 cells permeability experiments, which indicates that they could be substrates for the efflux transporters, such as p-glycoprotein [213, 214]. This could be potentially important, as these candidate compounds are intended for treatment of cancer, where substrates for such efflux transporters can be limited by multi-drug resistance developed by the cancerous cells [215-217]. In a previous study, primary samples from CLL patients also showed correlation between expression of p-glycoprotein and multi-drug resistance, which could be a possible concern for these compounds [217].

For most compounds, solubility was enhanced in acidic environment of FaSSGF (pH 1.6), owing to their weakly basic chemical properties (Table 6-2). All compounds showed higher solubility in FeSSIF than in FaSSIF which indicates that solubilisation of the compounds would be improved at fed state. The contents of GI lumen at fed state is different from the fasted state mainly in levels of phospholipids and bile acids, which leads to change in the pH, buffer capacity and surface tension of intestinal fluids [96, 218].

In the metabolic stability assay, it is generally considered that compounds with $F_h \leq 30\%$ are highly susceptible for extensive hepatic first-pass metabolism [102, 219]. Therefore, all the compounds except S3-138, HMKIII-41and HMKIII-17 were predicted to be highly influenced by the hepatic first-pass metabolism during the oral absorption process (Table 6-3).

The results of the *in vitro* biopharmaceutical evaluations were incorporated into GastroPlus™ and *in silico* simulation was performed to predict the pharmacokinetics in humans and rats following oral administration (Table 6-4). The properties of permeability, solubility and metabolic stability of the compounds are considered to be the most critical characteristics affecting the oral bioavailability [184, 188-191]. GastroPlus™ software was used as a tool that compiles the factors which could affect oral bioavailability and provide reasonable pharmacokinetic prediction [92, 220-223]. From the simulation results, it was predicted that compounds of HS3-77, HS3-72 and DF030263 compounds would have oral bioavailability of >50%.

To confirm that an orally bioavailable CDK9 inhibitor candidate was identified, *in vivo* pharmacokinetic experiments were performed with the most promising candidates (Figure 6-3 and Table 6-5). The mean oral bioavailability of HS3-77 was 42.7% which was not as high as predicted by the *in silico* simulation (90.0%). This indicated that there could be additional factors to permeability, solubility and metabolic stability that govern oral bioavailability which were overlooked in this study. Such factors could include formulation effect or precipitation rate of the compounds. Another reason could be that the models used in GastroPlus™ have not been validated. Additionally, more advanced techniques could have been applied for in vitro biopharmaceutical screening to improve the relevant *in vitro-in vivo* correlation (discussed further in Chapter 7).

Overall structure-property relationship analysis of the candidate CDK9 inhibitors is summarised in Figure 6-9. Substitution of the bicyclic ring group of DF030263 with a

methyl piperazine group increased permeability and solubility in FaSSGF (Panel A). Substitution of the *N*,4-dimethylthiazol-2-amine group of HS3-77 with a 2-methylimidazo[1,2-a]pyridine group resulted in comparable permeability and solubility but decreased metabolic stability (Panel B). To note, this substitution also caused acute toxicity. The methyl piperazine group of HS3-72 substituted with a sulfonamide group increased metabolic stability by removing a metabolically labile group but dramatically reduced permeability (Panel C). Addition of a cyanide group to HMKIII-41 also increased the metabolic stability but decreased solubility in all fluids (Panel D). This was unexpected as a cyanide group should increase the polarity of a compound and one could expect improved solubility from this substitution. When a methyl group was added to HMKIII-17, permeability was increased but the methyl group showed high liability for metabolic clearance (Panel E). The *N*,4-dimethylthiazol-2-amine group of DF030263 was substituted with a 2-methylimidazo[1,2-a]pyridine group and a cyanide group was added to DF030263. These structural changes resulted in decreased metabolic stability as seen with HS3-77 and HS3-72 and decreased permeability as seen with HMKIII-41 and HMKIII-17 (Panel F). Substitution of the bicyclic ring group of FS90-263 with a homopiperazine group increased metabolic stability but elimination of a tertiary amine resulted in decreased solubility in FaSSGF (Panel G). Substitution of the 7-membered ring group of S3-68 with a 6-membered ring group resulted in increased metabolic stability with comparable permeability and solubility; the cyanide group and the sulfonamide group of S3-138 resulted in minimal permeability and solubility (Panel G). Only statistically significant increase or decrease ($p<0.05$) are mentioned in the above structure-property relationship analysis.

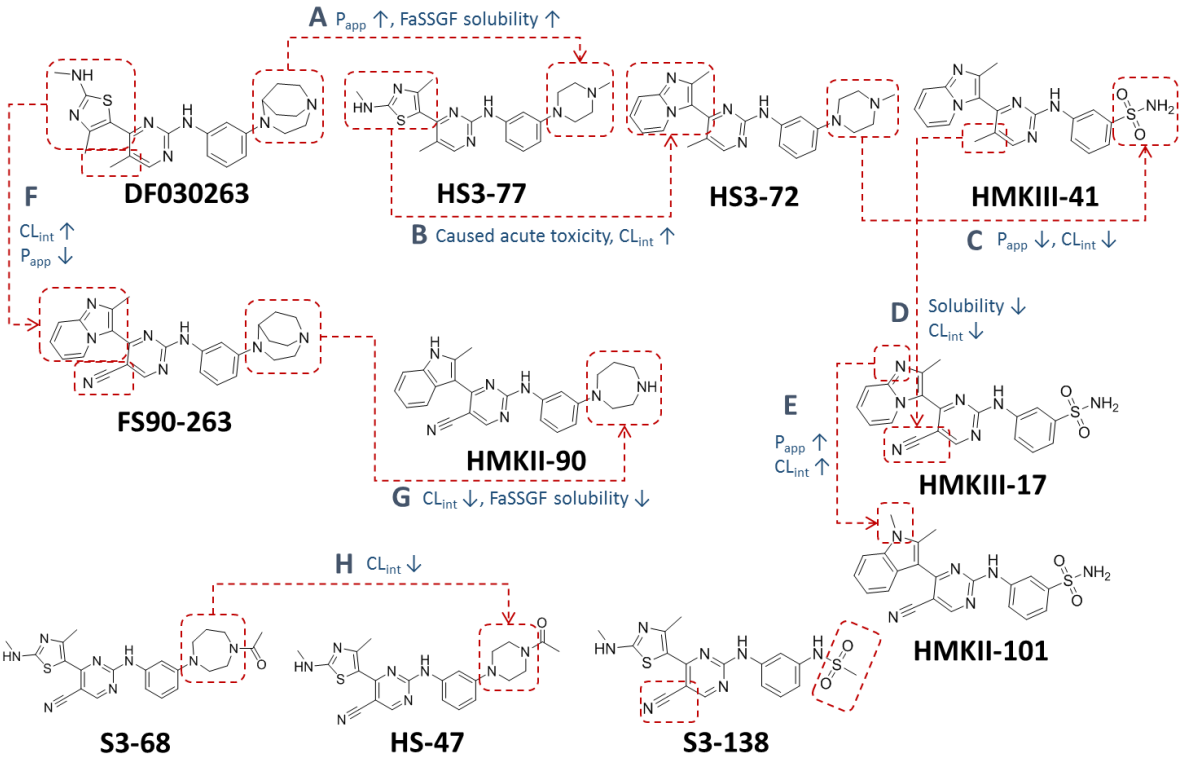


Figure 6-9. Structure-property relationship of the candidate CDK9 inhibitors.

Literature search shows that there are a number of studies in which *in vivo* pharmacokinetic screening was performed without any *in vitro* biopharmaceutical evaluations during identification of orally bioavailable therapeutic candidates [224-228]. Not only would this approach have been costly and time consuming, but also would result in sub-optimal implementation of the three Rs in preclinical research [194]. In addition, when some compounds did not show favourable pharmacokinetics *in vivo*, specific reasons behind these results could not be identified and therefore direction for design of additional candidates could not be derived efficiently. There are even some studies where a single lead candidate was selected for *in vivo* oral bioavailability experiments relying on *in vitro* efficacy profiles only [229, 230]. In these cases, candidates that are overall more promising might have been neglected

because optimisation of treatment should be a combination of pharmacokinetics and pharmacodynamics.

Moreover, many studies only applied one or two *in vitro* biopharmaceutical assessments before conducting *in vivo* pharmacokinetic studies [196-204]. However, oral bioavailability is a result of interplay between several factors; mainly solubility, permeability and metabolic stability [184, 188]. This is demonstrated in this current study where the bioavailable compound HS3-77 was not the most soluble, most permeable, or most metabolically stable compound from the list. It should be stressed, that if the candidates were chosen based on metabolic stability alone, as done in many other studies [198-204], HS3-77 would have been one of the least compounds to test *in vivo* pharmacokinetics. It has also been demonstrated in this study that chemical modification for optimisation of a single biopharmaceutical parameter might not result in improvement of the oral bioavailability, especially as it might affect other properties. This is exemplified by Panel C in Figure 6-9 where efforts to increase metabolic stability decreased permeability and therefore overall predicted bioavailability was reduced by 61-fold.

On the other hand, some studies actually had comprehensive evaluations of *in vitro* biopharmaceutical properties prior to *in vivo* experiments [231, 232]. However, the rationale behind the selection of candidates for *in vivo* experiments in these studies was often obscure and unexplained. Therefore there is a need for a justified approach to the integration of various *in vitro* biopharmaceutical parameters and utilisation of them in promoting the most desirable candidates. In this study, *in silico* simulation

using GastroPlus™ was utilised as a platform that can integrate the *in vitro* evaluation results. Such *in silico* simulation would be useful to give a rank-order of compounds and select those to be prioritised for further development.

6.4.2. Biopharmaceutical development of compound DF030263

6.4.2.1. *In vivo* oral bioavailability evaluation and the double-peak phenomenon

Following *in vivo* pharmacokinetic evaluation of compounds HS3-77 and HS3-72, DF030263 was also assessed *in vivo* as it was the third-ranked in predicted bioavailability and it has remarkable activity towards CDK9. In the initial *in vivo* oral bioavailability evaluation, DF030263 showed mean oral bioavailability of 23.8%. Interestingly, a distinct double-peak phenomenon was observed and it only appeared after oral administration of DF030263 (Figure 6-4). Similar double-peak phenomenon following oral administration has been reported for a number of drugs including acetaminophen [233], alprazolam [234], cimetidine [235], epinastine [236], furosemide [237], pafenolol [238], ranitidine [239] and veralipride [240]. This phenomenon is usually attributed to the following three main causes [234, 239, 241-244]: 1) enterohepatic recirculation where the drug in the systemic circulation is secreted via bile and reabsorbed from the GI tract; 2) variable absorption properties along the GI tract (also called "absorption windows"); 3) gastric emptying time is varied depending on motility of the GI tract, gastric pH or the lipidic formulation effect. In all cases, this erratic pattern of absorption can potentially be problematic for CDK9 inhibitors as relatively narrow therapeutic window is known to be one of their potential drawbacks [245].

In the case of DF030263 compound, enterohepatic recirculation was excluded from the possible reasons because the plasma concentration-time profile following intravenous administration did not show a double peak. Variance in gastric emptying time was also unlikely to be the reason because the time between the two peaks was as long as 3-6.5 h. Moreover, all four rats orally administered at fasted state displayed double-peaks. Therefore, absorption window of DF030263 in the GI tract was thought to be discontinuous and further studies were conducted to elaborate the two-site absorption windows hypothesis.

6.4.2.2. Two-site absorption windows hypothesis

Deconvolution of the plasma concentration-time profiles were conducted to elucidate absorption rate over time for DF030263 following oral administration. Deconvolution represents a mathematical process that can inversely uncover the input function when the oral administration profile is known and drug disposition characteristics are defined by the intravenous administration profile [246]. This allows determination of the absorption characteristics which can often be challenging to measure or quantify *in situ* [247]. As shown in Figure 6-5, the absorption function of DF030263 exhibited a biphasic process which leads to the two-site absorption.

The two-site absorption windows hypothesis was further supported with the results of the *in silico* simulation using GastroPlus™. The built-in ACAT and generic physiologically-based pharmacokinetic models in the software provide effective predictions of pharmacokinetic profiles in preclinical species and humans [248-251].

In this study, intestinal absorption of DF030263 in different compartments of the rat GI tract was predicted. The simulation results predicted clear discontinuation of absorption in the distal region of the small intestine and a second absorption window in the large intestine (Figure 6-7). Additionally, the secondary absorption phase following oral administration also corresponded to the oral-to-caecal transit time in rats (2-3 h) [238, 252]. This corroborated the assumption that a second absorption window exists in the large intestine. Such site-specific absorption of drugs is known to occur due to properties related to solubility, stability or interaction with luminal contents [253].

The luminal pH levels can differ in different segments of the GI tract and therefore *in vitro* solubility tests were carried out in a range of pH using simulated biorelevant media of FaSSGF, FaSSIF and FeSSIF. The solubility of DF030263 was maintained at the highest levels in the acidic environment of FaSSGF and the lower pH ranges of FaSSIF and FeSSIF (Figure 6-6). This is explained by the fact that DF030263 is a weak base with a pK_a of 10.7 (predicted by ACD/Labs, Toronto, Canada) and therefore would be solubilised more efficiently in such acidic environment. When the pH level was increased above 6.6, DF030263 showed pH-dependent solubility with decreasing solubility especially in the FaSSIF. This suggested that DF030263 could be precipitating in the regions of the GI tract where the pH is relatively high, such as the distal small intestine. The luminal pH in the rat small intestine increases as it reaches the distal region; from pH 6.5 in the duodenum to 7.1 in the ileum [209]. This possibility of precipitation in the small intestine with higher pH has been acknowledged especially for weakly basic compounds and it has been put forward as a critical drug development obstacle, significantly limiting the oral bioavailability of

these compounds [218]. The luminal pH drops again when it reaches the colon to 6.6 [209], which can provide opportunity for DF030263 to resolubilise and be available for absorption again. The pH-dependent solubility was therefore thought to be the main reason behind the two-site absorption windows. Since humans have a similar luminal pH levels pattern to rats, this phenomenon is likely to occur in humans as well [211, 254].

6.4.2.3. Exploitation of the two-site absorption windows

In order to improve the oral bioavailability of DF030263, the pH-dependent solubility and potential precipitation in the distal region of the small intestine had to be mitigated. Colonic administration mimicking controlled release of DF030263 in the large intestine and postprandial oral administration were tested for this purpose. Deconvolution and *in silico* simulation of the intestinal absorption both indicated a second absorption window in the large intestine. Additionally, when partial AUC is calculated for the oral administration profile at fasted state, the window between 2-12 h accounts for 86% of the total AUC. With all the above-mentioned factors, colonic administration was thought to possibly improve the bioavailability of DF030263.

Colonic administration was performed via a cannula inserted into the caecum and DF030263 solubilised in the dosing vehicle was infused for 1 h. Therefore it would not pass through the distal region of the small intestine where the pH is relatively higher and the solubility of DF030263 is lower. Consequently, potential loss in absorption of DF030263 due to the precipitation-resolubilisation process can be avoided.

As shown in Figure 6-8, colonic administration resulted in rapid absorption and only single peaks were observed in all rats tested. This is consistent with a previous study where pafenolol, which had double-peak following oral administration, showed a single peak when administered through an intraintestinal cannula to target a specific absorption window in the GI tract [238]. In spite of the single peak, colonic delivery did not improve the bioavailability of DF030263, but it was rather comparable to the oral administration at fasted state (Table 6-6). As a result, it was confirmed that the large intestine is indeed an absorption window but oral bioavailability cannot be improved by controlled release to this site. It is likely that the amount of dose that can be absorbed from the large intestine has been already absorbed from simple oral administration.

Postprandial oral administration was also tested mainly based on the premise that solubility is enhanced in fed conditions. The *in vitro* solubility results in Figure 6-6 clearly show that in FeSSIF, the solubility was higher and was less dependent on the change of pH. The presence of food in the GI tract modifies the luminal contents which leads to changes in pH, buffer capacity and surface tension thereby affecting solubilisation of drugs [218]. Therefore less precipitation of drugs can be anticipated at fed state especially for weak bases with poor solubility [218] which means that more drug can be available for absorption. Also an important food-effect is the delay in gastric emptying which alters the GI transit time [253]. This delay can allow the drug to reside longer time at the first absorption window which is the proximal region of the small intestine.

The plasma concentration-time profile following postprandial oral administration showed a single-peak with substantially improved bioavailability (Figure 6-8 and Table 6-6). Avoidance of the double-peak phenomenon by the food-effect has been previously reported [244, 252] but did not necessarily relate to increase in bioavailability. In the case of DF030263, higher solubility, less precipitation and prolonged exposure to the first absorption window had significantly positive effects towards improving the oral bioavailability. Delayed gastric emptying had also caused extended absorption phase resulting in T_{max} of 7 h. It is also noteworthy that the variability in the bioavailability was reduced at fed state (Table 3), which is crucial for drugs such as CDK inhibitors where the narrow therapeutic window is a limitation [245].

To note, there could be interspecies differences between the rats and the humans in the GI physiology and luminal contents which might result in different food effects. However, the changes of pH between fasted and fed states are similar between the two species and the rat intestinal fluid has slightly higher concentration of bile salt and phospholipid compared to the FeSSIF [210, 254, 255]. Therefore, similar pattern of food effect could be expected in humans although the extent might vary.

6.5. Conclusion

In this study, a rational development of CDK9 inhibitors is reported. Traditional *in vitro* biopharmaceutical experiments were coupled with *in silico* simulation tools in

order to efficiently identify the most promising candidate prior to *in vivo* experimentation. From these assessments, it was predicted that HS3-72, HS3-77 and DF030263 would have the highest oral bioavailability. The prediction was based on the combined net effect of permeability, solubility and metabolic stability on the oral bioavailability. *In vivo* oral bioavailability experiments were carried out in rats to confirm the findings. As a result, orally bioavailable candidate HS3-77 was has been identified, with bioavailability on rats as high as 42.7%. This study shows a rational approach in drug discovery involving pharmacokinetic assessments where various factors are integrated in identification of orally bioavailable drug candidates. This approach would not only improve efficiency in drug discovery and development but would also reinforce efficient implementation of the three Rs in preclinical research.

Further biopharmaceutical development with compound DF030263 demonstrated an *in vitro-in vivo-in silico* approach in improving the oral bioavailability. The two-site absorption windows hypothesis was suggested and supported by *in vitro* and *in silico* studies following observation of a double-peak phenomenon *in vivo*. Exploitation of the two-site absorption was attempted in order to improve the bioavailability. Colonic administration confirmed that the large intestine is a second absorption window but indicated that controlled release to the colon would not enhance the drug exposure. Instead, oral administration at fed state took advantage of the food-effect in terms of improved solubilization, reduced precipitation and delayed GI transit time, thereby increasing the bioavailability.

7. GENERAL DISCUSSION AND FURTHER WORK

7.1. General discussion

In this PhD project, optimisation of treatment of cancer was sought of based on principles of pharmacokinetics. It aimed to address some of the limitations of current treatments that arise due to insufficient systemic or tissue-specific exposure to the drugs.

The first approach was to take advantage of the physiological process of intestinal lymphatic transport in order to deliver anticancer agents to the mesenteric lymph nodes. Using this novel approach significantly higher concentrations of the active drugs were achievable in the MLNs without affecting the systemic exposure. Conventional chemotherapeutic agents rely on the fact that cancerous cells have higher proliferation rates compared to normal cells [256]. However, they hardly have any selectivity and therefore undesired exposure frequently results in side effects from chemotherapy [256]. Recent advancements in regards to site-specific delivery approach of anticancer agents include antibody drug conjugates [257], nanoparticles [258] and colloidal systems [259] aimed at tumour-specific delivery of drugs. Tumour-specific targeting can be achieved by those delivery systems that possess the ligands that have highly selective affinity towards cancer cells [256, 260]. Size-dependent disposition of the nanoparticles can result in high concentration of the anticancer agents in the tumours by the enhanced permeability and retention effect [261, 262]. Although these approaches offer some degree of site-specific delivery, most of them, if not all, are

limited to parenteral administration. This highlights the significance of the intestinal lymphatic delivery studied in this project because significant targeting of deep lymphatics can be achieved following oral administration.

Development and validation of novel bioanalytical method for determination of BEX in rat plasma was firstly performed prior to prodrug derivatisations [165]. BEX is a synthetic retinoid currently approved for cutaneous T-cell lymphoma and it also possesses therapeutic potential for other types of cancer [109, 111, 116, 165]. The bioanalytical method was a crucial part of the PhD project as all determination of concentrations in any samples was achieved by means of HPLC-UV. The LLOQ achieved by the method was 10 ng/mL, which was sufficient to describe the pharmacokinetics of BEX. The full validation included sample stability studies of short-term, long-term, freeze-thaw cycles and autosampler conditions that assured the integrity of samples throughout the project. Although modifications were applied to the method for quantification of prodrug concentrations and BEX generated from the prodrugs, the basis of a fully-validated method contributed in obtaining reliable and reproducible results.

Following design and synthesis of prodrugs of BEX, they were tested for their association with CM and conversion back to BEX. All prodrugs were designed to increase the lipophilicity and minimise the ionisability at pH 7.4, which are the main factors in CM association of compounds [61]. As a result, all prodrugs displayed increased association with CM compared to BEX (9%), which indicated their improved potential in targeting the intestinal lymphatics. The stability and conversion

of the prodrugs were assessed using rat plasma to represent the lymphatic system and FaSSIF with esterases to mimic the GI environment. Structure-activity relationships were observed where the half-lives of the prodrugs correlated with the lengths and bulkiness of the prodrug moieties. It could also be seen that the methyl group at position 1 of the prodrug moiety significantly delayed the conversion probably due to increased steric hindrance. Among the first-generation prodrugs, BET, the ethyl ester prodrug, showed the most rapid conversion in rat plasma ($t_{1/2}$ = 0.34 h) and a relatively high CM association of 37%.

Intestinal lymphatic targeting was confirmed by *in vivo* plasma pharmacokinetic and biodistribution studies. The initial set of studies with BET resulted in successful targeting of the prodrug to the intestinal lymphatics (6.0 to 41-fold higher than plasma). However, it did not release as much BEX and therefore BEX concentrations were comparable between the intestinal lymphatics and plasma. From these results, it was thought that stability of the prodrugs was the key determinant for successful delivery of the active drug. An ideal prodrug would be one that is stable in the GI environment but rapidly releases BEX upon reaching the lymphatic system. The first generations of the prodrugs showed that the stability in the lymphatic system was the limiting step and therefore activated ester prodrugs were designed to enhance the release of BEX in the lymphatics. BCY, the cyclic ester prodrug among the activated esters, had more rapid conversion than BET in rat plasma ($t_{1/2}$ = 0.13 h) and also higher association with CM (59%). As a result, more than 17-fold higher concentration of BEX could be achieved in the MLNs following administration of BCY compared to when BEX itself was administered. The activated ester prodrug moiety was also applied to RA which resulted in 2.4-fold higher targeting of the active drug to the MLNs, compared to when

RA was administered. In this study, the synergy between BEX and RA in cell growth inhibition was also demonstrated for the first time in DLBCL. Overall, it suggests that the lymphadenopathy in the MLNs could be more efficiently treated if BEX and RA are simultaneously delivered to the intestinal lymphatics by the activated ester prodrug approach.

Similar prodrug approaches have been researched by other groups but the main focus was on increasing the overall bioavailability where they mostly used long-chain or triglyceride mimetic prodrug moieties [62, 159]. However, in this project, through a series of stability and CM association studies, it was revealed that activated ester prodrugs is a very efficient approach for yielding high concentrations of active drugs in the MLNs. It was remarkable that 17- and 2.4-fold higher concentrations of the BEX and RA, respectively, were achievable in the MLNs without affecting the systemic exposure. This can be an extremely important factor as undesired increase in systemic exposure of anticancer agents can bring unwanted side effects.

A second approach of this PhD project was pharmacokinetic development and optimisation of CDK9 inhibitors. Before the optimisation work began, Caco-2 permeability assay was setup and its lab-to-lab variability was quantified [93]. The variability in the Caco-2 assays can originate from many various factors and it was shown that the results can differ significantly between laboratories. The results from the assays were applied to *in silico* simulation for prediction of fraction absorbed and it was demonstrated that the results can be substantially different. Therefore in this

study, a list of reference compounds were tested in order to enhance accuracy and predictability of the *in vitro* permeability assay.

The aims of pharmacokinetic development of CDK9 inhibitors were achieving sufficient systemic exposure of anticancer agents by identification of orally bioavailable candidate and further biopharmaceutical development in order to increase the systemic exposure. Recent trend of research on chemotherapy brings higher demand for orally bioavailable compounds [263]. More than half of CDK inhibitors already approved or under clinical trials are intended for oral administration and therefore sufficient oral bioavailability is indeed a crucial factor for a drug candidate to have a merit for further development [206]. Application of combinatorial chemistry allows increased number of molecules to be synthesised and efficient pharmacokinetic assessments are needed to identify the promising candidates with strong rationale [20, 263]. Although the concept of *in vitro* biopharmaceutical screening is not novel, reports of drug discovery studies that lack this process can often be found in public domain [224-228]. This PhD project has demonstrated the benefits of *in vitro-in silico-in vivo* approach for rational drug discovery and biopharmaceutical development of a promising candidate.

Eleven CDK9 inhibitor candidates were initially selected based on their *in vitro* efficacy and selectivity results. The rational drug discovery approach applied included *in vitro* biopharmaceutical assessments of solubility, permeability and metabolic stability. The solubility values of all compounds were in the micromolar range which meant that they were only slightly soluble in the tested media. None of the tested

compounds qualified as highly permeable from Caco-2 permeability assays. Therefore all candidate compounds would probably fall into BCS Class IV, but it cannot be ascertained as the solubility criteria depends on therapeutic dose which is not yet known for these novel compounds. Most compounds were classified as predicted to be highly affected by hepatic first-pass effect by the liver microsomal stability studies.

The results were then incorporated into *in silico* simulations for integration of the *in vitro* results. It was predicted that >50% bioavailability could be achieved with three compounds with rank-order of HS3-77>HS3-72>DF030263. The simulation results were then confirmed *in vivo* and oral bioavailability of HS3-77 was slightly above 42%. HS3-72 was also tested but toxicity was observed and therefore it was discontinued. DF030263 compound showed bioavailability of 24% and it also exhibited an interesting double-peak phenomenon, which led to further studies.

An *in vitro-in silico-in vivo* approach of biopharmaceutical development was applied to further enhance the oral bioavailability. Deconvolution of plasma pharmacokinetic profiles revealed distinct two phases of absorption. Intensive solubility studies in a range of pH showed that the solubility of DF030263 decreased dramatically when the pH increased over 6.6. *In silico* simulation of compartmentalised intestinal absorption indicated that the absorption would be discontinued in distal region of the small intestine and resumes in the large intestine. These results altogether suggested that there could be two absorption sites for DF030263 along the GI tract.

In vivo studies were conducted in order to exploit this two-site absorption phenomenon. Colonic administration was attempted to target the second site of absorption as it could avoid possible precipitation of the compound in the GI tract which might have been causing the discontinuation of absorption. However it resulted in bioavailability that was very similar to the existing result of 24%. It was then noted that the solubility study results suggested that fed state would not only increase the overall solubility but also prevent precipitation of the compound at high pH ranges. Therefore, oral administration at postprandial state was tested and the oral bioavailability was increased 2.6-fold, from 24% to 63%.

Overall, this PhD project describes pharmacokinetic optimisation of treatment of cancer. Two main approaches of site-specific targeting and improved systemic exposure were employed. Targeted delivery of anticancer agents by lipophilic prodrug approach would allow unnecessary systemic exposure to be mitigated whilst achieving substantially higher concentrations in the intestinal lymphatics. Rational drug discovery and development processes applied to CDK9 inhibitor candidates demonstrate efficient identification of orally bioavailable candidates and biopharmaceutical optimisation based on principles of pharmacokinetics. The results of the two approaches indicate that pharmacokinetic optimisation can be useful in development of anticancer agents to improve the treatment outcomes of cancer.

7.2. Further work

7.2.1. Intestinal lymphatic system targeting of anticancer agents by lipophilic prodrug approach

As a future work, a study involving fluorescein diacetate could be designed. Fluorescein diacetate itself is a non-fluorescent molecule. Within a living cell, it can be rapidly converted to fluorescein via hydrolysis by intracellular esterases. This fluorescein is fluorescent and hence its detection indicates intracellular esterase activity [264, 265]. Therefore, fluorescein diacetate could be used to monitor esterase activity in the MLN by fluorescent detection. This can be a useful information as the success of intestinal lymphatics targeting via prodrug approach depends on the release of the active drug from the prodrug in the intestinal lymphatics. However, the rate of release of the prodrug in the intestinal lymphatics *in situ* is not practically measurable. The use of fluorescein diacetate can help determine the relative esterase activity in the MLN compared to the *in vitro/ex vivo* assessment performed for prodrug conversion.

The current work of prodrug approach was a proof of concept where pharmacokinetic targeting of anticancer agent to the intestinal lymphatics was assessed. A proof of principle study could be designed as another future work where improved efficacy by the prodrug approach can be evaluated. For this purpose, *in vivo* systemic lymphoma models in mice or rats can be utilised [266, 267]. These models would have spontaneously developed lymphoma in the animals and therefore also the lymphadenopathy in the mesentery [267]. The prodrugs developed in the current project can be tested in these models and reduced lymphoma mass in the MLN would be the primary endpoint to assess the effectiveness of the prodrug approach.

7.2.2. Pharmacokinetic development of CDK9 inhibitors

A consequential future work for this approach would be to evaluate whether the systemic exposure achieved with the current candidates would be sufficient for them to be efficacious in preclinical models. For this purpose, systemic leukaemia or xenograft models of mice could be used with assessment of efficacy and safety [268, 269].

A future work more focused on pharmacokinetics could be conducted to investigate the discrepancy between *in silico* simulation and *in vivo* evaluation of the oral bioavailability. The three main factors (solubility, permeability and metabolic stability) that govern oral bioavailability of a compound were assessed *in vitro* and the results were incorporated into *in silico* simulation using GastroPlus^{TM}. However, the *in silico* simulation results differed by more than 2-fold for both HS3-77 (predicted F_{oral} = 90.0% and experimental F_{oral} = 42.7%) and DF030263 (predicted F_{oral} = 51.3% and experimental F_{oral} = 23.8%). There could have been potential limitations which will be further explained below: 1) *in vitro-in vivo* correlation of the *in vitro* biopharmaceutical assessments and 2) factors incorporated in the *in silico* simulation.

The *in vitro* biopharmaceutical assessments of solubility, permeability and metabolic stability applied in this project followed generally known protocols in the field. These protocols have been established based on the reasonable correlation that they have shown between *in vitro* and *in vivo* pharmacokinetics. However, there have been

various advances made in the field to improve this *in vitro-in vivo* correlation, Solubility was tested with biorelevant media of FaSSGF, FaSSIF and FeSSIF in this project but there are different compositions of these fluids proposed in the literature and improvements are made as physiological data is updated [270, 271]. For permeability tests, there have been improvements by application of different buffers [272, 273], cell culture methods [190, 274] and different membranes [275, 276]. The metabolic stability assay in this project utilized liver microsome and it has been proposed that improvements could be made when microsomal binding is considered [277]. Moreover, liver microsome mostly consists of phase I enzymes and therefore more accurate metabolism can be predicted when tissue slices or hepatocytes are used for the assay [278]. Overall, the methods for the *in vitro* assessment used in this project were useful in providing rank-order of the candidates but variations of the protocols could have helped improving the *in vitro-in vivo* correlations.

GastroPlus™ was used for *in silico* simulation of oral bioavailability based on the results from *in vitro* assessments. GastroPlus™ is a powerful *in silico* tool in predicting oral absorption and pharmacokinetics during drug discovery and development [279, 280]. However, it should be noted that this software is a compilation of available theories and principles established for *in vitro-in vivo* correlations. It is not able to offer accurate prediction without the input of critical factors. The fact that the simulation results were deviated more than 2-fold from experimental results even with input of solubility, permeability and metabolic stability indicates that there could more factors that can significantly affect the oral absorption. These could include factors such as the time a molecule takes to precipitate, saturation of the permeable membrane and effect of excipient used (PEG400 in this project). Investigation of these factors and

incorporating them into *in silico* simulation could enhance the predictive power of the simulation results.

APPENDICES

Appendix 1. Synthesis and characterisation results

General synthetic scheme for esterification

Ester prodrugs of BEX and RA were synthesised by adding 2.87 mmol of the desired alcohol to 0.287 mmol of BEX or RA. As catalysts, 0.431 mmol of 1-ethyl-3-(3-dimethylaminopropyl)carbodiimide and 0.057 mmol of 4-dimethylaminopyridine were added and 15 mL of dichloromethane was used as the solvent. The mixture was stirred using a magnetic stirrer overnight at room temperature. Purification was performed by flash chromatography using a 200-400 mesh silica gel-packed glass column and hexane:ethyl acetate, 50:2 (v/v) as the mobile phase. Specific details for compounds with different conditions are stated below for each compound.

Characterisation of synthesised prodrugs

^{1}H NMR and ^{13}C NMR spectra were obtained using Bruker 400 Ultrashield Spectrometer at 400 and 100 MHz, respectively. Bruker TOPSPIN 2.1 software was used to analyse the spectra. Chemical shifts were reported as parts per million (ppm) relative to the tetramethylsilane (internal standard) to the nearest 0.01 ppm and coupling constants (*J*) to the nearest 0.1 Hz. The following abbreviations were used while quoting the spectra: s, singlet; d, doublet; t, triplet; q, quartet; m, multiplet. High resolution mass spectrometry (HR-MS) was performed using Bruker MicroTOF operated with electrospray ionisation in positive mode. Purity of each compound was tested in respective chromatographic conditions as stated in Supplementary Material 2.

BME (bexarotene methyl ester). General synthetic scheme for esterification of BEX was used with methanol as the reactant. The final compound was obtained as white solid (82.0% yield), melting point 150-152 °C. Purity was >98% by HPLC-UV. ^{1}H NMR (400 MHz, $CDCl_3$): δ 7.98 (dt, J_1 = 8.4 Hz, J_2 =1.8 Hz, 2H), 7.37 (dt, J_1 = 8.4 Hz, J_2 = 1.8 Hz, 2H), 7.15 (s, 1H), 7.10 (s, 1H), 5.83 (d, J = 1.2 Hz, 1H), 5.34 (d, J = 1.2 Hz, 1H), 3.93 (s, 3H), 1.97 (s, 3H), 1.73 (s, 4H), 1.33 (s, 6H), 1.30 (s, 6H). ^{13}C NMR (100 MHz, $CDCl_3$): δ 167.12, 149.35, 145.74, 144.52, 142.48, 138.18, 132.88, 129.78, 129.13, 128.21, 128.17, 126.72, 116.94, 52.18, 35.36, 34.14, 34.03, 32.07, 32.03, 22.76, 20.07. HR-MS (ESI^+): *m/z* $[M+ H]^+$ calculated for $C_{25}H_{31}O_2$, 363.2319, found 363.2306.

BET (bexarotene ethyl ester). General synthetic scheme for esterification of BEX was used with ethanol as the reactant. The final compound was obtained as white crystal (66.9% yield), melting point 95-97 °C. Purity was >97% by HPLC-UV. ^{1}H NMR (400 MHz, $CDCl_3$): δ 7.98 (dt, J_1 = 8.5 Hz, J_2 =1.9 Hz, 2H), 7.35 (dt, J_1 = 8.5 Hz, J_2 = 1.9 Hz, 2H), 7.14 (s, 1H), 7.09 (s, 1H), 5.82 (d, J = 1.3 Hz, 1H), 5.34 (d, J = 1.3 Hz, 1H), 4.39 (q, J = 7.2 Hz, 2H), 1.96 (s, 3H), 1.72 (s, 4H), 1.40 (t, J = 7.1 Hz, 3H), 1.32 (s, 6H), 1.29 (s, 6H). ^{13}C NMR (100 MHz, $CDCl_3$): δ 166.63, 149.36, 145.61, 144.46, 142.44, 138.21, 132.86, 129.74, 129.48, 128.20, 128.17, 126.67, 116.81, 60.99, 35.36, 34.14, 34.03, 32.07, 32.03, 20.06, 14.48. HR-MS (ESI^+): *m/z* $[M+ H]^+$ calculated for $C_{26}H_{33}O_2$, 377.2475, found 377.2470.

BIP (bexarotene isopropyl ester). General synthetic scheme for esterification of BEX was used with isopropanol as the reactant. The final compound was obtained as white solid (45.0% yield), melting point 77-79 °C. Purity was >98% by HPLC-UV. ^{1}H NMR (400 MHz, $CDCl_3$): δ 7.98 (dt, J_1 = 8.6 Hz, J_2 =1.8 Hz, 2H), 7.35 (dt, J_1 = 8.6 Hz, J_2 = 1.8 Hz, 2H), 7.15 (s, 1H), 7.10 (s, 1H), 5.82 (d, J = 1.4 Hz, 1H), 5.34 (d, J = 1.3 Hz, 1H), 5.26 (septet, J = 6.2 Hz, 1H), 1.96 (s, 3H), 1.72(s, 4H), 1.38 (d, J = 6.2 Hz, 6H), 1.33 (s, 6H), 1.30 (s, 6H). ^{13}C NMR (100 MHz, $CDCl_3$): δ 166.11, 149.38, 145.50, 144.45, 142.43, 138.23, 132.86, 129.88, 129.69, 128.18, 128.15, 126.61, 116.71, 68.37, 35.37, 35.35, 34.13, 34.03, 32.07, 32.02, 22.09, 20.04. HR-MS (ESI^+): *m/z* $[M+ H]^+$ calculated for $C_{27}H_{35}O_2$, 391.2632, found 391.2636.

BIB (bexarotene isobutyl ester). General synthetic scheme for esterification of BEX was used with isobutanol as the reactant. The final compound was obtained as white solid (89.5% yield), melting point 62-64 °C. Purity was >97% by HPLC-UV. ^{1}H NMR (400 MHz, $CDCl_3$): δ 7.95 (dt, J_1 = 8.5 Hz, J_2 =1.8 Hz, 2H), 7.34 (dt, J_1 = 8.5 Hz, J_2 = 1.8 Hz, 2H), 7.12 (s, 1H), 7.08 (s, 1H), 5.81 (d, J = 1.3 Hz, 1H), 5.33 (d, J = 1.3 Hz, 1H), 4.47 (d, J = 6.3 Hz, 2H), 2.10 (nonet, J = 6.7 Hz, 1H), 1.98 (s, 3H), 1.73 (s, 4H), 1.34 (s, 6H), 1.31 (s, 6H), 1.05 (d, J = 6.8 Hz, 6H). ^{13}C NMR (100 MHz, $CDCl_3$): δ 166.63, 149.37, 145.61, 144.46, 142.45, 138.22, 132.85, 129.74, 129.49, 128.19, 128.16, 126.67, 116.78, 71.07, 41.50, 35.38, 35.36, 34.13, 34.03, 32.07, 32.03, 29.20, 28.07, 27.81, 22.75, 20.59, 20.04, 19.57, 19.32, 11.56. HR-MS (ESI^+): *m/z* $[M+ H]^+$ calculated for $C_{28}H_{37}O_2$, 405.2788, found 405.2779.

BDH (bexarotene 3,3'-dihydroxyisobutyl ester). General synthetic scheme for esterification of BEX was used with 2-hydroxymethyl-1,3-propanediol and *N*,*N*-dimethylformamide (DMF) as the reactant and the organic solvent, respectively. The flash chromatography for purification was also different from the general synthetic scheme that the following solvents were used for mobile phase: hexane:ethyl acetate = 50:50, 500 mL; hexane:ethyl acetate = 40:60, 250 mL; hexane:ethyl acetate = 30:70, 250 mL; hexane:ethyl acetate = 20:80, 500 mL. The final compound was obtained as white crystal (56.6% yield), melting point 116-118 °C. Purity was >98% by HPLC-UV. ^{1}H NMR (400 MHz, $CDCl_3$): δ 7.95 (dt, J_1 = 8.5 Hz, J_2 =1.8 Hz, 2H), 7.34 (dt, J_1 = 8.5 Hz, J_2 = 1.8 Hz, 2H), 7.12 (s, 1H), 7.08 (s, 1H), 5.81 (d, *J* = 1.3 Hz, 1H), 5.33 (d, *J* = 1.3 Hz, 1H), 4.47 (d, *J* = 6.3 Hz, 2H), 3.93-3.76 (m, 4H), 3.13 (broad s, 2H), 2.18 (septet, *J* = 5.5 Hz, 1H), 1.94 (s, 3H), 1.70 (s, 4H), 1.30 (s, 6H), 1.28 (s, 6H). ^{13}C NMR (100 MHz, $CDCl_3$): δ 166.97, 149.19, 145.93, 144.47, 142.43, 138.04, 132.76, 129.80, 128.79, 128.12, 126.70, 116.98, 62.97, 62.32, 42.71, 35.30, 35.28, 34.08, 33.97, 32.01, 31.96, 19.99. HR-MS (ESI^+): *m/z* $[M+H]^+$ calculated for $C_{28}H_{37}O_4$, 437.2686, found 437.2680.

BPR (bexarotene propyl ester). General synthetic scheme for esterification of BEX was used with 1-propanol as the reactant. The final compound was obtained as white solid (90.0% yield), melting point 66-68 °C. Purity was 98.0% by HPLC-UV. ^{1}H NMR (400 MHz, $CDCl_3$): δ 8.00 (dt, J_1 = 8.4 Hz, J_2 =1.9 Hz, 2H), 7.37 (dt, J_1 = 8.4 Hz, J_2 = 1.9 Hz, 2H), 7.16 (s, 1H), 7.11 (s, 1H), 5.84 (d, *J* = 1.1 Hz, 1H), 5.35 (d, *J* = 1.1 Hz, 1H), 4.30 (t, *J* = 6.7 Hz, 2H), 1.98 (s, 3H), 1.81 (sextet, *J* = 7.2 Hz, 2H), 1.73 (s, 4H), 1.34 (s, 6H), 1.31 (s, 6H) 1.05 (t, *J* = 7.4 Hz, 3H). ^{13}C NMR (100 MHz, $CDCl_3$): δ 166.69, 149.38, 145.61, 144.47, 142.45, 138.22, 132.87, 129.75, 129.50, 128.21,

128.17, 126.68, 116.80, 66.60, 41.51, 36.23, 35.38, 35.36, 34.14, 34.04, 33.88, 32.08, 32.03, 29.82, 29.52, 29.22, 29.04, 27.83, 22.85, 22.81, 22.76, 22.28, 20.60, 20.06, 19.58, 18.91, 14.46, 14.26, 11.57, 10.66. HR-MS (ESI^+): *m/z* $[M+ H]^+$ calculated for $C_{27}H_{35}O_2$, 391.2632, found 391.2636.

BBU (bexarotene butyl ester). General synthetic scheme for esterification of BEX was used with 1-butanol as the reactant. The final compound was obtained as white solid (102 mg, 87.8% yield), melting point 54-56 °C. Purity was >98% by HPLC-UV. ^1H NMR (400 MHz, $CDCl_3$): δ 7.99 (dt, J_1 = 8.4 Hz, J_2 =1.9 Hz, 2H), 7.37 (dt, J_1 = 8.4 Hz, J_2 = 1.9 Hz, 2H), 7.15 (s, 1H), 7.10 (s, 1H), 5.83 (d, *J* = 1.2 Hz, 1H), 5.34 (d, *J* = 1.2 Hz, 1H), 4.34 (t, *J* = 6.6 Hz, 2H), 1.97 (s, 3H), 1.77 (quintet, *J* = 8.0 Hz, 2H), 1.73 (s, 4H), 1.50 (sextet, *J* = 7.6 Hz, 2H), 1.33 (s, 6H), 1.30 (s, 6H), 1.00 (t, *J* = 7.4 Hz, 3H). ^{13}C NMR (100 MHz, $CDCl_3$): δ 166.70, 149.36, 145.60, 144.47, 142.44, 138.21, 132.86, 129.74, 129.49, 128.20, 128.16, 126.67, 116.80, 64.89, 41.50, 35.37, 35.35, 34.14, 34.03, 32.07, 32.03, 30.94, 29.85, 29.81, 29.51, 29.21, 29.04, 27.82, 22.76, 22.48, 20.06, 19.58, 19.43, 14.46, 14.26, 14.20, 13.90, 11.57. HR-MS (ESI^+): *m/z* $[M+ H]^+$ calculated for $C_{28}H_{37}O_2$, 405.2788, found 405.2777.

BHE (bexarotene hexyl ester). General synthetic scheme for esterification of BEX was used with 1-hexanol as the reactant. The final compound was obtained as white solid (91.8% yield), melting point 46-48 °C. Purity was >98% by HPLC-UV. ^1H NMR (400 MHz, $CDCl_3$): δ 7.99 (dt, J_1 = 8.5 Hz, J_2 =1.8 Hz, 2H), 7.37 (dt, J_1 = 8.5 Hz, J_2 = 1.8 Hz, 2H), 7.16 (s, 1H), 7.11 (s, 1H), 5.84 (d, *J* = 1.3 Hz, 1H), 5.35 (d, *J* = 1.3 Hz, 1H), 4.33 (t, *J* = 6.7 Hz, 2H), 1.97 (s, 3H), 1.78 (quintet, *J* = 7.9 Hz, 2H), 1.73 (s, 4H),

1.47 (quintet, *J* = 7.2 Hz, 2H), 1.40-1.34 (m, 4H), 1.33 (s, 6H), 1.31 (s, 6H), 0.93 (t, *J* = 7.0 Hz, 3H). ^{13}C NMR (100 MHz, $CDCl_3$): δ 166.72, 149.36, 145.60, 144.47, 142.45, 138.21, 132.87, 129.74, 129.51, 128.20, 128.16, 126.67, 116.82, 65.21, 35.37, 35.36, 34.14, 34.04, 32.08, 32.03, 31.62, 28.86, 25.87, 22.70, 20.06, 14.15. HR-MS (ESI^+): *m/z* $[M+ H]^+$ calculated for $C_{30}H_{41}O_2$, 433.3101, found 433.3097.

BOT (bexarotene octyl ester). General synthetic scheme for esterification of BEX was used with 1-octanol as the reactant. The final compound was obtained as white solid (87.1% yield), melting point 66-68°C. Purity was >98% by HPLC-UV. ^{1}H NMR (400 MHz, $CDCl_3$): δ 7.99 (dt, J_1 = 8.6 Hz, J_2 =1.8 Hz, 2H), 7.37 (dt, J_1 = 8.6 Hz, J_2 = 1.8 Hz, 2H), 7.16 (s, 1H), 7.11 (s, 1H), 5.84 (d, *J* = 1.4 Hz, 1H), 5.35 (d, *J* = 1.3 Hz, 1H), 4.33 (t, *J* = 6.7 Hz, 2H), 1.97 (s, 3H), 1.78 (quintet, *J* = 6.7 Hz, 2H), 1.73 (s, 4H), 1.51-1.42 (m, 2H), 1.40-1.26 (m, 20H), 0.91 (t, *J* = 7.0 Hz, 3H), 1.47 (quintet, *J* = 7.2 Hz, 2H), 1.40-1.34 (m, 4H), 1.32 (d, *J* = 11.2 Hz, 12H), 0.91 (t, *J* = 7.0 Hz, 3H). ^{13}C NMR (100 MHz, $CDCl_3$): δ 166.69, 149.36, 145.59, 144.46, 142.44, 138.22, 132.86, 129.74, 129.51, 128.20, 128.16, 126.67, 116.80, 65.20, 41.50, 35.37, 35.35, 34.13, 34.03, 32.07, 32.03, 31.94, 29.40, 29.34, 29.21, 29.04, 28.89, 26.21, 22.84, 22.79, 22.77, 20.59, 20.06, 19.58, 14.46, 14.23, 11.57. HR-MS (ESI^+): *m/z* $[M+ H]^+$ calculated for $C_{32}H_{45}O_2$, 461.3414, found 461.3392.

BUN (bexarotene undecanyl ester). General synthetic scheme for esterification of BEX was used with 1-undecanol as the reactant. The final compound was obtained as white solid (70.0% yield), melting point 38-40 °C. Purity was >98% by HPLC-UV. ^{1}H NMR (400 MHz, $CDCl_3$): δ 7.98 (dt, J_1 = 8.6 Hz, J_2 =1.8 Hz, 2H), 7.36 (dt, J_1 = 8.6

Hz, J_2 = 1.8 Hz, 2H), 7.15 (s, 1H), 7.09 (s, 1H), 5.83 (d, J = 1.4 Hz, 1H), 5.34 (d, J = 1.3 Hz, 1H), 4.32 (t, J = 6.6 Hz, 2H), 1.96 (s, 3H), 1.77 (quintet, J = 6.6 Hz, 2H), 1.72 (s, 4H), 1.50-1.41 (m, 2H), 1.41-1.20 (m, 26H), 0.90 (t, J = 6.6 Hz, 3H). ^{13}C NMR (100 MHz, $CDCl_3$): δ 166.71, 149.38, 145.60, 144.48, 142.46, 138.22, 132.87, 129.74, 129.52, 128.21, 128.17, 126.67, 116.80, 65.22, 35.38, 35.37, 34.15, 34.04, 32.08, 32.05, 32.04, 29.74, 29.73, 29.68, 29.47, 29.44, 29.90, 26.21, 22.83, 20.06, 14.25. HR-MS (ESI^+): *m/z* $[M+H]^+$ calculated for $C_{35}H_{51}O_2$, 503.3884, found 503.3884.

BOC (bexarotene octadecanyl ester). General synthetic scheme for esterification of BEX was used with 1-octadecanol as the reactant. The final compound was obtained as white solid (67.9% yield), melting point 62-64 °C. Purity was >98% by HPLC-UV. ^{1}H NMR (400 MHz, $CDCl_3$): δ 7.99 (dt, J_1 = 8.5 Hz, J_2 =1.8 Hz, 2H), 7.37 (dt, J_1 = 8.5 Hz, J_2 = 1.8 Hz, 2H), 7.16 (s, 1H), 7.10 (s, 1H), 5.83 (d, J = 1.3 Hz, 1H), 5.35 (d, J = 1.2 Hz, 1H), 4.33 (t, J = 6.6 Hz, 2H), 1.97 (s, 3H), 1.78 (quintet, J = 6.7 Hz, 2H), 1.73 (s, 4H), 1.51-1.42 (m, 2H), 1.42-1.20 (m, 40H), 0.91 (t, J = 6.6 Hz, 3H). ^{13}C NMR (100 MHz, $CDCl_3$): δ 166.69, 149.38, 145.59, 144.46, 142.45, 138.22, 132.86, 129.74, 129.52, 128.29, 128.16, 126.67, 116.79, 65.20, 35.38, 35.37, 34.14, 34.04, 32.08, 32.03, 29.85, 29.82, 29.74, 29.70, 29.51, 29.45, 28.91, 26.22, 22.84, 20.06, 14.26. HR-MS (ESI^+): *m/z* $[M+H]^+$ calculated for $C_{42}H_{65}O_2$, 601.4979, found 601.4943.

BOL (bexarotene oleyl ester). General synthetic scheme for esterification of BEX was used with oleyl alcohol as the reactant. The final compound was obtained as colourless gum (90.7% yield). Purity was >98% by HPLC-UV. ^{1}H NMR (400 MHz, $CDCl_3$): δ 7.99 (dt, J_1 = 8.5 Hz, J_2 =1.8 Hz, 2H), 7.37 (dt, J_1 = 8.5 Hz, J_2 = 1.8 Hz, 2H),

7.16 (s, 1H), 7.11 (s, 1H), 5.84 (d, J = 1.3 Hz, 1H), 5.38 (tt, J_1 = 5.5 Hz, J_2 = 1.8 Hz, 2H), 5.35 (d, J = 1.3 Hz, 1H), 4.33 (t, J = 6.6 Hz, 2H), 2.09-2.00 (m, 4H), 1.97 (s, 3H), 1.78 (quintet, J = 7.0 Hz, 2H), 1.73 (s, 4H), 1.51-1.42 (m, 2H), 1.42-1.21 (m, 32H), 0.91 (t, J = 6.7 Hz, 3H). ^{13}C NMR (100 MHz, $CDCl_3$): δ 166.67, 149.37, 145.59, 144.46, 142.44, 138.22, 132.86, 130.12, 129.93, 129.74, 129.51, 128.19, 128.16, 126.66, 116.78, 65.17, 35.38, 35.36, 34.14, 34.03, 32.07, 32.05, 32.03, 29.92, 29.88, 29.67, 29.58, 29.46, 29.42, 29.36, 28.90, 27.36, 27.33, 26.20, 22.83, 20.05, 14.25. HR-MS (ESI^+): *m/z* $[M+H]^+$ calculated for $C_{42}H_{63}O_2$, 599.4823, found 599.4828.

BTG (bexarotene triglyceryl ester). General synthetic scheme for esterification of BEX was used with glyceryl 1,3-dipalmitate as the reactant. The final compound was obtained as white solid (60.4% yield), melting point 46-48°C. Purity was >98% by HPLC-UV. ^{1}H NMR (400 MHz, $CDCl_3$): δ 7.97 (dt, J_1 = 8.5 Hz, J_2 =1.7 Hz, 2H), 7.37 (dt, J_1 = 8.5 Hz, J_2 = 1.7 Hz, 2H), 7.14 (s, 1H), 7.10 (s, 1H), 5.84 (d, J = 1.3 Hz, 1H), 5.52 (quintet, J = 4.4 Hz, 1H), 5.36 (d, J = 1.3 Hz, 1H), 4.44-4.30 (m, 4H), 2.33 (t, J = 7.4 Hz, 4H), 1.97 (s, 3H), 1.73 (s, 4H), 1.61 (quintet, J = 7.2 Hz, 4H), 1.37-1.21 (m, 60H), 0.91 (t, J = 6.6 Hz, 6H). ^{13}C NMR (100 MHz, $CDCl_3$): δ 173.46, 165.61, 149.25, 146.13, 144.54, 142.49, 138.09, 132.81, 130.01, 128.49, 128.18, 126.74, 117.06, 69.86, 62.28, 35.35, 34.22, 34.14, 34.03, 32.07, 32.02, 29.84, 29.80, 29.75, 29.57, 29.50, 29.37, 29.23, 25.01, 22.83, 22.75, 20.05, 14.25.

B22 (bexarotene 2-ethylbutyl ester). General synthetic scheme for esterification of BEX was used with 2-ethyl-1-butanol as the reactant. The final compound was obtained as colourless oil (90.5% yield). Purity was >98% by HPLC-UV. ^{1}H NMR

(400 MHz, $CDCl_3$): δ 7.99 (dt, J_1 = 8.5 Hz, J_2 =1.8 Hz, 2H), 7.37 (dt, J_1 = 8.5 Hz, J_2 = 1.8 Hz, 2H), 7.16 (s, 1H), 7.10 (s, 1H), 5.84 (d, J = 1.3 Hz, 1H), 5.35 (d, J = 1.3 Hz, 1H), 4.27 (d, J = 5.7 Hz, 2H), 1.97 (s, 3H), 1.73 (s, 4H), 1.68 (septet, J = 6.2 Hz, 1H), 1.48 (quintet, J = 7.2 Hz, 4H), 1.33 (s, 6H), 1.31 (s, 6H), 0.97 (t, J = 7.4 Hz, 6H). ^{13}C NMR (100 MHz, $CDCl_3$): δ 166.74, 149.37, 145.59, 144.46, 142.45, 138.22, 132.86, 129.74, 129.54, 128.19, 128.16, 126.67, 116.78, 67.01, 41.51, 40.71, 36.52, 36.23, 35.38, 35.36, 34.28, 34.14, 34.04, 33.88, 32.08, 32.03, 29.21, 29.04, 27.82, 25.98, 23.70, 22.76, 22.48, 20.59, 20.05, 19.58, 18.91, 14.46, 14.20, 11.57, 11.28. HR-MS (ESI^+): *m/z* $[M+H]^+$ calculated for $C_{30}H_{41}O_2$, 433.3101, found 433.3094.

B24 (bexarotene benzyl ester). General synthetic scheme for esterification of BEX was used with benzyl alcohol as the reactant. The final compound was obtained as colourless oil (83.4% yield). Purity was >98% by HPLC-UV. ^{1}H NMR (400 MHz, $CDCl_3$): δ 8.03 (dt, J_1 = 8.5 Hz, J_2 =1.6 Hz, 2H), 7.50-7.33 (m, 7H), 7.16 (s, 1H), 7.11 (s, 1H), 5.84 (d, J = 1.2 Hz, 1H), 5.39 (s, 2H), 5.36 (d, J = 1.2 Hz, 1H), 1.97 (s, 3H), 1.73 (s, 4H), 1.34 (s, 6H), 1.31 (s, 6H). ^{13}C NMR (100 MHz, $CDCl_3$): δ 166.42, 149.32, 145.85, 144.49, 142.46, 138.16, 136.29, 132.85, 129.92, 129.09, 128.72, 128.33, 128.24, 128.19, 128.18, 126.72, 116.92, 66.73, 41.50, 36.23, 35.67, 35.35, 34.27, 34.14, 34.03, 33.87, 32.07, 32.03, 29.21, 29.04, 27.82, 25.98, 22.76, 22.48, 20.59, 20.05, 19.58, 18.91, 14.46, 14.20, 11.57, 9.00. HR-MS (ESI^+): *m/z* $[M+H]^+$ calculated for $C_{31}H_{35}O_2$, 439.2632, found 439.2626.

B25 (bexarotene 1-phenylethyl ester). General synthetic scheme for esterification of BEX was used with 1-phenylethanol as the reactant. The final compound was obtained

as colourless oil (74.1% yield). Purity was >98% by HPLC-UV. ^{1}H NMR (400 MHz, $CDCl_3$): δ 8.03 (dt, J_1 = 8.5 Hz, J_2 =1.8 Hz, 2H), 7.51-7.29 (m, 7H), 7.16 (s, 1H), 7.11 (s, 1H), 6.15 (quartet, J = 6.6 Hz, 1H), 5.84 (d, J = 1.2 Hz, 1H), 5.35 (d, J = 1.2 Hz, 1H), 1.97 (s, 3H), 1.73 (s, 4H), 1.69 (d, J = 6.6 Hz, 3H), 1.34 (s, 6H), 1.31 (s, 6H). ^{13}C NMR (100 MHz, $CDCl_3$): δ 165.80, 149.34, 145.73, 144.48, 142.46, 142.01, 138.19, 132.85, 129.86, 129.49, 128.68, 128.18, 128.17, 127.99, 126.68, 126.17, 116.83, 72.96, 41.50, 36.51, 36.23, 35.37, 35.36, 34.27, 34.14, 34.04, 33.87, 32.07, 32.03, 29.21, 29.04, 27.82, 25.98, 22.76, 22.58, 22.48, 20.59, 20.04, 19.58, 18.91, 14.46, 14.34, 14.20, 11.57, 9.00. HR-MS (ESI^+): *m/z* $[M+H]^+$ calculated for $C_{32}H_{37}O_2$, 453.2788, found 453.2780.

B26 (bexarotene 1-ethylpropyl ester). General synthetic scheme for esterification of BEX was used with 3-pentanol as the reactant. The final compound was obtained as colourless oil (79 mg, 65.8% yield). Purity was >98% by HPLC-UV. ^{1}H NMR (400 MHz, $CDCl_3$): δ 8.00 (dt, J_1 = 8.5 Hz, J_2 =1.8 Hz, 2H), 7.37 (dt, J_1 = 8.5 Hz, J_2 = 1.8 Hz, 2H), 7.15 (s, 1H), 7.10 (s, 1H), 5.83 (d, J = 1.3 Hz, 1H), 5.34 (d, J = 1.3 Hz, 1H), 5.03 (quintet, J = 6.1 Hz, 1H), 1.98 (s, 3H), 1.73 (s, 4H), 1.72 (quintet, J = 7.4 Hz, 4H), 1.33 (s, 6H), 1.30 (s, 6H), 0.97 (t, J = 7.4 Hz, 6H). ^{13}C NMR (100 MHz, $CDCl_3$): δ 166.46, 149.38, 145.48, 144.45, 142.44, 138.25, 132.88, 129.85, 129.73, 128.18, 128.15, 126.63, 116.70, 41.51, 36.52, 36.24, 35.39, 35.37, 34.28, 34.14, 34.04, 33.88, 32.08, 32.04, 29.22, 29.05, 27.83, 26.70, 25.98, 22.76, 22.49, 20.59, 20.06, 19.58, 18.91, 14.46, 14.20, 11.57, 9.77, 9.00. HR-MS (ESI^+): *m/z* $[M+H]^+$ calculated for $C_{29}H_{39}O_2$, 419.2945, found 419.2936.

B27 (bexarotene 1-isopropyl-2-methyl-propyl ester). General synthetic scheme for esterification of BEX was used with 2,4-dimethyl-3-pentanol as the reactant. The final compound was obtained as colourless oil (117 mg, 91.3% yield). Purity was >98% by HPLC-UV. ^{1}H NMR (400 MHz, $CDCl_3$): δ 8.00 (dt, J_1 = 8.5 Hz, J_2 =1.8 Hz, 2H), 7.37 (dt, J_1 = 8.4 Hz, J_2 = 1.8 Hz, 2H), 7.14 (s, 1H), 7.10 (s, 1H), 5.83 (d, J = 1.2 Hz, 1H), 5.34 (d, J = 1.2 Hz, 1H), 4.85 (t, J = 6.1 Hz, 1H), 2.10-1.95 (m, 5H), 1.72 (s, 4H), 1.32 (s, 6H), 1.30 (s, 6H), 0.96 (d, J = 6.7 Hz, 12H). ^{13}C NMR (100 MHz, $CDCl_3$): δ 166.63, 149.36, 145.46, 144.45, 142.45, 138.25, 132.89, 129.83, 129.67, 128.18, 128.15, 126.65, 116.71, 83.33, 41.51, 36.52, 36.24, 35.37, 34.28, 34.15, 34.05, 33.88, 32.09, 32.04, 29.83, 29.22, 29.05, 27.83, 25.99, 22.77, 22.49, 20.59, 20.07, 19.79, 19.59, 18.92, 17.51, 14.47, 14.21, 11.58, 9.00. HR-MS (ESI^+): *m/z* $[M+H]^+$ calculated for $C_{31}H_{43}O_2$, 447.3258, found 447.3255.

BGA1 (bexarotene N,N-dimethylacetamide ester). BGA1 was synthesised by adding 0.344 mmol of 2-chloro-N,N-dimethylacetamide to 0.287 mmol of BEX. Catalysts of 0.412 mmol KI and 0.344 mmol K_2CO_3 were added and 4 mL of DMF was used as the solvent. The mixture was stirred at 100 °C using a magnetic stirrer overnight. Purification was performed by flash chromatography using hexane:ethyl acetate = 7:3 (v/v) as the mobile phase. The final compound was obtained as white solid (42.5% yield), melting point 134-136 °C. Purity was >97% by HPLC-UV. ^{1}H NMR (400 MHz, $CDCl_3$): δ 8.05 (dt, J_1 = 8.4 Hz, J_2 =1.8 Hz, 2H), 7.36 (dt, J_1 = 8.4 Hz, J_2 = 1.8 Hz, 2H), 7.14 (s, 1H), 7.09 (s, 1H), 5.82 (d, J = 1.2 Hz, 1H), 5.34 (d, J = 1.2 Hz, 1H), 4.96 (s, 2H), 3.06 (s, 3H), 3.01 (s, 3H), 1.95 (s, 3H), 1.71 (s, 4H), 1.32 (s, 6H), 1.29 (s, 6H). ^{13}C NMR (100 MHz, $CDCl_3$): δ 171.30, 166.60, 166.26, 149.35, 146.11, 144.49, 142.45, 138.14, 132.90, 130.19, 128.43, 128.22, 128.18, 126.75,

117.03, 61.98, 60.54, 41.50, 36.11, 35.76, 35.36, 34.14, 34.03, 29.20, 27.81, 13.97, 22.75, 21.17, 20.58, 20.07, 19.57, 18.90, 14.45, 14.33, 11.56. HR-MS (ESI^+): *m/z* [M+ H]$^+$ calculated for $C_{28}H_{36}NO_3$, 434.2690, found 434.2687.

BGA2 (bexarotene N,N-diethylacetamide ester). BGA2 was synthesised by adding 0.344 mmol of 2-chloro-N,N-diethylacetamide to 0.287 mmol of BEX. Catalysts of 0.412 mmol KI and 0.344 mmol K_2CO_3 were added and 4 mL of DMF was used as the solvent. The mixture was stirred at 100 °C using a magnetic stirrer overnight. Purification was performed by flash chromatography using DCM:MeOH with 0.7 N NH_3 = 50:2 (v/v) as the mobile phase. The final compound was obtained as white solid (59 mg, 29.7% yield), melting point 146-148 °C. Purity was >98% by HPLC-UV. ^{1}H NMR (400 MHz, $CDCl_3$): δ 8.05 (dt, J_1 = 8.5 Hz, J_2 =1.8 Hz, 2H), 7.36 (dt, J_1 = 8.5 Hz, J_2 =1.8 Hz, 2H), 7.14 (s, 1H), 7.09 (s, 1H), 5.82 (d, *J* = 1.2 Hz, 1H), 5.34 (d, *J* = 1.2 Hz, 1H), 4.96 (s, 2H), 3.44 (q, *J* = 7.2 Hz, 2H), 3.33 (q, *J* = 7.2 Hz, 2H), 1.95 (s, 3H), 1.71 (s, 4H), 1.32 (s, 6H), 1.29 (s, 6H), 1.27 (t, *J* = 7.2 Hz, 3H), 1.17 (t, *J* = 7.2 Hz, 3H). ^{13}C NMR (100 MHz, $CDCl_3$): δ 166.29, 165.70, 149.34, 146.04, 144.46, 142.42, 138.13, 132.88, 130.16, 128.49, 128.20, 128.16, 126.72, 117.00, 61.94, 53.55, 41.19, 40.61, 35.35, 35.33, 34.11, 34.01, 32.04, 32.00, 23.95, 20.04, 14.35, 13.04. HR-MS (ESI^+): *m/z* [M+ H]$^+$ calculated for $C_{30}H_{40}NO_3$, 462.3003, found 462.3007.

BAE1 (bexarotene dimethylaminoethyl ester). General synthetic scheme for esterification of BEX was used with 2-dimethylaminoethanol as the reactant. Flash chromatography was performed with DCM:MeOH with 0.7 N NH_3 = 50:2 as the mobile phase for purification of the product. The final compound was obtained as

yellowish gum (73.1% yield). Purity was >97% by HPLC-UV. ^{1}H NMR (400 MHz, $CDCl_3$): δ 7.98 (dt, J_1 = 8.5 Hz, J_2 =1.8 Hz, 2H), 7.36 (dt, J_1 = 8.5 Hz, J_2 =1.8 Hz, 2H), 7.14 (s, 1H), 7.09 (s, 1H), 5.82 (d, J = 1.3 Hz, 1H), 5.34 (d, J = 1.2 Hz, 1H), 4.46 (t, J = 5.8 Hz, 2H), 2.76 (t, J = 5.8 Hz, 2H), 2.38 (s, 6H), 1.95 (s, 3H), 1.72 (s, 4H), 1.32 (s, 6H), 1.29 (s, 6H). ^{13}C NMR (100 MHz, $CDCl_3$): δ 166.54, 149.32, 145.79, 144.48, 142.45, 138.15, 132.84, 129.85, 129.07, 128.18, 128.16, 126.70, 116.91, 62.92, 57.89, 53.54, 45.86, 35.35, 35.34, 34.13, 34.02, 32.06, 32.01, 20.04. HR-MS (ESI^+): *m/z* [M+ H]$^+$ calculated for $C_{28}H_{38}NO_2$, 420.2897, found 420.2909.

BAE2 (bexarotene diisopropylaminoethyl ester). General synthetic scheme for esterification of BEX was used with 2-diisopropylaminoethanol as the reactant. Flash chromatography was performed with DCM:MeOH with 0.7 N NH_3 = 50:2 as the mobile phase for purification of the product. The final compound was obtained as yellowish gum (80 mg, 36.5% yield). Purity was >97% by HPLC-UV. ^{1}H NMR (400 MHz, $CDCl_3$): δ 7.98 (dt, J_1 = 8.5 Hz, J_2 =1.8 Hz, 2H), 7.36 (dt, J_1 = 8.5 Hz, J_2 =1.8 Hz, 2H), 7.14 (s, 1H), 7.09 (s, 1H), 5.82 (d, J = 1.2 Hz, 1H), 5.34 (d, J = 1.2 Hz, 1H), 4.27 (broad s, 2H), 3.07 (broad s, 2H), 2.81 (broad s, 2H), 1.96 (s, 3H), 1.72 (s, 4H), 1.32 (s, 6H), 1.29 (s, 6H), 1.07 (broad s, 12H). ^{13}C NMR (100 MHz, $CDCl_3$): δ 166.63, 149.36, 144.48, 142.45, 138.19, 132.87, 129.79, 128.21, 128.17, 126.69, 116.88, 53.55, 49.50, 43.95, 35.36, 35.35, 34.14, 34.03, 32.07, 32.03, 20.99, 20.07. HR-MS (ESI^+): *m/z* [M+ H]$^+$ calculated for $C_{32}H_{46}NO_2$, 476.3523, found 476.3536.

BAM1 (bexarotene isopropyl carbonate ethyl ester). BAM1 was synthesised by adding 0.344 mmol of 1-chloroethyl isopropyl carbonate to 0.287 mmol of BEX.

Catalysts of 0.412 mmol KI and 0.344 mmol K_2CO_3 were added and 4 mL of DMF was used as the solvent. The mixture was stirred at 65 °C using a magnetic stirrer for 2 h. Purification was performed by the general synthetic scheme. The final compound was obtained as colourless oil (45.6% yield). Purity was >97% by HPLC-UV. ^{1}H NMR (400 MHz, $CDCl_3$): δ 7.99 (dt, J_1 = 8.5 Hz, J_2 =1.7 Hz, 2H), 7.36 (dt, J_1 = 8.5 Hz, J_2 =1.7 Hz, 2H), 7.14 (s, 1H), 7.10 (s, 1H), 7.04 (q, *J* = 5.4 Hz, 1H), 5.83 (d, *J* = 1.2 Hz, 1H), 5.35 (d, *J* = 1.2 Hz, 1H), 4.93 (septet, *J* = 6.2 Hz, 1H), 1.96 (s, 3H), 1.72 (s, 4H), 1.66 (d, 5.4 Hz, 3H), 1.33 (d, 6.2 Hz, 6H), 1.32 (s, 6H), 1.30 (s, 6H). ^{13}C NMR (100 MHz, $CDCl_3$): δ 164.51, 152.67, 149.26, 146.32, 144.55, 142.49, 138.06, 132.83, 130.15, 128.20, 128.16, 126.76, 117.18, 91.76, 72.84, 53.55, 35.36, 35.34, 34.14, 34.04, 32.07, 32.02, 21.82, 21.78, 20.05, 19.88. HR-MS (ESI^+): *m/z* $[M+ Na]^+$ calculated for $C_{30}H_{38}NaO_5$, 501.2611, found 501.2611.

BAM2 (bexarotene cyclohexyl carbonate ethyl ester). BAM2 was synthesised by adding 0.344 mmol of 1-chloroethyl cyclohexyl carbonate to 0.287 mmol of BEX. Catalysts of 0.412 mmol KI and 0.344 mmol K_2CO_3 were added and 4 mL of DMF was used as the solvent. The mixture was stirred at 65 °C using a magnetic stirrer for 2 h. Purification was performed by the general synthetic scheme. The final compound was obtained as colourless oil (109 mg, 48.8% yield). Purity was >98% by HPLC-UV. ^{1}H NMR (400 MHz, $CDCl_3$): δ 7.99 (dt, J_1 = 8.5 Hz, J_2 =1.7 Hz, 2H), 7.36 (dt, J_1 = 8.5 Hz, J_2 =1.7 Hz, 2H), 7.14 (s, 1H), 7.10 (s, 1H), 7.04 (q, *J* = 5.4 Hz, 1H), 5.83 (d, *J* = 1.2 Hz, 1H), 5.35 (d, *J* = 1.2 Hz, 1H), 4.66 (septet, *J* = 4.7 Hz, 1H), 1.99-1.90 (m, 2H), 1.95 (s, 3H), 1.82-1.69 (m, 2H), 1.72 (s, 4H), 1.66 (d, 5.4 Hz, 3H), 1.65-1.43 (m, 6H), 1.32 (s, 6H), 1.29 (s, 6H). ^{13}C NMR (100 MHz, $CDCl_3$): δ 164.51, 152.67, 149.26, 146.30, 144.54, 142.49, 138.07, 132.83, 130.15, 128.19, 126.76, 117.16, 91.79, 60.53,

41.50, 35.36, 35.34, 34.14, 34.03, 32.06, 32.02, 31.55, 31.53, 29.20, 25.30, 23.73, 22.75, 20.05, 19.88, 14.45, 14.34, 11.56. HR-MS (ESI^+): *m/z* $[M+ Na]^+$ calculated for $C_{33}H_{42}NaO_5$, 541.2924, found 541.2939.

BCY (bexarotene (5-methyl-2-oxo-1,3-dioxolen-4-yl)methyl ester). General synthetic scheme for esterification of BEX was used with (5-methyl-2-oxo-1,3-dioxolen-4-yl)methyl alcohol as the reactant. Purification was performed by using hexane:EA = 88:12 as the mobile phase. The final compound was obtained as white solid (170 mg, 85.6% yield), melting point 96-98 °C. Purity was >98% by HPLC-UV. ^1H NMR (400 MHz, $CDCl_3$): δ 7.98 (dt, J_1 = 8.5 Hz, J_2 =1.7 Hz, 2H), 7.38 (dt, J_1 = 8.5 Hz, J_2 =1.7 Hz, 2H), 7.14 (s, 1H), 7.10 (s, 1H), 5.84 (d, *J* = 1.2 Hz, 1H), 5.36 (d, *J* = 1.2 Hz, 1H), 5.09 (s, 2H), 2.26 (s, 3H), 1.96 (s, 3H), 1.72 (s, 4H), 1.32 (s, 6H), 1.29 (s, 6H). ^{13}C NMR (100 MHz, $CDCl_3$): δ 171.28, 165.97, 152.27, 149.17, 146.47, 144.58, 142.51, 140.30, 137.98, 133.80, 132.80, 130.04, 128.21, 128.18, 127.92, 126.87, 117.31, 60.52, 54.24, 35.33, 35.31, 34.13, 34.02, 32.05, 32.00, 23.96, 21.16, 20.04, 14.32, 9.57. HR-MS (ESI^+): *m/z* $[M+ H]^+$ calculated for $C_{29}H_{33}O_5$, 461.2323, found 461.2323.

RAE (retinoic acid ethyl ester). General synthetic scheme for esterification of RA was used with ethanol as the reactant. Purification was performed by using [(hexane:toluene, 50:50)]:ethyl acetate = 50:2 as the mobile phase. The final compound was obtained as yellow gum (70.6% yield). Purity was >98% by HPLC-UV. ^1H NMR (400 MHz, $CDCl_3$): δ 7.09 – 6.96 (m, 1H), 6.35 – 6.24 (m, 2H), 6.21 – 6.12 (m, 2H), 5.82 – 5.77 (m, 1H), 4.20 (q, *J* = 7.1 Hz, 2H), 2.12 – 1.97 (m, 3H), 2.06

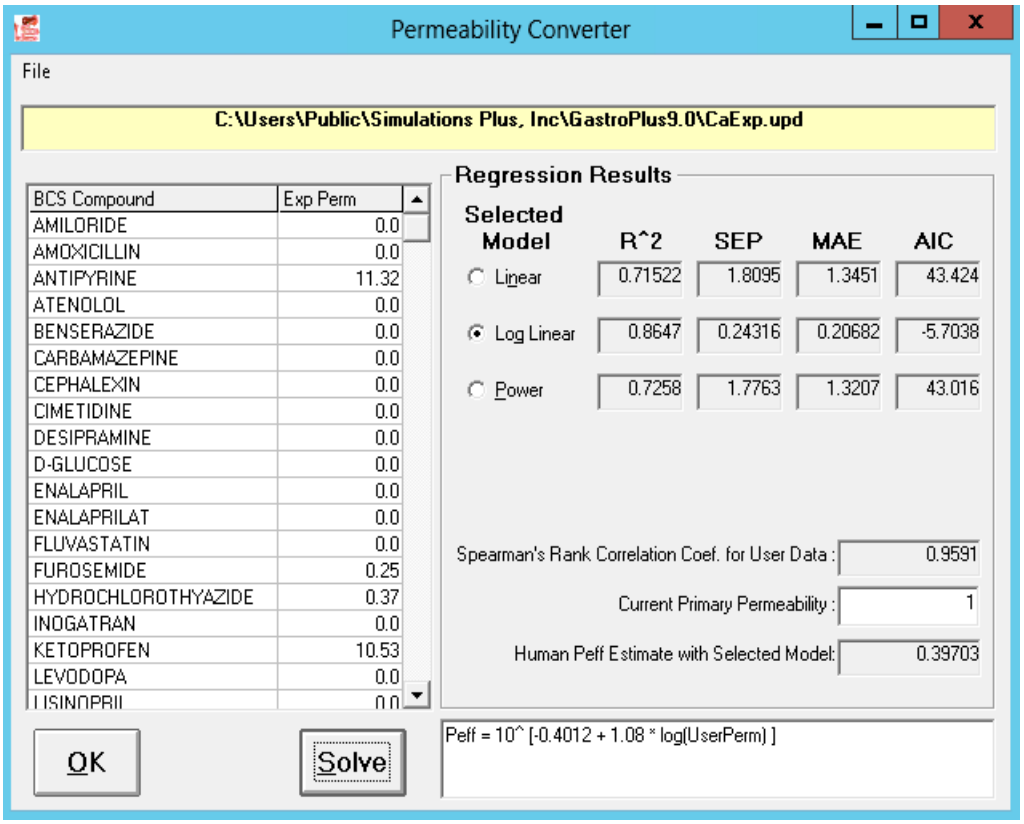
– 1.99 (m, 3H), 1.76 – 1.70 (m, 3H), 1.71 – 1.59 (m, 2H), 1.55 – 1.43 (m, 2H), 1.32 (t, J = 7.1 Hz, 3H), 1.05 (s, 6H). ^{13}C NMR (100 MHz, $CDCl_3$): δ 167.21, 152.70, 139.54, 137.70, 137.48, 137.28, 135.18, 132.13, 130.91, 130.35, 129.99, 129.50, 129.34, 128.63, 128.46, 118.60, 116.59, 59.64, 39.61, 34.27, 33.11, 28.96, 21.74, 19.23, 14.36, 13.83, 12.90. HR-MS (ESI^+): *m/z* $[M+ H]^+$ calculated for $C_{22}H_{33}O_2$, 329.2475, found 329.2476.

RAC (retinoic acid (5-methyl-2-oxo-1,3-dioxolen-4-yl)methyl ester). General synthetic scheme for esterification of RA was used with (5-methyl-2-oxo-1,3-dioxolen-4-yl)methyl alcohol as the reactant. Purification was performed by using hexane:EA = 90:10 as the mobile phase. The final compound was obtained as yellow gum (68.5% yield). Purity was >98% by HPLC-UV. ^{1}H NMR (400 MHz, $CDCl_3$): δ 7.07 (dd, J_1 = 11.4 Hz, J_2 = 15.0 Hz, 1H), 6.37 – 6.25 (m, 2H), 6.24 – 6.12 (m, 2H), 5.79 (s, 1H). ^{13}C NMR (100 MHz, $CDCl_3$): δ 207.07, 166.19, 154.99, 152.26, 140.41, 139.71, 137.65, 137.15, 134.58, 133.97, 133.27, 132.00, 130.23, 130.11, 129.31, 129.15, 129.03, 117.48, 116.63, 114.61, 52.97, 39.60, 39.53, 34.27, 33.12, 33.06, 30.93, 28.95, 21.74, 21.08, 19.20, 14.05, 12.95, 9.40. HR-MS (ESI^+): *m/z* $[M+ H]^+$ calculated for $C_{25}H_{33}O_5$, 413.2323, found 413.2308.

Appendix 2. Establishment of a "user-defined permeability model"

In GastroPlus™, P_{app} values of compounds with known P_{eff} can be given as input to establish a "user-defined permeability model". An example of a "user-defined permeability model" setup is shown in Appendix Figure 2-1. GastroPlus™ provides a list of compounds that the software has known values of P_{eff} (this P_{eff} value is not shown to the users). When the user inputs P_{app} values of these compounds, GastroPlus™ performs internal correlation between the input P_{app} values and their P_{eff} values. The users are then informed of the regression results of the internal correlation. The P_{app} value of the compound of interest can then be applied to this "user-defined permeability model" to give an estimate of the P_{eff} value.

Therefore establishing a "user-defined permeability model" represents calibrating the permeability model in GastroPlus™. Most importantly, same permeability value can result in different simulation results depending on how the "user-defined permeability model" is determined. In this study, same P_{app} values of application set compounds have been applied to different "user-defined permeability models" established by P_{app} values of training set compounds from different laboratories. This was to demonstrate the consequences of directly comparing P_{app} values of a compound across different laboratories.



Appendix Figure 2-1. Establishment of a "user-defined permeability model" in GastroPlus™. The "BCS Compound" refers to the list of reference compounds provided by GastroPlusTM. The P_{app} values of these reference compounds are given as input in the "Exp Perm" column. Following the internal correlation process (initiated by clicking the "Solve" button), regression results are shown for the correlation. The user can select the models between "Linear", "Log Linear" or "Power", after analysing the parameters of each model. Following this process, the user inputs the P_{app} value for the compound of interest in the "Current Primary Permeability" box. After all these processes, the P_{eff} value estimated by the "user-defined permeability model" will be given in the "Human Peff Estimate with Selected Model" box.

Appendix 3. TG measurements in each test medium used for further conversion studies of BET and BCY (mg/mL, n = 3)

	AVG	SD
Blank rat plasma	0.31	0.01
Rat plasma spiked with Intralipid®	0.33	0.02
Postprandial rat lymph	4.05	1.58

REFERENCES

1. World, et al., *World Cancer Report 2014.* WHO Press, 2014.
2. Lozano, R., et al., *Global and regional mortality from 235 causes of death for 20 age groups in 1990 and 2010: a systematic analysis for the Global Burden of Disease Study 2010.* Lancet, 2012. **380**(9859): p. 2095-128.
3. UK, C.R., *All cancers combined, Cancer statistics.* 2015.
4. Schroeder, A., et al., *Treating metastatic cancer with nanotechnology.* Nat Rev Cancer, 2012. **12**(1): p. 39-50.
5. Steeg, P.S., *Tumor metastasis: mechanistic insights and clinical challenges.* Nat Med, 2006. **12**(8): p. 895-904.
6. Ryan, G.M., L.M. Kaminskas, and C.J. Porter, *Nano-chemotherapeutics: maximising lymphatic drug exposure to improve the treatment of lymph-metastatic cancers.* J Control Release, 2014. **193**: p. 241-56.
7. Ries, L.A.G., et al., *SEER Survival Monograph: Cancer Survival Among Adults: U.S. SEER Program, 1988-2001, Patient and Tumor Characteristics.* National Cancer Institute, SEER Program, 2007. **NIH Pub. No. 07-6215, Bethesda, MD**.
8. Lammers, T., W.E. Hennink, and G. Storm, *Tumour-targeted nanomedicines: principles and practice.* Br J Cancer, 2008. **99**(3): p. 392-7.
9. Widakowich, C., et al., *Review: Side Effects of Approved Molecular Targeted Therapies in Solid Cancers.* The Oncologist, 2007. **12**: p. 1443-1455.
10. Porta, C., et al., *Uncovering Pandora's vase: the growing problem of new toxicities from novel anticancer agents. The case of sorafenib and sunitinib.* Clin Exp Med, 2007. **7**(4): p. 127-34.
11. Li, J., et al., *A review on various targeted anticancer therapies.* Target Oncol, 2012. **7**(1): p. 69-85.
12. Singh, Y., M. Palombo, and P.J. Sinko, *Recent trends in targeted anticancer prodrug and conjugate design.* Curr Med Chem, 2008. **15**(18): p. 1802-26.
13. Undevia, S.D., G. Gomez-Abuin, and M.J. Ratain, *Pharmacokinetic variability of anticancer agents.* Nat Rev Cancer, 2005. **5**(6): p. 447-58.
14. Masson, E. and W.C. Zamboni, *Pharmacokinetic optimisation of cancer chemotherapy. Effect on outcomes.* Clin Pharmacokinet, 1997. **32**(4): p. 324-43.
15. Kaestner, S.A. and G.J. Sewell, *Chemotherapy dosing part I: scientific basis for current practice and use of body surface area.* Clin Oncol (R Coll Radiol), 2007. **19**(1): p. 23-37.
16. Zhou, Q. and J.M. Gallo, *The pharmacokinetic/pharmacodynamic pipeline: translating anticancer drug pharmacology to the clinic.* AAPS J, 2011. **13**(1): p. 111-20.
17. Kaestner, S.A. and G.J. Sewell, *Chemotherapy dosing part II: alternative approaches and future prospects.* Clin Oncol (R Coll Radiol), 2007. **19**(2): p. 99-107.
18. Iliadis, A. and D. Barbolosi, *Optimizing drug regimens in cancer chemotherapy by an efficacy-toxicity mathematical model.* Comput Biomed Res, 2000. **33**(3): p. 211-26.
19. van den Bongard, H.J., et al., *Pharmacokinetically guided administration of chemotherapeutic agents.* Clin Pharmacokinet, 2000. **39**(5): p. 345-67.

20. Eddershaw, P.J., A.P. Beresford, and M.K. Bayliss, *ADME/PK as part of a rational approach to drug discovery.* Drug Discovery Today, 2000. **5**(9): p. 409-414.
21. Barton, P. and R.J. Riley, *A new paradigm for navigating compound property related drug attrition.* Drug Discov Today, 2016. **21**(1): p. 72-81.
22. Hellriegel, E.T., T.D. Bjornsson, and W.W. Hauck, *Interpatient variability in bioavailability is related to the extent of absorption: implications for bioavailability and bioequivalence studies.* Clin Pharmacol Ther, 1996. **60**(6): p. 601-7.
23. Li, A.P., *Screening for human ADME/Tox drug properties in drug discovery.* Drug Discov Today, 2001. **6**(7): p. 357-366.
24. Swartz, M.A., *The physiology of the lymphatic system.* Adv Drug Deliv Rev, 2001. **50**(1-2): p. 3-20.
25. Roman, E. and A.G. Smith, *Epidemiology of lymphomas.* Histopathology, 2011. **58**(1): p. 4-14.
26. Fisher, S.G. and R.I. Fisher, *The epidemiology of non-Hodgkin's lymphoma.* Oncogene, 2004. **23**(38): p. 6524-34.
27. Xie, Y., et al., *Drug delivery to the lymphatic system: importance in future cancer diagnosis and therapies.* Expert Opin Drug Deliv, 2009. **6**(8): p. 785-92.
28. Cao, Y., *Opinion: emerging mechanisms of tumour lymphangiogenesis and lymphatic metastasis.* Nat Rev Cancer, 2005. **5**(9): p. 735-43.
29. Nathanson, S.D., *Insights into the mechanisms of lymph node metastasis.* Cancer, 2003. **98**(2): p. 413-23.
30. McAllaster, J.D. and M.S. Cohen, *Role of the lymphatics in cancer metastasis and chemotherapy applications.* Adv Drug Deliv Rev, 2011. **63**(10-11): p. 867-75.
31. Wang, Y. and G. Oliver, *Current views on the function of the lymphatic vasculature in health and disease.* Genes Dev, 2010. **24**(19): p. 2115-26.
32. Kawada, K. and M.M. Taketo, *Significance and mechanism of lymph node metastasis in cancer progression.* Cancer Res, 2011. **71**(4): p. 1214-8.
33. Trevaskis, N.L., L.M. Kaminskas, and C.J. Porter, *From sewer to saviour - targeting the lymphatic system to promote drug exposure and activity.* Nat Rev Drug Discov, 2015. **14**(11): p. 781-803.
34. Nicolas, J.F. and B. Guy, *Intradermal, epidermal and transcutaneous vaccination: from immunology to clinical practice.* Expert Rev Vaccines, 2008. **7**(8): p. 1201-14.
35. Tseng, Y.C., et al., *Lipid-calcium phosphate nanoparticles for delivery to the lymphatic system and SPECT/CT imaging of lymph node metastases.* Biomaterials, 2014. **35**(16): p. 4688-98.
36. Dahlberg, A.M., et al., *The lymphatic system plays a major role in the intravenous and subcutaneous pharmacokinetics of trastuzumab in rats.* Mol Pharm, 2014. **11**(2): p. 496-504.
37. Lycke, N., *Recent progress in mucosal vaccine development: potential and limitations.* Nat Rev Immunol, 2012. **12**(8): p. 592-605.
38. Swartz, M.A., S. Hirosue, and J.A. Hubbell, *Engineering approaches to immunotherapy.* Sci Transl Med, 2012. **4**(148): p. 148rv9.
39. Gershkovich, P. and A. Hoffman, *Uptake of lipophilic drugs by plasma derived isolated chylomicrons: linear correlation with intestinal lymphatic bioavailability.* Eur J Pharm Sci, 2005. **26**(5): p. 394-404.

40. Gershkovich, P., et al., *Different impacts of intestinal lymphatic transport on the oral bioavailability of structurally similar synthetic lipophilic cannabinoids: dexanabinol and PRS-211,220.* Eur J Pharm Sci, 2007. **31**(5): p. 298-305.
41. Trevaskis, N.L., W.N. Charman, and C.J. Porter, *Lipid-based delivery systems and intestinal lymphatic drug transport: a mechanistic update.* Adv Drug Deliv Rev, 2008. **60**(6): p. 702-16.
42. Lucey, B.C., J.W. Stuhlfaut, and J.A. Soto, *Mesenteric lymph nodes seen at imaging: causes and significance.* Radiographics, 2005. **25**(2): p. 351-65.
43. Cole, S.M., *Computed tomography of lymphomatous involvement of mesenteric nodes.* Radiography, 1986. **52**(606): p. 299-301.
44. Mueller, P.R., et al., *Appearance of lymphomatous involvement of the mesentery by ultrasonography and body computed tomography: the "sandwich sign".* Radiology, 1980. **134**(2): p. 467-73.
45. Horton, K.M., L.P. Lawler, and E.K. Fishman, *CT findings in sclerosing mesenteritis (panniculitis): spectrum of disease.* Radiographics, 2003. **23**(6): p. 1561-7.
46. Hardy, S.M., *The sandwich sign.* Radiology, 2003. **226**(3): p. 651-2.
47. Anis, M. and A. Irshad, *Imaging of abdominal lymphoma.* Radiol Clin North Am, 2008. **46**(2): p. 265-85, viii-ix.
48. Manzella, A., et al., *Abdominal manifestations of lymphoma: spectrum of imaging features.* ISRN Radiol, 2013. **2013**: p. 483069.
49. Salemis, N.S., et al., *Diffuse large B cell lymphoma of the mesentery: an unusual presentation and review of the literature.* J Gastrointest Cancer, 2009. **40**(3-4): p. 79-82.
50. DeVita, V.T., T.S. Lawrence, and S.A. Rosenberg, *Devita, Hellman, and Rosenberg's cancer : principles & practice of oncology*. 10th edition. ed. 2015, Philadelphia: Wolters Kluwer. xlv, 2234 pages.
51. Mindelzun, R.E., et al., *The misty mesentery on CT: differential diagnosis.* AJR Am J Roentgenol, 1996. **167**(1): p. 61-5.
52. Sabate, J.M., et al., *Sclerosing mesenteritis: imaging findings in 17 patients.* AJR Am J Roentgenol, 1999. **172**(3): p. 625-9.
53. Yenarkarn, P., R.F. Thoeni, and D. Hanks, *Case 107: lymphoma of the mesentery.* Radiology, 2007. **242**(2): p. 628-31.
54. Goffinet, D.R., et al., *Clinical and surgical (laparotomy) evaluation of patients with non-Hodgkin's lymphomas.* Cancer Treat Rep, 1977. **61**(6): p. 981-92.
55. Goffinet, D.R., et al., *Abdominal irradiation in non-Hodgkin's lymphomas.* Cancer, 1976. **37**(6): p. 2797-805.
56. Solimando, A.G., et al., *Targeting B-cell non Hodgkin lymphoma: New and old tricks.* Leuk Res, 2016.
57. Ansell, S.M., *Non-Hodgkin Lymphoma: Diagnosis and Treatment.* Mayo Clin Proc, 2015. **90**(8): p. 1152-63.
58. Nishioka, Y. and H. Yoshino, *Lymphatic targeting with nanoparticulate system.* Adv Drug Deliv Rev, 2001. **47**(1): p. 55-64.
59. Charman, W.N. and C.J.H. Porter, *Lipophilic prodrugs designed for intestinal lymphatic transport.* Advanced Drug Delivery Reviews, 1996. **19**(2): p. 149-169.
60. Edwards, G.A., et al., *Animal models for the study of intestinal lymphatic drug transport.* Adv Drug Deliv Rev, 2001. **50**(1-2): p. 45-60.

61. Gershkovich, P., et al., *The role of molecular physicochemical properties and apolipoproteins in association of drugs with triglyceride-rich lipoproteins: in-silico prediction of uptake by chylomicrons.* J Pharm Pharmacol, 2009. **61**(1): p. 31-9.
62. Borkar, N., et al., *Lipophilic prodrugs of apomorphine I: preparation, characterisation, and in vitro enzymatic hydrolysis in biorelevant media.* Eur J Pharm Biopharm, 2015. **89**: p. 216-23.
63. Zgair, A., et al., *Oral administration of cannabis with lipids leads to high levels of cannabinoids in the intestinal lymphatic system and prominent immunomodulation.* Scientific Reports, 2017. **7**(1).
64. Zgair, A., et al., *Dietary fats and pharmaceutical lipid excipients increase systemic exposure to orally administered cannabis and cannabis-based medicines.* Am J Transl Res, 2016. **8**(8): p. 3448-59.
65. Zgair, A., et al., *Targeting Cannabidiol to the Intestinal Lymphatic System for Enhanced Immunomodulatory Effects in the Treatment of Autoimmune Diseases.* Proceedings of Annual Meeting of American Association of Pharmaceutical Scientists, 2016. **Denver, USA, 16 Nov**
66. Hu, L., et al., *Glyceride-Mimetic Prodrugs Incorporating Self-Immolative Spacers Promote Lymphatic Transport, Avoid First-Pass Metabolism, and Enhance Oral Bioavailability.* Angew Chem Int Ed Engl, 2016. **55**(44): p. 13700-13705.
67. Khanna, I., *Drug discovery in pharmaceutical industry: productivity challenges and trends.* Drug Discov Today, 2012. **17**(19-20): p. 1088-102.
68. Yu, H. and A. Adedoyin, *ADME-Tox in drug discovery: integration of experimental and computational technologies.* Drug Discov Today, 2003. **8**(18): p. 852-61.
69. Di, L. and E.H. Kerns, *Profiling drug-like properties in discovery research.* Curr Opin Chem Biol, 2003. **7**(3): p. 402-8.
70. Kassel, D.B., *Applications of high-throughput ADME in drug discovery.* Curr Opin Chem Biol, 2004. **8**(3): p. 339-45.
71. Dressman, J.B., K. Thelen, and S. Willmann, *An update on computational oral absorption simulation.* Expert Opinion on Drug Metabolism & Toxicology, 2011. **7**(11): p. 1345-1364.
72. Bergstrom, C.A., et al., *Early pharmaceutical profiling to predict oral drug absorption: current status and unmet needs.* Eur J Pharm Sci, 2014. **57**: p. 173-99.
73. Selick, H.E., A.P. Beresford, and M.H. Tarbit, *The emerging importance of predictive ADME simulation in drug discovery.* Drug Discov Today, 2002. **7**(2): p. 109-16.
74. Smith, D.A., *Evolution of ADME science: where else can modeling and simulation contribute?* Mol Pharm, 2013. **10**(4): p. 1162-70.
75. O'Neill, V.J. and C.J. Twelves, *Oral cancer treatment: developments in chemotherapy and beyond.* Br. J. Cancer, 2002. **87**(9): p. 933-7.
76. Thanki, K., et al., *Oral delivery of anticancer drugs: challenges and opportunities.* J. Control. Release, 2013. **170**(1): p. 15-40.
77. Barillet, M., et al., *Oral antineoplastic agents: how do we care about adherence?* Br J Clin Pharmacol, 2015. **80**(6): p. 1289-302.
78. Ruddy, K., E. Mayer, and A. Partridge, *Patient adherence and persistence with oral anticancer treatment.* CA. Cancer J. Clin., 2009. **59**(1): p. 56-66.

79. Banna, G.L., et al., *Anticancer oral therapy: emerging related issues.* Cancer Treat. Rev., 2010. **36**(8): p. 595-605.
80. Lapenna, S. and A. Giordano, *Cell cycle kinases as therapeutic targets for cancer.* Nat Rev Drug Discov, 2009. **8**(7): p. 547-66.
81. Wang, S. and P.M. Fischer, *Cyclin-dependent kinase 9: a key transcriptional regulator and potential drug target in oncology, virology and cardiology.* Trends Pharmacol Sci, 2008. **29**(6): p. 302-13.
82. Shao, H., et al., *Substituted 4-(thiazol-5-yl)-2-(phenylamino)pyrimidines are highly active CDK9 inhibitors: synthesis, X-ray crystal structures, structure-activity relationship, and anticancer activities.* J Med Chem, 2013. **56**(3): p. 640-59.
83. Walsby, E., et al., *A novel Cdk9 inhibitor preferentially targets tumor cells and synergizes with fludarabine.* Oncotarget, 2014. **5**(2): p. 375-85.
84. Liu, X., et al., *CDKI-71, a novel CDK9 inhibitor, is preferentially cytotoxic to cancer cells compared to flavopiridol.* Int J Cancer, 2012. **130**(5): p. 1216-26.
85. Shao, H., et al., *Synthesis, structure-activity relationship and biological evaluation of 2,4,5-trisubstituted pyrimidine CDK inhibitors as potential anti-tumour agents.* Eur J Med Chem, 2013. **70**: p. 447-55.
86. Rumondor, A.C., S.S. Dhareshwar, and F. Kesisoglou, *Amorphous Solid Dispersions or Prodrugs: Complementary Strategies to Increase Drug Absorption.* J Pharm Sci, 2016. **105**(9): p. 2498-508.
87. Aungst, B.J., *Intestinal permeation enhancers.* J Pharm Sci, 2000. **89**(4): p. 429-42.
88. DeMario, M.D. and M.J. Ratain, *Oral chemotherapy: rationale and future directions.* J Clin Oncol, 1998. **16**(7): p. 2557-67.
89. Stappaerts, J., et al., *Rapid conversion of the ester prodrug abiraterone acetate results in intestinal supersaturation and enhanced absorption of abiraterone: in vitro, rat in situ and human in vivo studies.* Eur J Pharm Biopharm, 2015. **90**: p. 1-7.
90. Taha, D.A., et al., *The role of acid-base imbalance in statin-induced myotoxicity.* Transl Res, 2016.
91. Taha, D.A., et al., *Hyperlipidaemia alone and in combination with acidosis can increase the incidence and severity of statin-induced myotoxicity.* Eur J Pharm Sci, 2017. **100**: p. 163-175.
92. Qazzaz, M.E., et al., *In vitro anticancer properties and biological evaluation of novel natural alkaloid jerantinine B.* Cancer Lett, 2016. **370**(2): p. 185-97.
93. Lee, J.B., et al., *Quantitative analysis of lab-to-lab variability in Caco-2 permeability assays.* Eur J Pharm Biopharm, 2017. **114**: p. 38-42.
94. Hubatsch, I., E.G. Ragnarsson, and P. Artursson, *Determination of drug permeability and prediction of drug absorption in Caco-2 monolayers.* Nat Protoc, 2007. **2**(9): p. 2111-9.
95. Dressman, J.B., et al., *Estimating drug solubility in the gastrointestinal tract.* Adv Drug Deliv Rev, 2007. **59**(7): p. 591-602.
96. Vertzoni, M., et al., *Simulation of fasting gastric conditions and its importance for the in vivo dissolution of lipophilic compounds.* Eur J Pharm Biopharm, 2005. **60**(3): p. 413-7.
97. Merchant, H.A., et al., *Gastrointestinal characterisation and drug solubility determination in animals.* J Pharm Pharmacol, 2015. **67**(5): p. 630-9.
98. Taha, D.A., et al., *The role of acid-base imbalance in statin-induced myotoxicity.* Transl Res, 2016. **174**: p. 140-160 e14.

99. Obach, R.S., et al., *The prediction of human pharmacokinetic parameters from preclinical and in vitro metabolism data.* J Pharmacol Exp Ther, 1997. **283**(1): p. 46-58.
100. Obach, R.S., *Prediction of human clearance of twenty-nine drugs from hepatic microsomal intrinsic clearance data: An examination of in vitro half-life approach and nonspecific binding to microsomes.* Drug Metab Dispos, 1999. **27**(11): p. 1350-9.
101. Naritomi, Y., et al., *Prediction of human hepatic clearance from in vivo animal experiments and in vitro metabolic studies with liver microsomes from animals and humans.* Drug Metab Dispos, 2001. **29**(10): p. 1316-24.
102. Kwon, Y., *Handbook of Essential Pharmacokinetics, Pharmacodynamics and Drug Metabolism for Industrial Scientists*. 2001: Kluwer Academic Publishers.
103. Kromdijk, W., et al., *Quantitative determination of oseltamivir and oseltamivir carboxylate in human fluoride EDTA plasma including the ex vivo stability using high-performance liquid chromatography coupled with electrospray ionization tandem mass spectrometry.* J Chromatogr B Analyt Technol Biomed Life Sci, 2012. **891-892**: p. 57-63.
104. Kim, M.S., et al., *Determination of a peroxisome proliferator-activated receptor gamma agonist, 1-(trans-methylimino-N-oxy)-6-(2-morpholinoethoxy-3-phenyl-1H-indene-2-carboxylic acid ethyl ester (KR-62980) in rat plasma by liquid chromatography-tandem mass spectrometry.* J Pharm Biomed Anal, 2011. **54**(1): p. 121-6.
105. Parkinson, C.M., et al., *Diagnostic necropsy and selected tissue and sample collection in rats and mice.* J Vis Exp, 2011(54).
106. Kagan, L., et al., *The role of the lymphatic system in subcutaneous absorption of macromolecules in the rat model.* Eur J Pharm Biopharm, 2007. **67**(3): p. 759-65.
107. Farol, L.T. and K.B. Hymes, *Bexarotene: a clinical review.* Expert Rev Anticancer Ther, 2004. **4**(2): p. 180-8.
108. Boehm, M.F., et al., *Synthesis and structure-activity relationships of novel retinoid X receptor-selective retinoids.* J Med Chem, 1994. **37**(18): p. 2930-41.
109. Abbott, R.A., et al., *Bexarotene therapy for mycosis fungoides and Sezary syndrome.* Br J Dermatol, 2009. **160**(6): p. 1299-307.
110. Duvic, M., et al., *Phase 2 and 3 clinical trial of oral bexarotene (Targretin capsules) for the treatment of refractory or persistent early-stage cutaneous T-cell lymphoma.* Arch Dermatol, 2001. **137**(5): p. 581-93.
111. Mehta, N., et al., *Bexarotene is active against subcutaneous panniculitis-like T-cell lymphoma in adult and pediatric populations.* Clin Lymphoma Myeloma Leuk, 2012. **12**(1): p. 20-5.
112. Dragnev, K.H., et al., *A proof-of-principle clinical trial of bexarotene in patients with non-small cell lung cancer.* Clin Cancer Res, 2007. **13**(6): p. 1794-800.
113. Rigas, J.R. and K.H. Dragnev, *Emerging role of rexinoids in non-small cell lung cancer: focus on bexarotene.* Oncologist, 2005. **10**(1): p. 22-33.
114. Wakelee, H.A., et al., *A phase I pharmacokinetic study of bexarotene with vinorelbine and cisplatin in patients with advanced non-small-cell lung cancer (NSCLC).* Cancer Chemother Pharmacol, 2012. **69**(3): p. 815-24.

115. Blumenschein, G.R., Jr., et al., *Phase III trial comparing carboplatin, paclitaxel, and bexarotene with carboplatin and paclitaxel in chemotherapy-naive patients with advanced or metastatic non-small-cell lung cancer: SPIRIT II.* J Clin Oncol, 2008. **26**(11): p. 1879-85.
116. Welch, J.S., et al., *A phase I dose escalation study of oral bexarotene in combination with intravenous decitabine in patients with AML.* Am J Hematol, 2014. **89**(8): p. E103-8.
117. Tsai, D.E., et al., *A phase I study of bexarotene, a retinoic X receptor agonist, in non-M3 acute myeloid leukemia.* Clin Cancer Res, 2008. **14**(17): p. 5619-25.
118. Dragnev, K.H., et al., *Bexarotene and erlotinib for aerodigestive tract cancer.* J Clin Oncol, 2005. **23**(34): p. 8757-64.
119. Esteva, F.J., *Multicenter Phase II Study of Oral Bexarotene for Patients With Metastatic Breast Cancer.* Journal of Clinical Oncology, 2003. **21**(6): p. 999-1006.
120. Liu, Y.Y., et al., *Bexarotene increases uptake of radioiodide in metastases of differentiated thyroid carcinoma.* Eur J Endocrinol, 2006. **154**(4): p. 525-31.
121. Marquez, C.B., et al., *Multiple keratoacanthomas arising in the setting of sorafenib therapy: novel chemoprophylaxis with bexarotene.* Cancer Control, 2009. **16**(1): p. 66-9.
122. Aicardi, G., *New hope from an old drug: fighting Alzheimer's disease with the cancer drug bexarotene (targretin)?* Rejuvenation Res, 2013. **16**(6): p. 524-8.
123. Tousi, B., *The emerging role of bexarotene in the treatment of Alzheimer's disease: current evidence.* Neuropsychiatr Dis Treat, 2015. **11**: p. 311-5.
124. Cramer, P.E., et al., *ApoE-directed therapeutics rapidly clear beta-amyloid and reverse deficits in AD mouse models.* Science, 2012. **335**(6075): p. 1503-6.
125. Bomben, V., et al., *Bexarotene reduces network excitability in models of Alzheimer's disease and epilepsy.* Neurobiol Aging, 2014. **35**(9): p. 2091-5.
126. Schafer, A., E.S. Burstein, and R. Olsson, *Bexarotene prodrugs: targeting through cleavage by NQO1 (DT-diaphorase).* Bioorg Med Chem Lett, 2014. **24**(8): p. 1944-7.
127. Tesseur, I. and B. De Strooper, *When the dust settles: what did we learn from the bexarotene discussion?* Alzheimers Res Ther, 2013. **5**(6): p. 54.
128. LaClair, K.D., et al., *Treatment with bexarotene, a compound that increases apolipoprotein-E, provides no cognitive benefit in mutant APP/PS1 mice.* Mol Neurodegener, 2013. **8**: p. 18.
129. Hanifin, J.M., et al., *Novel treatment of chronic severe hand dermatitis with bexarotene gel.* Br J Dermatol, 2004. **150**(3): p. 545-53.
130. Krathen, R.A., S. Ward, and M. Duvic, *Bexarotene Is a New Treatment Option for Lymphomatoid Papulosis.* Dermatology, 2003. **206**(2): p. 142-147.
131. Smit, J.V., et al., *A phase II multicenter clinical trial of systemic bexarotene in psoriasis.* J Am Acad Dermatol, 2004. **51**(2): p. 249-56.
132. Talpur, R., et al., *Phase I/II randomized bilateral half-head comparison of topical bexarotene 1% gel for alopecia areata.* J Am Acad Dermatol, 2009. **61**(4): p. 592 e1-9.
133. George, M., et al., *Newer antipsychotics and upcoming molecules for schizophrenia.* Eur J Clin Pharmacol, 2013. **69**(8): p. 1497-509.
134. Tritos, N.A. and B.M. Biller, *Advances in medical therapies for Cushing's syndrome.* Discov Med, 2012. **13**(69): p. 171-9.

135. Qu, L. and X. Tang, *Bexarotene: a promising anticancer agent.* Cancer Chemother Pharmacol, 2010. **65**(2): p. 201-5.
136. Kizaki, M., et al., *Effects of novel retinoid X receptor-selective ligands on myeloid leukemia differentiation and proliferation in vitro.* Blood, 1996. **87**(5): p. 1977-84.
137. Cesario, R.M., et al., *Differentiation and growth inhibition mediated via the RXR:PPARgamma heterodimer in colon cancer.* Cancer Lett, 2006. **240**(2): p. 225-33.
138. Yen, W.C. and W.W. Lamph, *A selective retinoid X receptor agonist bexarotene (LGD1069, Targretin) prevents and overcomes multidrug resistance in advanced prostate cancer.* Prostate, 2006. **66**(3): p. 305-16.
139. Yen, W.C., et al., *A selective retinoid X receptor agonist bexarotene (LGD1069, targretin) inhibits angiogenesis and metastasis in solid tumours.* Br J Cancer, 2006. **94**(5): p. 654-60.
140. Wang, Y., et al., *Prevention of lung cancer progression by bexarotene in mouse models.* Oncogene, 2006. **25**(9): p. 1320-9.
141. Wang, Y., et al., *Preventive effects of bexarotene and budesonide in a genetically engineered mouse model of small cell lung cancer.* Cancer Prev Res (Phila), 2009. **2**(12): p. 1059-64.
142. Kim, H.T., et al., *Identification of biomarkers modulated by the rexinoid LGD1069 (bexarotene) in human breast cells using oligonucleotide arrays.* Cancer Res, 2006. **66**(24): p. 12009-18.
143. Janakiram, N.B., et al., *Chemopreventive Effects of RXR-Selective Rexinoid Bexarotene on Intestinal Neoplasia of ApcMin/+ Mice.* Neoplasia, 2012. **14**(2): p. 159-168.
144. Xu, L., et al., *Bexarotene reduces blood-brain barrier permeability in cerebral ischemia-reperfusion injured rats.* PLoS One, 2015. **10**(4): p. e0122744.
145. McFarland, K., et al., *Low dose bexarotene treatment rescues dopamine neurons and restores behavioral function in models of Parkinson's disease.* ACS Chem Neurosci, 2013. **4**(11): p. 1430-8.
146. Lalloyer, F., et al., *The RXR agonist bexarotene improves cholesterol homeostasis and inhibits atherosclerosis progression in a mouse model of mixed dyslipidemia.* Arterioscler Thromb Vasc Biol, 2006. **26**(12): p. 2731-7.
147. Lalloyer, F., et al., *Rexinoid bexarotene modulates triglyceride but not cholesterol metabolism via gene-specific permissivity of the RXR/LXR heterodimer in the liver.* Arterioscler Thromb Vasc Biol, 2009. **29**(10): p. 1488-95.
148. Chen, L., et al., *Bexarotene nanocrystal-Oral and parenteral formulation development, characterization and pharmacokinetic evaluation.* Eur J Pharm Biopharm, 2014. **87**(1): p. 160-9.
149. Li, L., et al., *Preparation, in vitro and in vivo evaluation of bexarotene nanocrystals with surface modification by folate-chitosan conjugates.* Drug Deliv, 2016. **23**(1): p. 79-87.
150. van de Merbel, N.C., et al., *Validated liquid chromatographic method for the determination of bexarotene in human plasma.* J Chromatogr B Analyt Technol Biomed Life Sci, 2002. **775**(2): p. 189-95.
151. Services, U.S.D.o.H.a.H., *Guidance for Industry, Bioanalyical Method Validation.* 2001.

152. Miller, V.A., et al., *Initial clinical trial of a selective retinoid X receptor ligand, LGD1069.* J Clin Oncol, 1997. **15**(2): p. 790-5.
153. Howell, S.R., et al., *Bexarotene metabolism in rat, dog, and human, synthesis of oxidative metabolites, and in vitro activity at retinoid receptors.* Drug Metab Dispos, 2001. **29**(7): p. 990-8.
154. Gershkovich, P., et al., *A simple and sensitive method for determination of vitamins D3 and K1 in rat plasma: application for an in vivo pharmacokinetic study.* Drug Dev Ind Pharm, 2014. **40**(3): p. 338-44.
155. Zgair, A., et al., *Development of a simple and sensitive HPLC-UV method for the simultaneous determination of cannabidiol and Delta(9)-tetrahydrocannabinol in rat plasma.* J Pharm Biomed Anal, 2015. **114**: p. 145-51.
156. Watzl, B., S. Girrbach, and M. Roller, *Inulin, oligofructose and immunomodulation.* Br J Nutr, 2005. **93 Suppl 1**: p. S49-55.
157. Miura, S., et al., *Modulation of intestinal immune system by dietary fat intake: relevance to Crohn's disease.* J Gastroenterol Hepatol, 1998. **13**(12): p. 1183-90.
158. Zgair, A., J.C.M. Wong, and P. Gershkovich, *Targeting Immunomodulatory Agents to the Gut-Associated Lymphoid Tissue,* in *Neuro-Immuno-Gastroenterology*, C. Constantinescu, R. Arsenescu, and V. Arsenescu, Editors. 2016, Springer International Publishing: Cham. p. 237-261.
159. Han, S., et al., *Targeted delivery of a model immunomodulator to the lymphatic system: comparison of alkyl ester versus triglyceride mimetic lipid prodrug strategies.* J Control Release, 2014. **177**: p. 1-10.
160. Estaquier, J. and B. Hurtrel, *[Mesenteric lymph nodes, a sanctuary for the persistance of HIV. Escape mechanisms]*. Med Sci (Paris), 2008. **24**(12): p. 1055-60.
161. Gershenwald, J.E. and I.J. Fidler, *Cancer. Targeting lymphatic metastasis.* Science, 2002. **296**(5574): p. 1811-2.
162. Zheng, X., et al., *Tracking Cancer Metastasis In Vivo by Using an Iridium-Based Hypoxia-Activated Optical Oxygen Nanosensor.* Angew Chem Int Ed Engl, 2015. **54**(28): p. 8094-9.
163. Amory, J.K., et al., *Oral testosterone-triglyceride conjugate in rabbits: single-dose pharmacokinetics and comparison with oral testosterone undecanoate.* J Androl, 2003. **24**(5): p. 716-20.
164. Malec, J., et al., *In silico modelling of chylomicron association to predict lymphatic absorption of small molecules.* Proceedings of Annual Meeting of Population Approach Group in Europe, 2017. **June 2017**.
165. Lee, J.B., et al., *Simple and sensitive HPLC-UV method for determination of bexarotene in rat plasma.* J Chromatogr B Analyt Technol Biomed Life Sci, 2017. **1040**: p. 73-80.
166. Tallarida, R.J., *Quantitative methods for assessing drug synergism.* Genes Cancer, 2011. **2**(11): p. 1003-8.
167. Manouilov, K.K., et al., *Lymphatic distribution of 3'-azido-3'-deoxythymidine and 3'-azido-2',3'-dideoxyuridine in mice.* Drug Metab Dispos, 1995. **23**(6): p. 655-8.
168. Fletcher, C.V., et al., *Persistent HIV-1 replication is associated with lower antiretroviral drug concentrations in lymphatic tissues.* Proc Natl Acad Sci U S A, 2014. **111**(6): p. 2307-12.

169. Fanous, M.Y., A.J. Phillips, and J.A. Windsor, *Mesenteric lymph: the bridge to future management of critical illness.* JOP, 2007. **8**(4): p. 374-99.
170. Woodnutt, G., V. Berry, and L. Mizen, *Effect of protein binding on penetration of beta-lactams into rabbit peripheral lymph.* Antimicrob Agents Chemother, 1995. **39**(12): p. 2678-83.
171. Bala, V., et al., *Lipophilic Prodrugs of SN38: Synthesis and in Vitro Characterization toward Oral Chemotherapy.* Mol Pharm, 2016. **13**(1): p. 287-94.
172. Borde, A.S., et al., *Assessment of enzymatic prodrug stability in human, dog and simulated intestinal fluids.* Eur J Pharm Biopharm, 2012. **80**(3): p. 630-7.
173. Crauste-Manciet, S., et al., *Cefpodoxime-proxetil protection from intestinal lumen hydrolysis by oil-in-water submicron emulsions.* International Journal of Pharmaceutics, 1998. **165**(1): p. 97-106.
174. Beaumont, K., et al., *Design of ester prodrugs to enhance oral absorption of poorly permeable compounds: challenges to the discovery scientist.* Curr Drug Metab, 2003. **4**(6): p. 461-85.
175. Altucci, L., et al., *RAR and RXR modulation in cancer and metabolic disease.* Nat Rev Drug Discov, 2007. **6**(10): p. 793-810.
176. Dawson, M.I. and Z. Xia, *The retinoid X receptors and their ligands.* Biochim Biophys Acta, 2012. **1821**(1): p. 21-56.
177. Irvine, J.D., et al., *MDCK (Madin-Darby canine kidney) cells: A tool for membrane permeability screening.* J Pharm Sci, 1999. **88**(1): p. 28-33.
178. Li, C., et al., *Development of in vitro pharmacokinetic screens using Caco-2, human hepatocyte, and Caco-2/human hepatocyte hybrid systems for the prediction of oral bioavailability in humans.* J Biomol Screen, 2007. **12**(8): p. 1084-91.
179. Zhu, C., et al., *A comparative study of artificial membrane permeability assay for high throughput profiling of drug absorption potential.* Eur J Med Chem, 2002. **37**(5): p. 399-407.
180. Skolnik, S., et al., *Towards prediction of in vivo intestinal absorption using a 96-well Caco-2 assay.* J Pharm Sci, 2010. **99**(7): p. 3246-65.
181. Kerns, E.H., et al., *Combined application of parallel artificial membrane permeability assay and Caco-2 permeability assays in drug discovery.* J Pharm Sci, 2004. **93**(6): p. 1440-53.
182. Volpe, D.A., *Variability in Caco-2 and MDCK cell-based intestinal permeability assays.* J Pharm Sci, 2008. **97**(2): p. 712-25.
183. Alsenz, J. and E. Haenel, *Development of a 7-day, 96-well Caco-2 permeability assay with high-throughput direct UV compound analysis.* Pharm Res, 2003. **20**(12): p. 1961-9.
184. Larregieu, C.A. and L.Z. Benet, *Distinguishing between the permeability relationships with absorption and metabolism to improve BCS and BDDCS predictions in early drug discovery.* Mol Pharm, 2014. **11**(4): p. 1335-44.
185. Varma, M.V., K. Sateesh, and R. Panchagnula, *Functional role of P-glycoprotein in limiting intestinal absorption of drugs: contribution of passive permeability to P-glycoprotein mediated efflux transport.* Mol Pharm, 2005. **2**(1): p. 12-21.
186. Yazdanian, M., et al., *Correlating partitioning and caco-2 cell permeability of structurally diverse small molecular weight compounds.* Pharm Res, 1998. **15**(9): p. 1490-4.

187. Muirhead, G.J., et al., *Comparative human pharmacokinetics and metabolism of single-dose oral and intravenous sildenafil.* Br J Clin Pharmacol, 2002. **53 Suppl 1**: p. 13S-20S.
188. Amidon, G.L., et al., *A theoretical basis for a biopharmaceutic drug classification: the correlation of in vitro drug product dissolution and in vivo bioavailability.* Pharm Res, 1995. **12**(3): p. 413-20.
189. Augustijns, P., et al., *A review of drug solubility in human intestinal fluids: implications for the prediction of oral absorption.* Eur J Pharm Sci, 2014. **57**: p. 322-32.
190. Lee, J.B., et al., *A novel in vitro permeability assay using three-dimensional cell culture system.* J Biotechnol, 2015. **205**: p. 93-100.
191. Lennernas, H., *Regional intestinal drug permeation: biopharmaceutics and drug development.* Eur J Pharm Sci, 2014. **57**: p. 333-41.
192. Balls, M. and J.H. Fentem, *The validation and acceptance of alternatives to animal testing.* Toxicol In Vitro, 1999. **13**(4-5): p. 837-46.
193. Hakkinen, P.J. and D.K. Green, *Alternatives to animal testing: information resources via the Internet and World Wide Web.* Toxicology, 2002. **173**(1-2): p. 3-11.
194. Russell, W.M.S. and R.L. Burch, *The principles of humane experimental technique*. 1959, London,: Methuen. 238 p.
195. Kroeger, M., *How omics technologies can contribute to the '3R' principles by introducing new strategies in animal testing.* Trends Biotechnol, 2006. **24**(8): p. 343-6.
196. Schroeder, G.M., et al., *Discovery of N-(4-(2-amino-3-chloropyridin-4-yloxy)-3-fluorophenyl)-4-ethoxy-1-(4-fluorophenyl)-2-oxo-1,2-dihydropyridine-3-carboxamide (BMS-777607), a selective and orally efficacious inhibitor of the Met kinase superfamily.* J Med Chem, 2009. **52**(5): p. 1251-4.
197. Tian, X., et al., *Discovery of orally bioavailable 1,3,4-trisubstituted 2-oxopiperazine-based melanocortin-4 receptor agonists as potential antiobesity agents.* J Med Chem, 2008. **51**(19): p. 6055-66.
198. Liu, Q., et al., *Discovery of 9-(6-aminopyridin-3-yl)-1-(3-(trifluoromethyl)phenyl)benzo[h][1,6]naphthyridin-2(1H)-one (Torin2) as a potent, selective, and orally available mammalian target of rapamycin (mTOR) inhibitor for treatment of cancer.* J Med Chem, 2011. **54**(5): p. 1473-80.
199. Augeri, D.J., et al., *Discovery and preclinical profile of Saxagliptin (BMS-477118): a highly potent, long-acting, orally active dipeptidyl peptidase IV inhibitor for the treatment of type 2 diabetes.* J Med Chem, 2005. **48**(15): p. 5025-37.
200. Yeh, V.S., et al., *Discovery of orally active butyrolactam 11beta-HSD1 inhibitors.* Bioorg Med Chem Lett, 2006. **16**(21): p. 5555-60.
201. Cai, Z.W., et al., *Discovery of orally active pyrrolopyridine- and aminopyridine-based Met kinase inhibitors.* Bioorg Med Chem Lett, 2008. **18**(11): p. 3224-9.
202. Miller, W.H., et al., *Discovery of orally active nonpeptide vitronectin receptor antagonists based on a 2-benzazepine Gly-Asp mimetic.* J Med Chem, 2000. **43**(1): p. 22-6.
203. Choi, H., et al., *Discovery of potent, selective, and orally bioavailable PDE5 inhibitor: Methyl-4-(3-chloro-4-methoxybenzylamino)-8-(2-hydroxyethyl)-7-*

methoxyquinazolin-6 -ylmethylcarbamate (CKD 533). Bioorg Med Chem Lett, 2010. **20**(1): p. 383-6.
204. Hughes, R.O., et al., *Investigation of aminopyridiopyrazinones as PDE5 inhibitors: Evaluation of modifications to the central ring system.* Bioorg Med Chem Lett, 2009. **19**(15): p. 4092-6.
205. Panchagnula, R. and N.S. Thomas, *Biopharmaceutics and pharmacokinetics in drug research.* International Journal of Pharmaceutics, 2000. **201**(2): p. 131-150.
206. Sanchez-Martinez, C., et al., *Cyclin dependent kinase (CDK) inhibitors as anticancer drugs.* Bioorg Med Chem Lett, 2015. **25**(17): p. 3420-35.
207. Santo, L., K.T. Siu, and N. Raje, *Targeting Cyclin-Dependent Kinases and Cell Cycle Progression in Human Cancers.* Semin Oncol, 2015. **42**(6): p. 788-800.
208. Wang, S. and P.M. Fischer, *Cyclin-dependent kinase 9: a key transcriptional regulator and potential drug target in oncology, virology and cardiology.* Trends Pharmacol. Sci., 2008. **29**(6): p. 302-13.
209. Smith, H.W., *Observations on the Flora of the Alimentary Tract of Animals and Factors Affecting Its Composition.* J Pathol Bacteriol, 1965. **89**: p. 95-122.
210. Ward, F.W. and M.E. Coates, *Gastrointestinal pH measurement in rats: influence of the microbial flora, diet and fasting.* Lab Anim, 1987. **21**(3): p. 216-22.
211. Evans, D.F., et al., *Measurement of gastrointestinal pH profiles in normal ambulant human subjects.* Gut, 1988. **29**(8): p. 1035-41.
212. Agoram, B., W.S. Woltosz, and M.B. Bolger, *Predicting the impact of physiological and biochemical processes on oral drug bioavailability.* Advanced Drug Delivery Reviews, 2001. **50**: p. S41-S67.
213. Polli, J.W., et al., *Rational use of in vitro P-glycoprotein assays in drug discovery.* Journal of Pharmacology and Experimental Therapeutics, 2001. **299**(2): p. 620-628.
214. Mensch, J., et al., *Application of PAMPA-models to predict BBB permeability including efflux ratio, plasma protein binding and physicochemical parameters.* Int J Pharm, 2010. **395**(1-2): p. 182-97.
215. Nobili, S., et al., *Overcoming tumor multidrug resistance using drugs able to evade P-glycoprotein or to exploit its expression.* Med Res Rev, 2012. **32**(6): p. 1220-62.
216. Patel, N.R., et al., *Nanopreparations to overcome multidrug resistance in cancer.* Adv Drug Deliv Rev, 2013. **65**(13-14): p. 1748-62.
217. Sparrow, R.L., et al., *Common expression of the multidrug resistance marker P-glycoprotein in B-cell chronic lymphocytic leukaemia and correlation with in vitro drug resistance.* Leuk Res, 1993. **17**(11): p. 941-7.
218. Kostewicz, E.S., et al., *Predicting the precipitation of poorly soluble weak bases upon entry in the small intestine.* J Pharm Pharmacol, 2004. **56**(1): p. 43-51.
219. Houston, J.B., *Utility of in vitro drug metabolism data in predicting in vivo metabolic clearance.* Biochem Pharmacol, 1994. **47**(9): p. 1469-79.
220. Kocic, I., et al., *A case study on the in silico absorption simulations of levothyroxine sodium immediate-release tablets.* Biopharm Drug Dispos, 2012. **33**(3): p. 146-59.

221. Parrott, N. and T. Lave, *Applications of physiologically based absorption models in drug discovery and development.* Mol Pharm, 2008. **5**(5): p. 760-75.
222. Sinha, V.K., et al., *From preclinical to human--prediction of oral absorption and drug-drug interaction potential using physiologically based pharmacokinetic (PBPK) modeling approach in an industrial setting: a workflow by using case example.* Biopharm Drug Dispos, 2012. **33**(2): p. 111-21.
223. Hosea, N.A. and H.M. Jones, *Predicting pharmacokinetic profiles using in silico derived parameters.* Mol Pharm, 2013. **10**(4): p. 1207-15.
224. Duplantier, A.J., et al., *Discovery, SAR, and pharmacokinetics of a novel 3-hydroxyquinolin-2(1H)-one series of potent D-amino acid oxidase (DAAO) inhibitors.* J Med Chem, 2009. **52**(11): p. 3576-85.
225. Wu, C., et al., *Discovery, modeling, and human pharmacokinetics of N-(2-acetyl-4,6-dimethylphenyl)-3-(3,4-dimethylisoxazol-5-ylsulfamoyl)thiophene-2 -carboxamide (TBC3711), a second generation, ETA selective, and orally bioavailable endothelin antagonist.* J Med Chem, 2004. **47**(8): p. 1969-86.
226. Springthorpe, B., et al., *From ATP to AZD6140: the discovery of an orally active reversible P2Y12 receptor antagonist for the prevention of thrombosis.* Bioorg Med Chem Lett, 2007. **17**(21): p. 6013-8.
227. Hughes, R.O., et al., *Optimization of the aminopyridopyrazinones class of PDE5 inhibitors: discovery of 3-[(trans-4-hydroxycyclohexyl)amino]-7-(6-methoxypyridin-3-yl)-1-(2-propoxyethyl) pyrido[3,4-b]pyrazin-2(1H)-one.* Bioorg Med Chem Lett, 2009. **19**(17): p. 5209-13.
228. Wu, W.L., et al., *Discovery of orally efficacious tetracyclic metabotropic glutamate receptor 1 (mGluR1) antagonists for the treatment of chronic pain.* J Med Chem, 2007. **50**(23): p. 5550-3.
229. Owen, D.R., et al., *Identification, synthesis and SAR of amino substituted pyrido[3,2b]pyrazinones as potent and selective PDE5 inhibitors.* Bioorg Med Chem Lett, 2009. **19**(15): p. 4088-91.
230. Dorsey, B.D., et al., *Discovery of a potent, selective, and orally active proteasome inhibitor for the treatment of cancer.* J Med Chem, 2008. **51**(4): p. 1068-72.
231. Rawson, D.J., et al., *The discovery of UK-369003, a novel PDE5 inhibitor with the potential for oral bioavailability and dose-proportional pharmacokinetics.* Bioorg Med Chem, 2012. **20**(1): p. 498-509.
232. Sutherlin, D.P., et al., *Discovery of a potent, selective, and orally available class I phosphatidylinositol 3-kinase (PI3K)/mammalian target of rapamycin (mTOR) kinase inhibitor (GDC-0980) for the treatment of cancer.* J Med Chem, 2011. **54**(21): p. 7579-87.
233. Clements, J.A., et al., *Kinetics of acetaminophen absorption and gastric emptying in man.* Clin Pharmacol Ther, 1978. **24**(4): p. 420-31.
234. Wang, Y., et al., *A double-peak phenomenon in the pharmacokinetics of alprazolam after oral administration.* Drug Metab Dispos, 1999. **27**(8): p. 855-9.
235. Takamatsu, N., et al., *Variability in cimetidine absorption and plasma double peaks following oral administration in the fasted state in humans: correlation with antral gastric motility.* Eur J Pharm Biopharm, 2002. **53**(1): p. 37-47.

236. Ogiso, T., et al., *Pharmacokinetics of epinastine and a possible mechanism for double peaks in oral plasma concentration profiles.* Biol Pharm Bull, 2001. **24**(7): p. 790-4.
237. Hammarlund, M.M., L.K. Paalzow, and B. Odlind, *Pharmacokinetics of furosemide in man after intravenous and oral administration. Application of moment analysis.* Eur J Clin Pharmacol, 1984. **26**(2): p. 197-207.
238. Lennernas, H. and C.G. Regardh, *Regional gastrointestinal absorption of the beta-blocker pafenolol in the rat and intestinal transit rate determined by movement of 14C-polyethylene glycol (PEG) 4000.* Pharm Res, 1993. **10**(1): p. 130-5.
239. Yin, O.Q., et al., *A modified two-portion absorption model to describe double-peak absorption profiles of ranitidine.* Clin Pharmacokinet, 2003. **42**(2): p. 179-92.
240. Plusquellec, Y., et al., *A double-peak phenomenon in the pharmacokinetics of veralipride after oral administration: a double-site model for drug absorption.* J Pharmacokinet Biopharm, 1987. **15**(3): p. 225-39.
241. Wagner, J.G., *Unusual pharmacokinetics*, in *Pharmacokinetics: A Modern View*, L.Z. Benet, G. Levy, and B.L. Ferraiolo, Editors. 1984, Plenum Press: New York. p. 173-189.
242. Godfrey, K.R., et al., *Modelling the Double Peak Phenomenon in pharmacokinetics.* Comput Methods Programs Biomed, 2011. **104**(2): p. 62-9.
243. Williams, M.F., et al., *Influence of gastrointestinal site of drug delivery on the absorption characteristics of ranitidine.* Pharm Res, 1992. **9**(9): p. 1190-4.
244. Charman, W.N., et al., *Absorption of danazol after administration to different sites of the gastrointestinal tract and the relationship to single- and double-peak phenomena in the plasma profiles.* J Clin Pharmacol, 1993. **33**(12): p. 1207-13.
245. Guha, M., *Cyclin-dependent kinase inhibitors move into Phase III.* Nat Rev Drug Discov, 2012. **11**(12): p. 892-4.
246. Roush, J.A., *Evaluation of gastrointestinal motility directly from human pharmacokinetic data.* Int J Pharm, 2011. **419**(1-2): p. 43-51.
247. Kakhi, M. and J. Chittenden, *Modeling of pharmacokinetic systems using stochastic deconvolution.* J Pharm Sci, 2013. **102**(12): p. 4433-43.
248. Heikkinen, A.T., et al., *Application of PBPK modeling to predict human intestinal metabolism of CYP3A substrates - an evaluation and case study using GastroPlus.* Eur J Pharm Sci, 2012. **47**(2): p. 375-86.
249. Mathias, N.R. and J. Crison, *The use of modeling tools to drive efficient oral product design.* AAPS J, 2012. **14**(3): p. 591-600.
250. Parrott, N., et al., *Application of full physiological models for pharmaceutical drug candidate selection and extrapolation of pharmacokinetics to man.* Basic Clin Pharmacol Toxicol, 2005. **96**(3): p. 193-9.
251. De Buck, S.S., et al., *Prediction of human pharmacokinetics using physiologically based modeling: a retrospective analysis of 26 clinically tested drugs.* Drug Metab Dispos, 2007. **35**(10): p. 1766-80.
252. Suttle, A.B. and K.L. Brouwer, *Regional gastrointestinal absorption of ranitidine in the rat.* Pharm Res, 1995. **12**(9): p. 1311-5.
253. Davis, S.S., *Formulation strategies for absorption windows.* Drug Discov Today, 2005. **10**(4): p. 249-57.

254. Berghausen, J., et al., *Simulated rat intestinal fluid improves oral exposure prediction for poorly soluble compounds over a wide dose range.* Admet & Dmpk, 2016. **4**(1): p. 35.
255. McConnell, E.L., A.W. Basit, and S. Murdan, *Measurements of rat and mouse gastrointestinal pH, fluid and lymphoid tissue, and implications for in-vivo experiments.* J Pharm Pharmacol, 2008. **60**(1): p. 63-70.
256. Allen, T.M., *Ligand-targeted therapeutics in anticancer therapy.* Nat Rev Cancer, 2002. **2**(10): p. 750-63.
257. Lin, K. and J. Tibbitts, *Pharmacokinetic considerations for antibody drug conjugates.* Pharm Res, 2012. **29**(9): p. 2354-66.
258. Brannon-Peppas, L. and J.O. Blanchette, *Nanoparticle and targeted systems for cancer therapy.* Advanced Drug Delivery Reviews, 2012. **64**: p. 206-212.
259. Kim, C.K. and S.J. Lim, *Recent progress in drug delivery systems for anticancer agents.* Arch Pharm Res, 2002. **25**(3): p. 229-39.
260. Sapra, P. and T.M. Allen, *Ligand-targeted liposomal anticancer drugs.* Prog Lipid Res, 2003. **42**(5): p. 439-62.
261. Bertrand, N., et al., *Cancer nanotechnology: the impact of passive and active targeting in the era of modern cancer biology.* Adv Drug Deliv Rev, 2014. **66**: p. 2-25.
262. Wang, J., M. Sui, and W. Fan, *Nanoparticles for tumor targeted therapies and their pharmacokinetics.* Curr Drug Metab, 2010. **11**(2): p. 129-41.
263. Chabner, B.A. and T.G. Roberts, Jr., *Timeline: Chemotherapy and the war on cancer.* Nat Rev Cancer, 2005. **5**(1): p. 65-72.
264. Afrimzon, E., et al., *Intracellular esterase activity in living cells may distinguish between metastatic and tumor-free lymph nodes.* Clin Exp Metastasis, 2008. **25**(3): p. 213-24.
265. Eisenthal, A., et al., *Decrease of intracellular fluorescein fluorescence polarization (IFFP) in human peripheral blood lymphocytes undergoing stimulation with phytohaemagglutinin (PHA), concanavalin A (ConA), pokeweed mitogen (PWM) and anti-CD3 antibody.* Biol Cell, 1996. **86**(2-3): p. 145-50.
266. Matar, P., et al., *Th2/Th1 switch induced by a single low dose of cyclophosphamide in a rat metastatic lymphoma model.* Cancer Immunol Immunother, 2002. **50**(11): p. 588-96.
267. Harris, A.W., et al., *The E mu-myc transgenic mouse. A model for high-incidence spontaneous lymphoma and leukemia of early B cells.* J Exp Med, 1988. **167**(2): p. 353-71.
268. Mohammad, R.M., et al., *Establishment of a human B-CLL xenograft model: utility as a preclinical therapeutic model.* Leukemia, 1996. **10**(1): p. 130-7.
269. Bichi, R., et al., *Human chronic lymphocytic leukemia modeled in mouse by targeted TCL1 expression.* Proc Natl Acad Sci U S A, 2002. **99**(10): p. 6955-60.
270. Fotaki, N. and M. Vertzoni, *Biorelevant Dissolution Methods and Their Applications in In Vitro-In Vivo Correlations for Oral Formulations.* The Open Drug Delivery Journal, 2010. **4**: p. 2-13.
271. Prasad, D., C.H. Gu, and A. Kuldipkumar, *Comparison of biorelevant simulated media mimicking the intestinal environment to assess the solubility profiles of poorly soluble drugs.* Pharm Dev Technol, 2016. **21**(4): p. 511-7.
272. Fossati, L., et al., *Use of simulated intestinal fluid for Caco-2 permeability assay of lipophilic drugs.* Int J Pharm, 2008. **360**(1-2): p. 148-55.

273. Saha, P. and J.H. Kou, *Effect of bovine serum albumin on drug permeability estimation across Caco-2 monolayers.* Eur J Pharm Biopharm, 2002. **54**(3): p. 319-24.
274. Liang, E., K. Chessic, and M. Yazdanian, *Evaluation of an accelerated Caco-2 cell permeability model.* J Pharm Sci, 2000. **89**(3): p. 336-45.
275. Lennernas, H., et al., *Regional jejunal perfusion, a new in vivo approach to study oral drug absorption in man.* Pharm Res, 1992. **9**(10): p. 1243-51.
276. Di, L., et al., *Development of a new permeability assay using low-efflux MDCKII cells.* J Pharm Sci, 2011. **100**(11): p. 4974-85.
277. Riley, R.J., D.F. McGinnity, and R.P. Austin, *A unified model for predicting human hepatic, metabolic clearance from in vitro intrinsic clearance data in hepatocytes and microsomes.* Drug Metab Dispos, 2005. **33**(9): p. 1304-11.
278. Masimirembwa, C.M., U. Bredberg, and T.B. Andersson, *Metabolic stability for drug discovery and development: pharmacokinetic and biochemical challenges.* Clin Pharmacokinet, 2003. **42**(6): p. 515-28.
279. Jiang, W., et al., *The role of predictive biopharmaceutical modeling and simulation in drug development and regulatory evaluation.* Int J Pharm, 2011. **418**(2): p. 151-60.
280. Hamalainen, M.D. and A. Frostell-Karlsson, *Predicting the intestinal absorption potential of hits and leads.* Drug Discov Today Technol, 2004. **1**(4): p. 397-405.